UNIVERSIDAD AUTÓNOMA DE CHIHUAHUA
FACULTAD DE INGENIERÍA
SECRETARIA DE INVESTIGACIÓN Y POSGRADO
DOCTORADO EN INGENIERÍA

A SIMPLIFIED METHOD TO DEVELOP LRFD PRELIMINARY DESIGN CHARTS FOR PRESTRESSED CONCRETE BRIDGES

TESIS

PARA OBTENER EL GRADO DE DOCTOR EN INGENIERÍA

PRESENTA

Ph.D. JORGE MÁRQUEZ BALDERRAMA

CHIHUAHUA, CHIH. SEPTIEMBRE 2016

UNIVERSIDAD AUTÓNOMA DE CHIHUAHUA

FACULTAD DE INGENIERÍA

SECRETARIA DE INVESTIGACIÓN Y POSGRADO

DOCTORADO EN INGENIERÍA

A SIMPLIFIED METHOD TO DEVELOP LRFD PRELIMINARY DESIGN CHARTS FOR PRESTRESSED CONCRETE BRIDGES

TESIS

PARA OBTENER EL GRADO DE DOCTOR EN INGENIERÍA

APROBADO:

DRA. CECILIA OLIVIA OLAGUE CABALLERO, Presidente

DR. GILBERTO WENGLAS LARA, Secretario

DR. MARIO CESAR RODRÍGUEZ RAMIREZ, Vocal

DR. JOSE CASTAÑEDA AVILA, Vocal 1

DR. ALEJANDRO VILLALOBOS ARAGON, Vocal 2

SEPTIEMBRE, 2016

CHIHUAHUA, CHIH.

por

Ph.D. JORGE MARQUEZ BALDERRAMA

2016

12 de septiembre de 2016

Ph.D. JORGE MÁRQUEZ BALDERRAMA

Presente

En atención a su solicitud relativa al trabajo de tesis para obtener el grado de Doctor en Ingeniería, nos es grato transcribirle el tema aprobado por esta Dirección, propuesto y dirigido por el director **Ph.D. David V. Jauregui** para que lo desarrolle como tesis, con el título: **"A SIMPLIFIED METHOD TO DEVELOP LRFD PRELIMINARY DESIGN CHARTS FOR PRESTRESSED CONCRETE BRIDGES"**

CHAPTER 1

INTRODUCTION

1.1 Preliminary Design Charts

1.2 Effects of Design Parameters

1.3 Need for Research

1.4 Research Goal and Objectives

1.5 Overview of Dissertation

CHAPTER 2

LITERATURE REVIEW

2.1 Fereig (1985)

2.2 PCI (2003)

2.3 Hanna et al. (2010)

2.4 PCI (2011)

2.5 Jeon et al. (2012)

2.6 Summary of Literature Review

CHAPTER 3

DESCRIPTION OF PRESTRESSED GIRDER MODEL FOR SIMPLE SPANS

3.1 Design Criteria

3.2 Transition Points and Design Regions

3.3. Comparison with PCI-03 Charts

UNIVERSIDAD AUTÓNOMA DE CHIHUAHUA
Facultad de Ingeniería

Solicitamos a Usted tomar nota de que el título del trabajo se imprima en lugar visible de los ejemplares de las tesis.

A T E N T A M E N T E
"naturam subiecit aliis"

FACULTAD DE INGENIERÍA U.A.CH.

EL DIRECTOR	**EL SECRETARIO DE INVESTIGACIÓN Y POSGRADO**
M.I. RICARDO RAMÓN TORRES KNIGHT	**DR. MARIO CÉSAR RODRÍGUEZ RAMÍREZ**

CHIHUAHUA Facultad de Ingeniería DIRECCION

Facultad de Ingeniería
Circuito No. 1, Campus Universitario 2
Chihuahua, Chih. C.P. 31125
Tel. (614) 442-9500 www.fing.uach.mx

UNIVERSIDAD INTERNACIONAL

Dedicatoria

A Dios por su Amor, Fortaleza y Protección.
A mis Padres que lo Dieron Todo por mí, Gracias a Ellos Soy lo que Soy.
A mi Esposa Karina por su Amor, Cariño y Apoyo Incondicional.
A mis Hijos Priscy y Jorgito por su Amor, Cariño y Admiración.
A mis Hermanos por su Apoyo y Cariño.

ACKNOWLEDGEMENTS

I owe my deepest gratitude to God who has made this dissertation possible and for whom my graduate experience, family, and friends have been one that I will never forget.

I would like to acknowledge the most generous assistance that I received from Dr. Dávid V. Jauregui, my advisor, who wisely guided me through this research. Encouragement, sharp and constructive criticism, and most of all, the patience and passion for civil engineering received from Dr. Jáuregui helped the author to complete this investigation before the imposed deadline. I have been extremely fortunate to have such an advisor and professor.

To my wife Karina and children Priscyla and Jorge thank you for all your continuous encouragement, love, friendship and support. Karina thank you for your help and prayers in the most stressful days. This dissertation would not be possible without your love and patience.

Mom, Dad, thank you for your encouragement, many phone calls, but most of all for your unconditional support and love. To my brothers and sisters thank you for your valuable help, friendship and prayers every time I needed it.

I would like to acknowledge my co-advisor, Dr. Brad Weldon, for always providing me advice and constructive criticism during my graduate studies. Dr. Craig Newtson thank you for your valuable help every time I needed it. I would also like to thank Dr. Ruinian Jiang for having had the time to serve in my final defense.

To all my close friends, graduate, and undergraduate students, along with the faculty and staff of the Department of Civil Engineering at New Mexico State University for sharing your experiences and for your friendship and support.

(PROMEP), and Consejo Nacional de Ciencia y Tecnologia (CONACYT) for the financial support for my research. Special thanks to the faculty and staff of the Department of Civil Engineering at the University of Chihuahua for their confidence and support.

ABSTRACT

A SIMPLIFIED METHOD TO DEVELOP LRFD PRELIMINARY DESIGN CHARTS FOR PRESTRESSED CONCRETE BRIDGES

BY

JORGE MÁRQUEZ BALDERRAMA, M.A.Sc.

Doctor of Philosophy in Civil Engineering

New Mexico State University

Las Cruces, New Mexico, 2015

Dr. David V. Jáuregui, Chair

Dr. Brad D. Weldon, Co-Chair

The 2011 PCI Bridge Design Manual provides preliminary design charts for selecting the girder size and number of prestressing strands for a given span length and beam spacing but only for f'_c = 8,000 psi (55.2 MPa). This single strength limits the use of the charts, particularly for states considering ultra-high performance concrete (UHPC). Accordingly, this dissertation presents a simplified procedure to develop preliminary design charts for prestressed concrete bulb-tee girders considering service load stress limits, flexural strength and stresses at release. The results for a BT-72 beam are first compared with the 2003 PCI design charts originally developed based on the AASHTO Standard Specifications. The procedure is then adapted to the AASHTO

LRFD Bridge Design Specifications and verified with the prevailing 2011 PCI design charts. Finally, new LRFD charts are generated for NSC, HPC, and UHPC with 0.5, 0.6, and 0.7-in. (13, 15 and 18 mm) strands for simple and two-span continuous bridges to illustrate the simplified procedure and potential impact of UHPC, larger strand size, and continuity on bridge girders.

The new LRFD charts are shown to be accurate for the design assumptions made since an excellent agreement (within 2% and 4%) resulted between the preliminary design charts developed in this study and those given in the 2003 and 2011-PCI Bridge Design Manuals. The "transition point" is identified which provides the information needed for a designer to distinguish the zones between fully prestressed (uncracked), partially prestressed, and non-prestressed (cracked) members. The preliminary design charts demonstrate the effect of using UHPC and/or larger strand size and/or two-span continuous layouts. The effect of implementing continuity with the combination of UHPC and a larger strand diameter was shown to be much more significant than just increasing the concrete compressive strength or the strand diameter or using two-span continuous layouts. However, the use of longer full-span girders poses significant challenges for fabrication, transportation, erection, span-to-depth ratios, and live and dead load deflections of prestressed concrete bridges and, consequently, should be considered carefully for the final design of the bridge.

TABLE OF CONTENTS

LIST OF TABLES

LIST OF FIGURES

CHAPTER 1:

CHAPTER 2:

CHAPTER 3:

CHAPTER 4:

CHAPTER 5:

NOMENCLATURE

A	= cross-section area of beam
A_g	= gross area of non-composite beam section
A_{ps}	= area of prestressing steel
A_s	= area of nonprestressed tension reinforcement
A_{st}	= area of one strand
c	= distance from extreme compression fiber to neutral axis
c_1, c_2, c_3, c_4	= constants
CR_c	= loss of prestress due to creep of concrete
CR_s	= loss of prestress due to relaxation of pretensioning steel
dia	= diameter
d_e	= distance from the center of the exterior beam and the interior edge of the curb or traffic barrier
d_p	= distance from extreme compression fiber to extreme tension steel
e	= coefficient factor $\geq$ 1.0 to determine LRFD distribution factor for exterior I-beams without midspan diaphragms for two or more design lanes loaded
e_g	= distance between the centers of gravity of the beam and deck
e_m	= average prestressing steel eccentricity at midspan
E_c	= modulus of elasticity of concrete
E_{ci}	= modulus of elasticity for girder at release
E_p	= modulus of elasticity of prestressing steel

E_s = modulus of elasticity for pretensioning strands

ES = loss of prestress due to elastic shortening

f_b = bottom concrete stresses at transfer

f_{b1} = flexural bottom stresses due to live and dead loads

f_{b2} = flexural bottom stresses due to prestress after all losses

f_c = average compressive stress in concrete slice based on nonlinear behavior

f'_c = specified compressive strength of concrete at 28 days

f'_{ci} = concrete stress at release

f_{cir} = average concrete stress at the center of gravity of the pretensioning steel due to pretensioning force and dead load of girder immediately after transfer

f_{cds} = concrete stress at the center of gravity of the pretensioning steel due to all dead loads except the dead load present at the time the pretensioning force is applied

f_{pbt} = stress in prestressing steel prior to transfer

f_{pe} = effective prestress force

f_{pi} = prestressing steel stress immediately prior to transfer = $0.75f_{pu}$

f_{ps} = stresses in the prestressing steel

f_{pu} = specified tensile strength of prestressing steel

f_{py} = yield strength of prestressing steel

f'_s = ultimate pretensioning strands stress

f_{se} = effective final prestress

f_{si} = initial pretensioning

f_t	= top concrete stresses at transfer
f_y	= specified yield strength of reinforcing bars
F_b	= tension stress limit at service loads
F_{cr}	= allowable compressive stress at release
F_{tr}	= allowable tensile stress at release
g	= distribution factor for exterior I-beams without midspan diaphragms for two or more design lanes loaded
HL-93	= highway loading, developed in 1993
HPC	= high performance concrete
HS-20	= highway semi-trailer, 20 TON (40 kips) weight of the tractor (1st two axles)
I	= live load impact factor
I_g	= moment of inertia of non-composite beam section
k	= factor to increase post-peak decay in stress for nonlinear concrete stress-strain curves
K_g	= longitudinal stiffness
L	= span length
M_b	= simple span bending moment due to barrier weight
$M_{b\ (two-span)}$	= two-span bending moment due to barrier weight
M_{b+ws}	= bending moment due to barrier and wearing surface weight
M_g	= bending moment at midspan due to girder weight
$M_{HS-20(two-span)}$	= bending moments at $\frac{2}{5}L$ from the left support due to the HS-20 design truck for a two-span continuous system

$M_{lane(two-span)}$	= bending moments at $\frac{2}{5}L$ from the left support due to lane loading of 0.64 kip/ft (953.3 kg/m) for a two-span continuous system
M_{LL}	= bending moment per lane due to live load at midspan
M_{LL+I}	= bending moment per lane due to live load plus impact at midspan
$M_{LL+I(HS-20)}$	= live load bending moment plus impact due to HS-20 truck loading at midspan
M_{HL-93}	= bending moment due to HL-93 live loading
$M_{LL+I(HL-93)}$	= midspan bending moment due to HL-93 live loading plus impact
M_{lane}	= bending moment at midspan due to lane loading of 0.64 kip/ft
$M_{LL+I(HL-93)s}$	= simulated bending moment due to HL-93 live loading plus impact
M_{SE}	= bending moments for the LRFD Service III limit state
M_s	= bending moment due to the slab weight and haunch
M_{ws}	= simple span bending moment due to wearing surface weight
$M_{ws\ (two-span)}$	= two-span bending moment due to wearing surface weight
M_u	= ultimate flexural moment
mg	= moment distribution factor
n	= modular ratio between beam and deck material
n_s	= curve fitting factor for nonlinear concrete stress-strain curves
N	= number of prestressing strands
N_L	= number of loaded lanes under consideration

N_b = number of beams

NSC = normal strength concrete

P = 40 and 30 kips (177.9 and 133.4 kN) for HS-25 and HS-20 truck loading, respectively

P_{se} = effective pretension force after all losses

PPR = partial prestress ratio

R = reaction on exterior beam in terms of lanes

RH = relative humidity

S = girder spacing

SH = loss of prestress due to concrete shrinkage

t_s = slab thickness

UHPC = ultra-high performance concrete

w_c = unit weight of concrete

w_h = haunch weight

w_g = girder weight

w_s = slab weight

x = horizontal distance from the center of gravity of the pattern of beams to each beam

X_{ext} = horizontal distance from the center of gravity of the pattern of beams to the exterior beam

ε'_c = concrete strain when f_c reaches f'_c

ε_{cf} = concrete strain above the neutral axis at the center of each slice

ε_{ps} = strain in the prestressing steel

Δf_{pES} = instantaneous prestress losses due to elastic shortening

Δf_{pLT} = long term prestress losses due to creep, concrete shrinkage and steel relaxation

Δf_{pR} = loss of prestress due to relaxation of pretensioning steel

Δf_{pT} = total prestress losses for the Service III limit state

γ_h = correction factor for relative humidity of the ambient air

γ_L = live load factor (equal to 0.8)

γ_{st} = correction factor for concrete strength at time of transfer

$\emptyset$ = strength reduction factor

$\emptyset M_n$ = flexural design strength

CHAPTER 1

INTRODUCTION

Precast prestressed concrete girder bridges have grown into the most commonly used bridge systems in the United States. Preliminary design is an essential first step in designing a safe and economical bridge of this type. For a given span length and based on standard concrete strengths, the preliminary design mainly includes selection of the girder size and shape; girder spacing; diameter and number of prestressing strands; and deck thickness. In 2003, the Precast/Prestressed Concrete Institute (PCI) Bridge Design Manual provided preliminary design charts that were based on the American Association of State Highway and Transportation Officials (AASHTO) Standard Specifications (2002) for 28-day concrete compressive strengths of f'_c = 7,000 and 12,000 psi (48.3 and 82.8 MPa) with 0.5-in. (13 mm) and 0.6-in. (15 mm) diameter strands, respectively. In 2011, PCI revised the charts based on the AASHTO Load and Resistance Factor Design (LRFD) Bridge Design Specifications (2010), but only for f'_c = 8,000 psi (55.2 MPa) and 0.6-in. (15 mm) diameter strands. Preliminary design charts provide bridge engineers an effective tool to optimize the final design of prestressed concrete bridge girders. In addition, these design aids can reduce the time-consuming selection process and eliminate unnecessary design iterations of numerous options required to achieve a feasible and economical bridge design.

The remainder of this chapter provides a description of the general types of charts found in the literature related to the design of prestressed concrete bridge girders and a discussion of the usefulness of these graphs for preliminary design purposes. The effects of design parameters including concrete properties, prestressing strand size, and span continuity on the design of a prestressed concrete girder are discussed and illustrated. The need for a simplified method to develop LRFD preliminary design charts is explained and discussed. The research goal and objectives are given and described. Finally, an overview of this dissertation is provided.

1.1 Preliminary Design Charts

Generally, two types of charts can be found in the literature related to preliminary design of prestressed concrete bulb-tee (BT) bridge girders: (1) those that show the maximum attainable span length versus girder spacing for different girder sizes as shown in Figure 1.1, and (2) those that show the number of strands versus span length for different girder spacings as shown in Figure 1.2. These charts provide the designer an excellent starting point for a preliminary design.

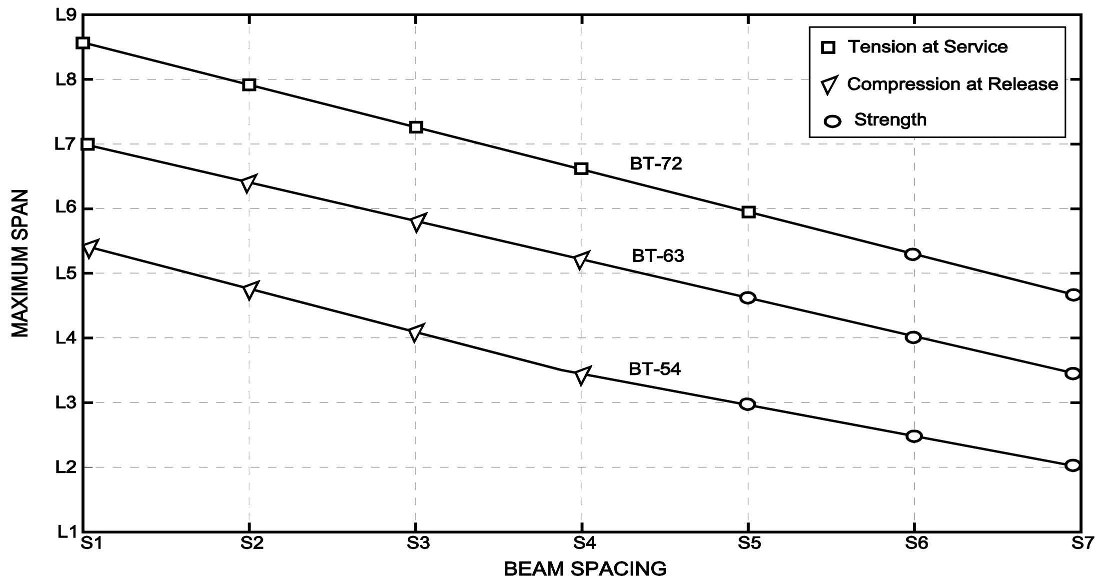

Figure 1.1. Maximum span length versus girder spacing for different BT girder shapes.

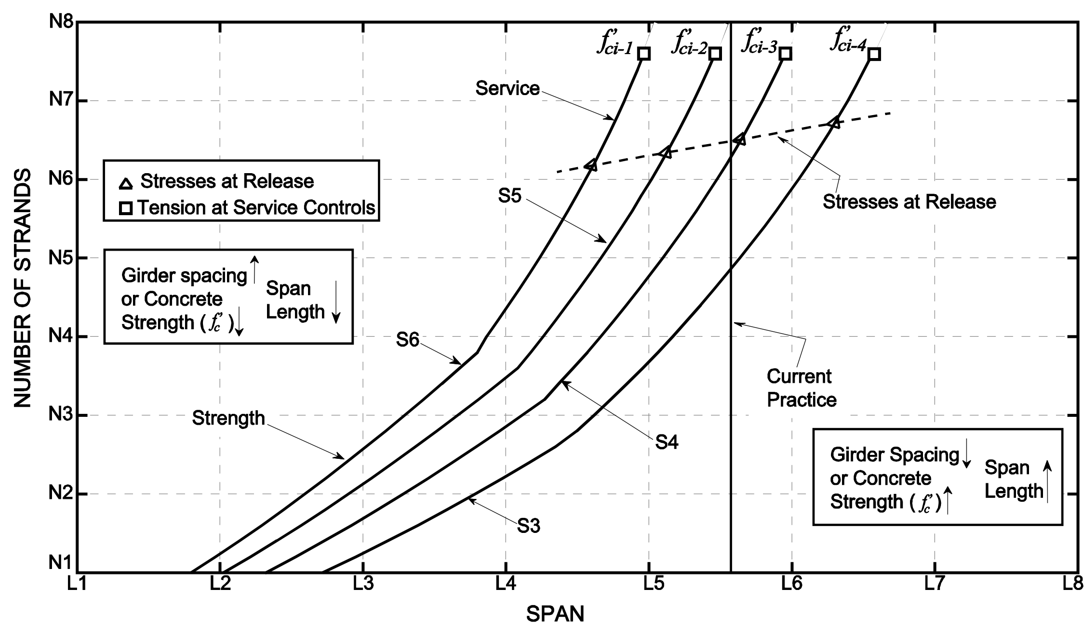

Figure 1.2. Number of strands versus span length for different girder spacings and a given concrete strength.

The first chart (Figure 1.1) provides the designer an estimate of the maximum span length when the girder spacing, concrete strength and girder size are known. On the other hand, if the maximum length and girder size are provided, the girder spacing can be determined. Notice that the governing limit state is provided for each girder shape in the graph. Normally, stresses at release or service govern at longer span lengths. Charts of this type were developed for different standard cross sections including box beams, bulb-tees, and I-beams in the PCI Bridge Design Manuals (2003, 2011). For each cross section, different girder sizes were considered such as the BT-54, BT-63, and BT-72 for bulb-tees. In addition to the standard AASHTO shapes, new shapes have been introduced in bridge design practice in the U.S. and used successfully. For example, the PCI Bridge Design Manual (2011) includes a U-beam, a non-composite deck bulb-tee girder, and a double-tee stemmed beam known as the NEXT beam as shown in Figure 1.3.

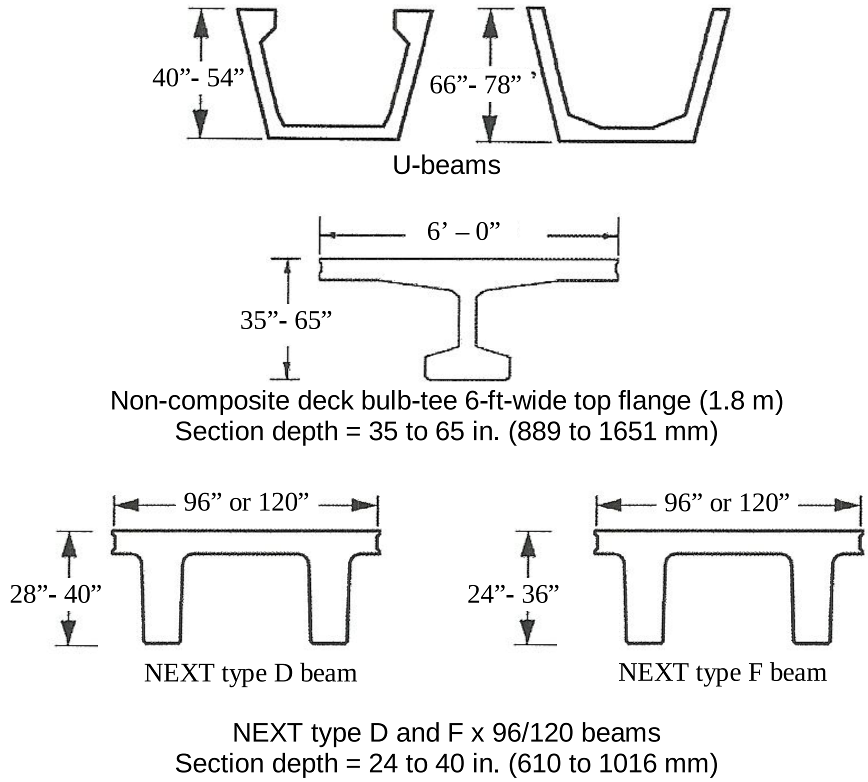

Figure 1.3. New shapes in bridge design: U-beam, non-composite deck bulb-tee girder and NEXT beam (PCI 2011). Note: 1 in. = 25.4 mm, 1 ft = 304.8 mm

States such as Washington, Texas, Nebraska, Utah, Florida, Pennsylvania, and the New England states have developed their own girder shapes based on typical AASHTO-PCI bulb-tee sections, AASHTO I-beams, and multi-web stemmed beams given in the PCI Bridge Design Manuals (2003, 2011). Preliminary design charts similar to the one shown in Figure 1.1 have been developed by many of these states providing the span capability of local products. It is important to point out that knowledge of the local marketplace is essential to determine the optimal configuration for a bridge. Using local girder shapes helps to minimize the cost of a bridge due to transportation and local production issues.

The second chart (Figure 1.2) provides the required number of strands given the girder spacing, span length, concrete strengths (at release and 28 days) and strand diameter for a specific girder section. This chart can alternatively provide the span length given the number of strands and girder spacing for a specific girder size and concrete strength. Girder spacings of 6, 8, 10 and 12 ft (1.8, 2.4, 3.0 and 3.7 m) are normally chosen which represent feasible upper and lower limits used in current practice (PCI 2011). For this range of girder spacings, the exterior girder typically governs the design for the narrower spacing and the interior girder usually governs for wider spacings. This is attributed mainly to the differences in the LRFD live-load distribution factor for exterior and interior girders. It is also generally found that the controlling beam (interior or exterior) demands just a few more strands than the rest of the beams or the maximum span length only reduces by 5 to 10 ft (1.5 to 3 m) (PCI 2011). Note that as the girder spacing decreases or the concrete strength increases, the span length increases. On the contrary, if the girder spacing increases or the concrete strength decreases, the span length decreases.

The use of longer full-span girders has limitations on fabrication, transportation, and erection. Some states restrict the maximum transportable girder length to 120 ft (36.6 m) and the weight to 70 tons (PCI 2011). Precast beams up to 210 ft (64 m) in length and more than 150 tons in weight, however, have been allowed in Pennsylvania, Washington, Nebraska and Florida (PCI 2011). The size of the erection equipment may be limited by the access to the site or by the availability to the contractor. In addition, transportation of long beams may also be restricted by access to the construction site. Depending on the current regulations of girder lengths in each state, the designer can determine the most practical and economical configuration. This length restriction can be represented as shown in Figure 1.2 by a vertical line labeled as “Current Practice”.

1.2 Effects of Design Parameters

For a given span length and based on standard concrete strengths, the design of an economical prestressed concrete girder generally starts with a preliminary estimate of the girder size, shape, and spacing; diameter and number of prestressing strands; and deck thickness. Full-span girders are simple-span girders with no intermediate concrete girder splices or concrete joints. These girders can also be used as continuous span girders with continuity diaphragms or girder splices at interior piers. Full-span girders are the most cost-effective and practical for precast, prestressed concrete girder bridges which can be used in simple-span and continuous span structural systems (PCI 2011). The most common systems are simple-supported bridges which have been used effectively in the U.S. for over 60 years (Hueste et al. 2012); however, these systems become limiting when longer spans are desired due to a growing need in the transportation industry to limit the impact of construction on the the traveling public. The effects of different material properties (including the concrete strength, strand size and type, and lightweight aggregate) and span continuity on the girder design are discussed in the following paragraphs.

1.2.1 Concrete Properties

The use of high performance concrete (HPC) is the most effective method to extend prestressed concrete girder spans (Jeon et al. 2011). Concrete strengths for this type of concrete can range from 7,250 psi to 14,500 psi (50 to 100 MPa) (PCA 1994) as shown in Table 1.1.

Table 1.1. Typical strength classification for different types of concrete (PCA 1994).

Normal strength concrete (NSC)	High-performance concrete (HPC)	Very-high-strength concrete	Ultra-high-performance concrete (UHPC)
< 7,250 (50)	7,250-14,500 (50-100)	14,500-21,750 (100-150)	> 21,750 (150 MPa)

Note: concrete strength given in psi (MPa).

In general, as the girder concrete strength increases, longer span lengths can be attained and the number of piers and girders can be reduced and consequently, the total volume of concrete. However, material cost generally rises when HPC is used. For example, increasing the concrete strength from f'_c = 7 ksi (48.3 MPa) to 14 ksi (96.6 MPa), can double the material cost from \$70 to \$140/yd^3 (\$91.7 to \$183.4/m^3) (PCI 2011). If the strength increment is only 3 ksi (20.7 MPa), then the additional cost can be \$10 to \$20/yd^3 (\$13.1 to \$26.2/m^3) (PCI 2011). For a preliminary design, the rise in material cost in using HPC needs to be weighed against savings due to reductions in the volume of concrete. According to PCI (2011), initial savings due to reductions of the volume of concrete and improved durability properties indicate that the use of HPC is feasible.

Ultra-high performance concrete (UHPC), a new class of cementitious composite material, began with the development of reactive powder concrete (RPC) in the early 1980's. This development can be credited to researchers Bache (1981) and Richard and Cheyrezy (1995). Richard and Cheyrezy (1995) implemented several new principles to produce UHPC. This type of concrete is different from normal strength concrete (NSC) and HPC in several ways. Mainly, coarse sand is replaced by fine sand and high strength steel fibers. Consequently, UHPC has been shown to develop a compressive strength greater than 21.7 ksi (150 MPa) and the steel fibers result in a sustained post-cracking tensile strength greater than 0.72 ksi (5 MPa) (Graybeal 2009). Since both the compressive and tensile strengths are greater for UHPC, the design of structural elements may be better optimized. Additionally, because its main aggregate is fine sand, the porosity of the concrete decreases and thus, penetration of liquids reduces significantly, improving durability (Graybeal 2011). Hence, the mechanical and durability properties of UHPC make it a promising material for the construction of new prestressed concrete bridges as well as an option for repair and replacement of older bridges to address highway infrastructure deterioration (Graybeal 2009). Typical strength ranges of HPC and UHPC are shown in Table 1.1.

The reduction of a girder's weight by using structural concrete lightweight aggregate (LWA) has been used extensively to support heavy superimposed dead and live loads as well as to achieve higher span capacities (PCI 2011). The most significant contributions of LWA concrete have been in bridge construction. Structural LWA concrete has been used in highway bridges for more than 50 years in North America.

There are over 200 concrete bridges in the U.S. and Canada that have been built with this type of aggregates (Ramirez et al. 2000). As the span length increases, the self-weight of the structure increases and becomes of greatest importance. About one-third of the total load resisted by a prestressed concrete bridge girder corresponds to its own weight and the load increases proportionally as the span increases (PCI 2011). Structural concrete made with lightweight aggregates is usually 20 to 30% lighter than normal concrete (Ramirez et al. 2000). Densities of lightweight or a combination of lightweight aggregate and normal-weight aggregate (NWA) are generally between 70 and 120 lb/ft^3 (1120 and 1920 kg/m^3) (ACI 2013). Reductions up to 30% of the superstructure weight are possible that results in cost savings for materials (mild reinforcement, prestressing steel); substructure elements (foundations, piers); and formwork, transportation, and handling where ground conditions are severe (Ramirez et al. 2000). However, LWA concrete requires a larger amount of cement than normal concrete to achieve a high strength (50% more cement content than normal concrete) and as a result, the initial cost of LWA concrete may be higher (Ramirez et al. 2000). Overall, more than 10% of the cost of a bridge can be estimated as net savings after having considered cost savings due to reductions in materials and the higher initial cost of lightweight aggregates (Ramirez et al. 2000).

Structural lightweight concrete has a minimum compressive strength of 2465 psi (17 MPa) (Ramirez et al. 2000). However, experimental research conducted by Meyer et al. (2002) proved that bridge girders can be built with high strength, lightweight aggregate concrete (HSLWC) achieving concrete compressive strengths up to 12 ksi (83 MPa), thereby reducing the girder weight up to 20% and increasing the length of simple-span AASHTO I-girders and AASHTO-PCI bulb-tee girders by up to 4% and 3% respectively.

1.2.2 Prestressing Strand Size

Using high strength concrete and larger diameter strands it is possible to obtain longer span lengths, shallower section depths, and wider girder spacings. Larger prestressing forces can be achieved by increasing the strand size which consequently reduces the number of strands required. Furthermore, lowering the center of gravity of the strands results in additional flexural capacity. This lowers the material and labor costs since the number of strands and clamps needed in the prestressing process is reduced. The use of 0.6 and 0.7-in. (15 and 18 mm) diameter strands rather than 0.5-in. (13 mm) results in a more efficient girder. For example, a 20% increase in strand diameter from 0.5 to 0.6-in. (13 to 15 mm) provides 40% more pretensioning force (PCI 2011).

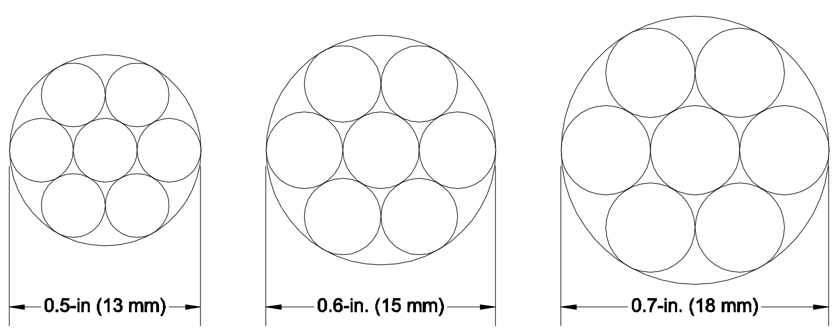

Figure 1.4. Sketch of 0.5, 0.6 and 0.7-in. (13, 15 and 18 mm) diameter strands (scale 1: 2).

Designers have quickly accepted the use of 0.6-in. (15 mm) diameter strands. Further improvement occurs when 0.7-in. (18 mm) diameter strands are used. A 17% increase from 0.6 to 0.7-in. (15 to 18 mm) diameter strand gives 35% more prestressing force and a 40% increase from 0.5 to 0.7 inch (13 to 15 mm) produces a 92% increase in the prestressing force (Hanna et al. 2010). Therefore, the increase in prestressing force is about double the increase in strand diameter.

Experimental and analytical research work have shown the benefits of 0.7-in. (18 mm) diameter strands in bridge girder design. Vadivelu et al. (2008) conducted an analytical study and showed that a BT-72 girder with 0.6-in. (15 mm) diameter strands could be reduced to a BT-54 girder with 0.7-in. (18 mm) diameter strands and achieve the same capacity. Morcous et al. (2011) performed an experimental study using 0.7-in. (18 mm) diameter strands in pretensioned bridge girders. This investigation evaluated the challenges of implementing I-girders with 0.7-in. (18 mm) diameter strands in bridge construction. Two full-scale Nebraska University (NU) 900 I-girders were fabricated and tested which showed that the design provisions from the AASHTO LRFD Bridge Design Specifications (2010) and current production practices for 0.7-in. (18 mm) strand can be used without significant changes.

Using HPC, the allowable concrete stress in compression and tension are increased and consequently, longer spans and/or wider girder spacings are possible but larger pretension tensile forces are needed. The number and/or the strand diameter must increase to handle the required pretension force. Furthermore, the more prestressing steel area that is provided in the bottom flange, the greater the capacity to resist positive moment. It is important to note that the bottom flange dimensions determines the number and size of the strands that can be used. Therefore, the designer should consider girder sections with larger bottom flanges if longer spans are demanded and HPC is used. For example, longer span lengths are possible with the NU I-girders, Washington super girders (WF##G), and New England bulb-tee (NEBT) beams than the AASHTO-PCI bulb-tee section because they have larger bottom flanges as shown in Figure 1.5. The NU I-girders have been widely used in Canada and the U.S. in Nebraska, Missouri, and Texas (Hanna et al. 2010).

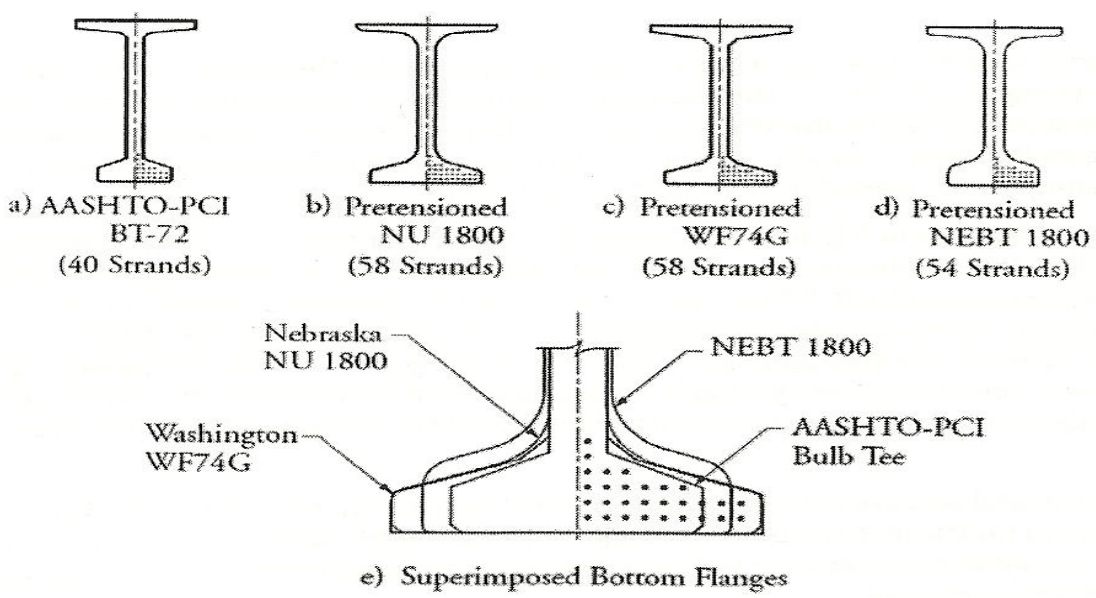

Figure 1.5. Comparison of bulb tee with I-beam shapes with large bottom flanges to accommodate more strands (PCI 2011).

1.2.3 Span Continuity

Simple-supported precast prestressed concrete girders have been used in the U.S. for more than sixty years (Hueste et al. 2012). Span lengths are commonly limited to about 150 ft (46 m) due to weight and length restrictions during girder transportation (Hueste et al. 2012). Longer span bridges are advantageous when traffic and congestion increase in urban areas. There are several engineering techniques to extend the span length of prestressed concrete bridges including the use of HPC and UHPC, lightweight concrete, larger strand size, and modified girder sections (Abdel-Karim et al. 1995). In addition, the span length can be increased using continuous span girders. Designing for continuity involves two basic steps; girders are typically constructed simple for dead load (step 1) and continuous for live load (step 2). In the first step, precast, prestressed girders are erected as simple spans, as shown in Figure 1.6.

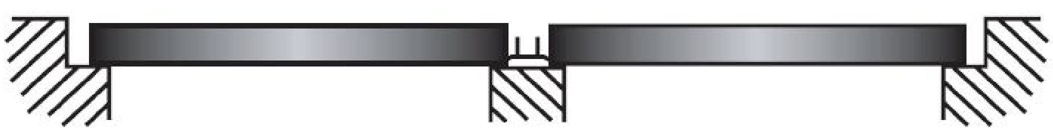

Figure 1.6. Precast, prestressed girders erected as simple spans.

The non-composite structure is analyzed as simple span for girder, slab and haunch self-weights and effects of prestress at release. In the second step, the bridge is made continuous and composite with a cast-in-place deck and a diaphragm as shown in Figure 1.7.

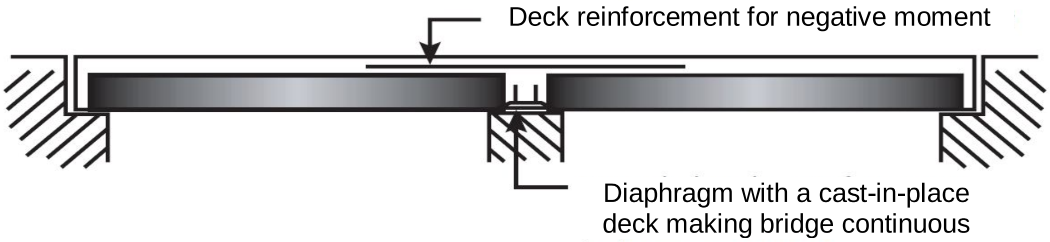

Figure 1.7. Precast, prestressed girders made continuous and composite with a cast-in-place deck and diaphragm.

Composite and continuous girders are then analyzed for live loads (e.g. HL-93 live loading plus impact), and superimposed dead loads (e.g. future wearing surface and barriers weight) and time dependent effects (shrinkage, creep and temperature).

Spliced precast, prestressed concrete girders have been preferred by contractors in performance-based bids of projects in some states (Castrodale et al. 2004). Advantages of these types of construction are that bridge deck joints are eliminated over the piers thereby reducing maintenance cost and improving durability (Hueste et al. 2012). Based on the bridge span length and the urban demands, simple and continuous span girders are preliminary design options that should be carefully examined to maximize structural performance and minimize the bridge cost.

1.3 Need for Research

Current PCI preliminary design charts are based on the AASTHO LRFD Bridge Design Specifications (2010) and provide useful design aids but they limit the designer to a single girder concrete strength of f'_c = 8,000 psi (55.2 MPa) and 0.6-in. (15 mm) diameter strands. In addition, these charts were developed only for simple spans.

Longer spans may be needed in urban areas due to traffic and congestion problems during construction. The construction of longer spans is also beneficial in the development of an effective infrastructure for economic and environmental reasons. As previously discussed, there are several techniques for extending spans including the use of high strength concrete, lightweight aggregates, larger diameter strand, and modified girder sections (Abdel-Karim et al. 1995). In addition, span continuity is an effective method to increase the span length (Hueste et al. 2012). Consequently, preliminary design charts should include not only the option to evaluate simple spans, but also continuous spans particularly when longer spans are required. Advances in bridge technology demands that different parameters be considered including, but not limited to, concrete girder and deck strengths; constitutive relationships for concrete and steel; girder section and spacing; strand size and prestress loss equations; and allowable concrete stress limits for tension and compression. Therefore, a versatile simplified design method that is capable of evaluating various combinations of these parameters for simple and continuous spans is needed to give preliminary options that aid the engineer in optimizing the final girder design.

1.4 Research Goal and Objectives

The major goal of this research was to develop a simplified method for generating LRFD preliminary design charts for prestressed concrete girders for simple and continuous span bridges. The specific objectives of this research are:

- Develop an analytical girder model to generate preliminary design charts for simple-supported prestressed concrete bulb-tee girders following the AASHTO Standard Specifications (2002) to obtain a closed-form solution. Use a BT-72 girder to illustrate the analytical procedure and verify the results with the PCI (2003) design charts.
- Adapt the simple-supported girder model to the LRFD Specifications (2010) through modification of the dead and live load effects, and prestress losses and verify the results with the PCI (2011) design charts. Modify the prestressed girder model to satisfy the LRFD Service III and Strength I limit states for simple span bridges.
- Adapt the LRFD-based prestressed girder model from simple span to two-span continuous bridges. Generate LRFD preliminary charts for different combinations of concrete strength including NSC, HPC, and UHPC with 0.5-in. (13 mm), 0.6-in. (15 mm.) and 0.7-in. (18 mm) diameter strands, respectively, to illustrate the utility of the prestressed girder model and potential impact on design for simple and continuous span bridges.

1.5 Overview of Dissertation

The remainder of this dissertation is organized into five additional chapters. Chapter 2 gives a literature review related to preliminary design charts for prestressed concrete girders including past development and current state of practice. Chapter 3 presents the design criteria that was followed to develop the prestressed girder model for simple spans based on service, strength, and release limit states using the AASHTO Standard Specifications (2002). Chapter 4 explains the procedure that was followed to adapt the prestressed girder model to the AASHTO LRFD Bridge Design Specifications (2010) including the modifications for the Service III and Strength I limit states. This chapter also explains the adaptation of the girder model from simple spans to two-span continuous bridges and consideration of release stresses. Chapter 5 evaluates the impact of using different combination of concrete strengths including NSC, HPC, and UHPC with 0.5-in. (13 mm), 0.6-in. (15 mm.) and 0.7-in. (18 mm) diameter strands for simple and two-span continuous bridges. Practical implications are also discussed in this chapter. Chapter 6 presents a summary of the research and conclusions followed by recommendations for future work.

CHAPTER 2

LITERATURE REVIEW

This chapter gives a literature review related to the development and use of preliminary design charts for prestressed concrete bridge girders. Most of the graphical design aids found in the literature are for simple spans. However, the consideration of span continuity in bridge design is discussed and illustrated with the few reported studies for continuous span girders. For each reference, the design criteria and assumptions including, dead and live loads, deck and girder properties, allowable stresses, and prestressing strands and spacing are described. Subsequently, the charts of each reference are briefly described and the findings are summarized.

2.1 Fereig (1985)

Preliminary design charts for simple prestressed concrete bridge girders were first developed by Fereig (1985) in Canada. A mathematical model was provided in this study that was based on linear programming to obtain the required prestressing force versus the span length for different girder spacings. Ferguson (1998) defines a linear programming problem as "a problem of maximizing or minimizing a linear function subjected to linear constraints". Charts were generated for interior girders of prestressed concrete simple span bridges. Standard sections of the Canadian Prestressed Concrete Institute (CPCI) with different span lengths and girder spacings were evaluated.

2.1.1 Design Criteria and Assumptions

The charts were developed in accordance with the CAN3-S6-M78 standard (1978) for design of highway bridges published by the Canadian Standards (CSA). The preliminary designs were conducted for simple-span, interior CPCI girders under MS200-77 loading with a composite, cast-in-place concrete deck. Several parameters were considered including different span lengths and girder spacings; allowable stresses at transfer and service; physical limitations for the prestressing force eccentricity (i.e., maximum eccentricities); ultimate moment capacities; and steel ratio limits. Concrete compressive strengths of 5.08 ksi (35 MPa) and 4.35 ksi (30 MPa) were assumed at 28 days and transfer, respectively. Maximum allowable tensile stresses of $f_t = 3\sqrt{f'_c}$ in psi ($0.25\sqrt{f'_c}$ in MPa) and $f_t = 6\sqrt{f'_c}$ in psi ($0.5\sqrt{f'_c}$ in MPa) at service were assumed to develop the first and second set of charts, respectively. For a given CPCI girder section and spacing, the required prestressing force after losses was determined versus the girder span length. The preliminary design model was based on nine constraints, each representing a design criterion that was satisfied in the linear program. A summary of these constraints is given in Table 2.1.

Table 2.1. Constraints of the Fereig (1985) preliminary design model.

Constraint	Design Consideration
1-4	Allowable stresses at transfer and service at the top and bottom of the girder
5	Maximum eccentricity
6, 7	Ultimate flexural capacity
8, 9	Steel ratio limit

In the linear program developed in this study, the function that is maximized is $\frac{1}{P}$ where P is the prestressing force. Using the simplex method (a mathematical procedure to solve linear programming problems), the minimum prestressing force is determined versus the span length for different girder spacings. The prestressing force is obtained by solving the dual linear program (Philips et al. 1976) for the two controlling constraints. For example, a criteria designation of (1, 4) signifies that the stresses at transfer and service at the top and bottom of the girder, respectively, governs the design. Hence, by solving the linear programming model, the nine constraints mentioned earlier are satisfied and the two design controlling conditions are identified.

2.1.1.1 Dead and Live Loads

The self-weight of the CPCI 1200, 1400, 1900 and 2300 prestressed concrete I-girders were considered in computing the noncomposite dead load and the self-weight of a 7.5-in. (19 mm) thick reinforced concrete deck. The bridge was assumed to have two lanes and composite dead loads consisted of two traffic barriers with a total uniform load of 680 lb/ft (10 kN/m) distributed equally among the bridge girders, a future asphalt wearing surface with a 2.95 in. (75 mm) thickness, and 7.87 in. (200 mm) steel diaphragms. Live load was based on MS200-77 truck loading as given in the CSA standard (1978). Discussion of the live-load-distribution factors and the analytical procedure used to compute the live-load girder moments was not provided in the paper.

2.1.1.2 Deck Properties

As mentioned previously, a deck thickness of 7.5 in. (190 mm) was assumed to develop the preliminary design charts. The concrete compressive strength of the deck was taken as 4.35 ksi (30 MPa). A parametric study was conducted to study the influence of varying the deck thickness by ± 0.5 in. (12 mm) on the magnitude of the required prestressing force and it was found that the force changed by less than 1%.

2.1.1.3 Girder Properties and Allowable Stresses

Figure 2.1 and Table 2.2 show the dimensions and section properties of the CPCI prestressed girders that were investigated by the author.

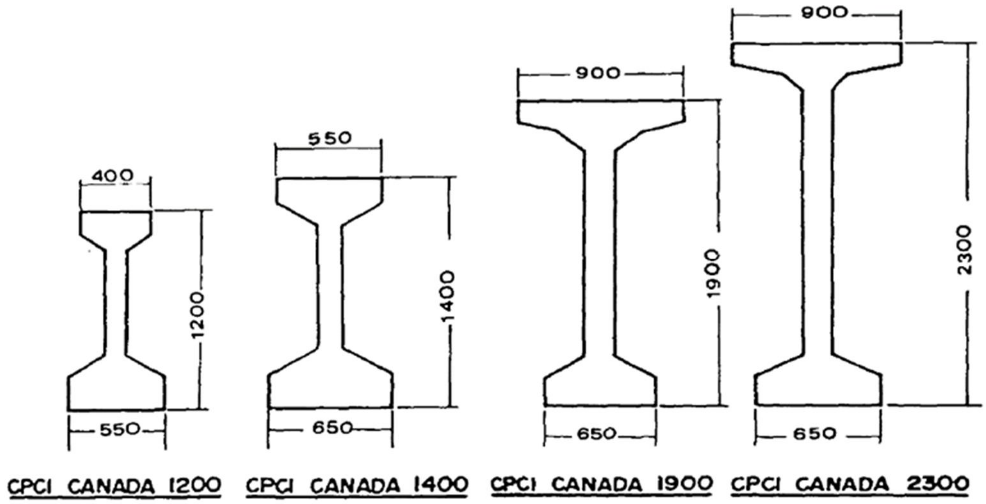

Figure 2.1. Dimensions of standard CPCI prestressed girders (Fereig 1985). Note: 1 ft = 304.8 mm.

Table 2.2. Section properties for standard CPCI prestressed girders (Fereig 1985).

Type	Section property Area ($mm^2 \times 10^3$)	$\overline{Y}$ (mm)	I ($mm^4 \times 10^6$)
1200	320	527	53 868
1400	413	635	102 580
1900	544	940	268 420
2300	604	1135	431 790

Note: 1 in. = 25.4 mm, 1 in.^{2} = 645.2 mm^2, 1 in.^{4} = 416231 mm^4.

2.1.1.4 Prestressing Strands and Spacing

This study determined the required prestressing force after losses and not the number of strands or strand layout. However, the number of strands and spacing can be easily estimated from the prestressing force by assuming a strand diameter.

2.1.2 Chart Description

In this paper, eight charts are presented for different girder span lengths and spacings. The first set of charts was developed for an allowable tensile concrete stress after prestress losses, $f_t = 3\sqrt{f'_c}$ psi ($0.25\sqrt{f'_c}$ MPa), and the second set for $f_t = 6\sqrt{f'_c}$ psi ($0.5\sqrt{f'_c}$ MPa). In each set, four CPCI prestressed concrete I-beams (CPCI 1200, 1400, 1900 and 2300) were studied. Figures 2.2 and 2.3 show the two charts for a CPCI 1200 girder.

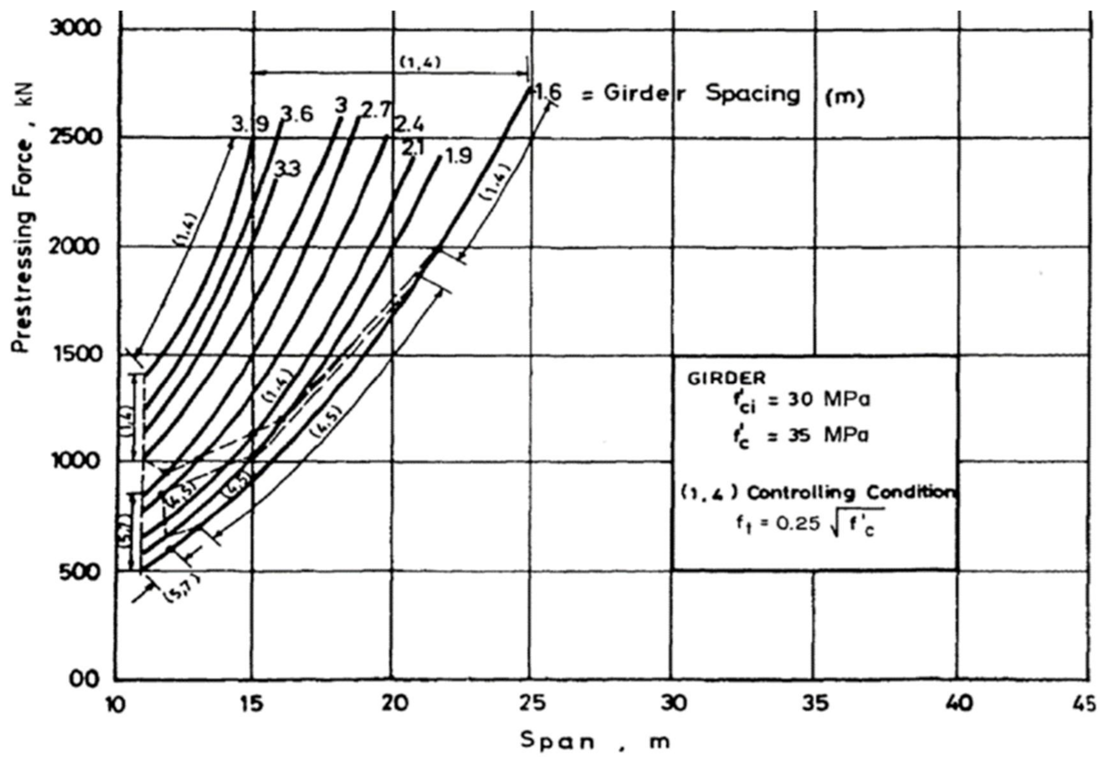

Figure 2.2. Preliminary design chart for CPCI 1200 girder based on $f_t = 3\sqrt{f'_c}$ psi ($0.25\sqrt{f'_c}$ MPa) (Fereig 1985).

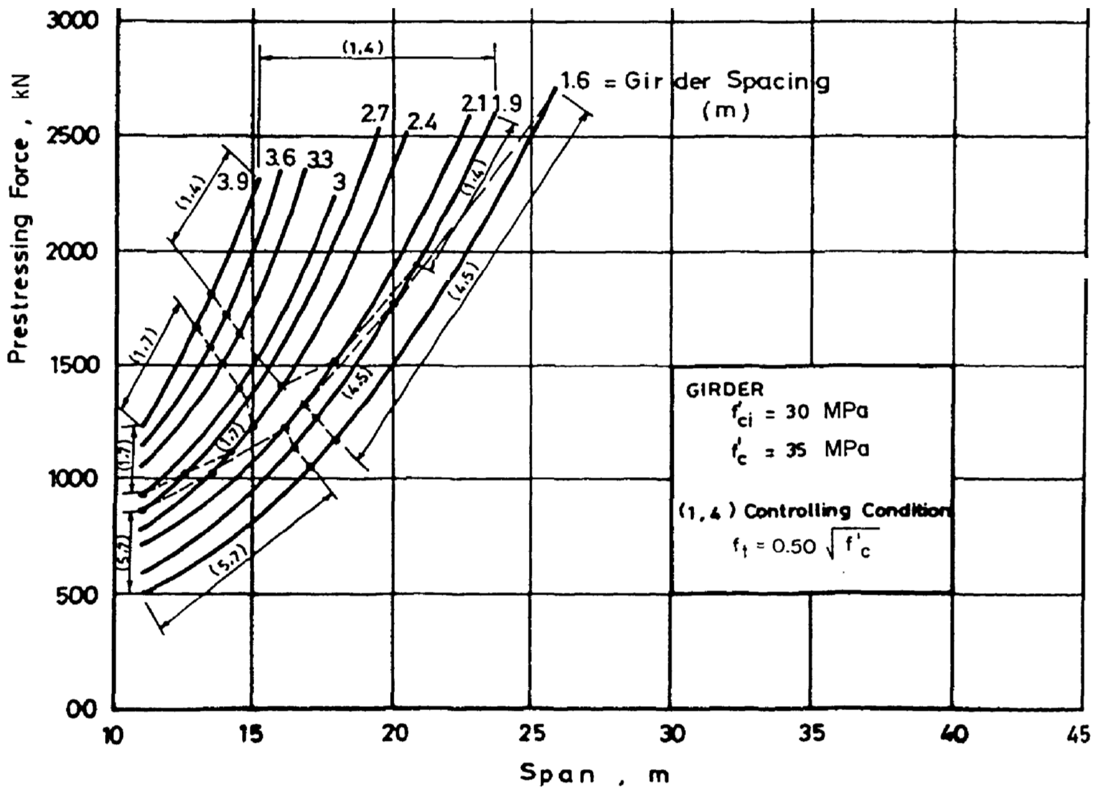

Figure 2.3. Preliminary design chart for CPCI 1200 girder based on $f_t = 6\sqrt{f'_c}$ psi ($0.5\sqrt{f'_c}$ MPa) (Fereig 1985).

The mathematical model was based on nine constraints that represent the conditions that govern the girder design as discussed earlier (see Table 2.1). The governing constraints are shown in parentheses in Figures 2.2 and 2.3 (e.g. (1, 4)). A parametric study was carried out based on the chart design parameters. The major conclusions were as follows:

- Variation in the required prestressing force was less than 1% when the 7.5 in. (190 mm) deck thickness was increased or decreased by 0.5 in. (12 mm);

- The required prestressing force is reduced by 3% on average when the girder concrete strength was increased from 5075 to 5800 psi (35 to 40 MPa);
- Varying the prestressing force after losses to the initial prestressing force ratio from 0.8 by 5% affected the required prestressing force by less than 2% on average; and
- The required prestressing force did not change when the effective prestressing force after losses to the ultimate strength of the prestressing steel ratio was varied from 0.52 to 0.58.

2.2 PCI (2003)

This section covers the preliminary design charts provided in the 2nd Edition of the PCI Bridge Design Manual (2003). The charts are hereafter referred to as the PCI-03 preliminary design charts and were developed to satisfy the strength and serviceability limit states of the AASHTO Standard Specifications (2002) for 28-day concrete compressive strengths of f'_c = 7,000 and 12,000 psi (48.3 and 82.8 MPa) with 0.5-in. (13 mm) and 0.6-in. (15 mm) diameter strands, respectively.

2.2.1 Design Criteria and Assumptions

In the next sections, a brief review of the assumptions used in the development of the PCI-03 preliminary design charts is provided.

2.2.1.1 Dead and Live Loads

The PCI-03 preliminary design charts were developed based on the live-load effects of an AASHTO HS25 truck which is 1.25 times the standard HS20 design truck. The live-load distribution factor for moment was taken as (S/5.5) under wheel loading where S is the girder spacing in feet. The AASHTO Standard Specifications (2002) employ this factor for interior I-beam systems under multiple lane loading. This formula does not include the effects of span length, slab thickness, and composite girder stiffness in computing the distribution factor as in the LRFD Bridge Design Specifications (AASHTO 2010). For example, in LRFD Article A4.6.2.2.2b, the moment distribution factor (mg) under axle loading for an interior girder under HL-93 and multiple design lanes is computed as:

$$mg = 0.075 + \left[\frac{S}{9.5}\right]^{0.6} \left[\frac{S}{L}\right]^{0.2} \left[\frac{K_g}{12Lt_s^3}\right]^{0.1} \tag{2.1}$$

where L = span length (ft); S = girder spacing (ft); and t_s = slab thickness (in). The longitudinal stiffness, K_g, is computed as:

$$K_g = n\left[I_g + Ae_g{}^2\right] \tag{2.2}$$

where n = modular ratio between beam and deck material; I_g = moment of inertia of beam (in^4); A = cross-sectional area of beam (in^2); and e_g = distance between the centers of gravity of the beam and deck (in.). The live load impact factor, I, used in developing the PCI-03 charts was computed as:

$$I = \frac{50}{L+125} \leq 30\% \qquad (2.3)$$

The girder, slab, and haunch weights were considered as non-composite dead loads. For composite dead load, a value of 40 psf (1915 N/m^2) superimposed dead load was assumed to account for the barriers and railing weight and a 2 in. (51 mm) concrete overlay was assumed for the future wearing surface.

2.2.1.2 Deck Properties

An 8-in. (203 mm) thick, concrete deck with a 28–day compressive strength of f'_c = 4000 psi (28 MPa) and a 0.5-in. (13 mm) haunch were assumed to develop the PCI-03 charts. It is important to note that using the same thickness for different girder spacings, may not be the most feasible at larger spacings because it would require a significant amount of steel reinforcement and therefore, the cost of the reinforced concrete deck would be excessive. In actuality, the deck thickness should increase with the beam spacing to achieve a more cost-effective design. For instance, the New Mexico Department of Transportation (NMDOT) uses a standard slab thickness that increases from 8 to 11 in. (191 to 279 mm) for beam spacings ranging from 6’-7” to 11’-10” (2.00 to 3.61 m) as specified in the NMDOT Bridge Procedures and Design Guide (2005).

2.2.1.3 Girder Properties and Allowable Stresses

The concrete compressive strengths for the girders were taken as f'_{ci} = 5500 psi (38 MPa) at release and f'_{c} = 7,000 psi (48.3 MPa) at service. In accordance with the AASHTO Standard Specifications (2002), the allowable tension limits were taken as $7.5\sqrt{f'_{ci}}$ psi ($0.63\sqrt{f'_{ci}}$ MPa) at release and $6\sqrt{f'_{c}}$ psi ($0.5\sqrt{f'_{c}}$ MPa) at service while the allowable compression limits were taken as $0.6f'_{ci}$ at release and $0.6f'_{c}$ at service. High-strength concretes ranging from 10,000 to 15,000 psi (69 to 103.4 MPa) have been recently used in the U.S bridge industry (PCI 2003 and 2011). Accordingly, the PCI-03 preliminary design charts for I-beams and bulb-tee girders also considered f'_{ci} = 8,000 psi (55.2 MPa) and f'_{c} = 12,000 psi (82.8 MPa). In the state of New Mexico, a 28-day compressive strength up to 9,500 psi (66 MPa) is currently the standard, but prestressing plants may provide up to 12,000 psi (82.8 MPa) using a 56-day curing period (NMDOT 2005). For the higher strength concrete, the allowable tensile stresses at release and service were assumed 33 percent higher than normal strength concrete (PCI 2003). That is, the allowable tensile stresses were set at $10\sqrt{f'_{ci}}$ psi ($0.83\sqrt{f'_{ci}}$ MPa) at release and $8\sqrt{f'_{c}}$ psi ($0.66\sqrt{f'_{ci}}$ MPa) at service, while the allowable compressive stresses were left the same (i.e., $0.6f'_{ci}$ and $0.6f'_{c}$).

2.2.1.4 Prestressing Strands and Spacing

For normal strength concrete, 0.5-in. (13 mm) diameter, seven-wire, 270 ksi (1.86 GPa) low relaxation strands were used. The center-to-center strand spacing was

2 in. (51 mm) and all strands were assumed to have an initial tension of 202.5 ksi (1.40 GPa) at release. End stresses can be controlled either by strand debonding (shielding) and/or harping but no information was provided as to which method was used in the PCI-03 charts. The PCI-03 charts for high strength concrete were developed using 0.6-in. (15 mm) diameter strands at 2 in. (51 mm) spacing. Note that a 0.6-in. (15 mm) diameter strand provides 40% more tensile capacity than a 0.5-in (13 mm) diameter strand.

Prestress losses were computed using the following equation from Article 9.16.2 of the AASHTO (2002) Standard Specifications:

$$Total\ Losses = SH + ES + CR_c + CR_s \quad \text{[STD Eq. 9-3]} \tag{2.4}$$

where SH = loss of prestress due to concrete shrinkage (ksi); ES = loss of prestress due to elastic shortening (ksi); CR_c = loss of prestress due to creep (ksi); and CR_s = loss of prestress due to relaxation of prestressing steel (ksi). A relative humidity value of RH equal to 70% was assumed. Loss of prestress due to concrete shrinkage was computed using the following equation:

$$SH = 17{,}000 - 150RH \quad \text{[STD Eq. 9-4]} \tag{2.5}$$

The elastic shortening prestress loss was computed as follows:

$$ES = \frac{E_s}{E_{ci}} f_{cir} \text{ [STD Eq. 9-6]} \tag{2.6}$$

where E_s = modulus of elasticity for pretensioning strands = 28,500 psi (196.5 MPa); f_{cir} = average concrete stress at the center of gravity of the pretensioning steel due to pretensioning force and dead load of girder immediately after transfer; and E_{ci} = modulus of elasticity for girder at release = $w_c{}^{1.5}(33)\sqrt{f'_{ci}}$ with w_c = unit weight of concrete = 150 pcf (2403 kg/m^3). Creep of concrete was estimated as follows:

$$CR_c = 12 f_{cir} - 7 f_{cds} \text{ [STD Eq. 9-9]} \tag{2.7}$$

where f_{cds} = concrete stress at the center of gravity of the pretensioning steel due to all dead loads except the dead load present at the time the pretensioning force is applied. Finally, loss of prestress due to relaxation of prestensioning steel was determined with the following equation:

$$CR_s = 5{,}000 - 0.10 ES - 0.05(SH + CR_c) \text{ [STD Eq. 9-10A]} \tag{2.8}$$

In the PCI-03 charts, it is not specified if the required number of strands for the resulting span lengths and girder spacings is feasible for local producers. Only a few producers in U.S. have a prestressing bed capable of handling 90 tensioned strands (PCI 2003). The number of prestressing strands was determined based only on flexural requirements. No attempt was made to determine the girder shear capacity, and deflections and camber limitations were not considered. Therefore, a complete check of the girder should be made in the final design stage.

2.2.2 Chart Description

The PCI-03 preliminary design charts were developed for different girder shapes including AASHTO box beams, AASHTO-PCI standard bulb-tees, AASHTO standard I-beams, double stemmed beams and voided slab beams. For each shape, different girder sizes were considered such as the PCI BT-54, BT-63, and BT-72 for bulb-tees. The first chart type for each shape provides the maximum span length versus girder spacing for the different girder sizes (see Figure 1.1). These particular charts are used in the early stages of design to select the girder size based on span length and girder spacing. The second chart type for each shape provides the number of prestressing strands required for a specified span length and beam spacing (see Figure 1.2). This dissertation focuses on both chart types mentioned above. The charts were developed only for simple span and interior girders based on the AASHTO Standard Specifications (2002). No distinction between service and strength was made in the charts as done by Fereig (1985). Figures 2.4 and 2.5 show the PCI-03 charts for the BT-72 girder section.

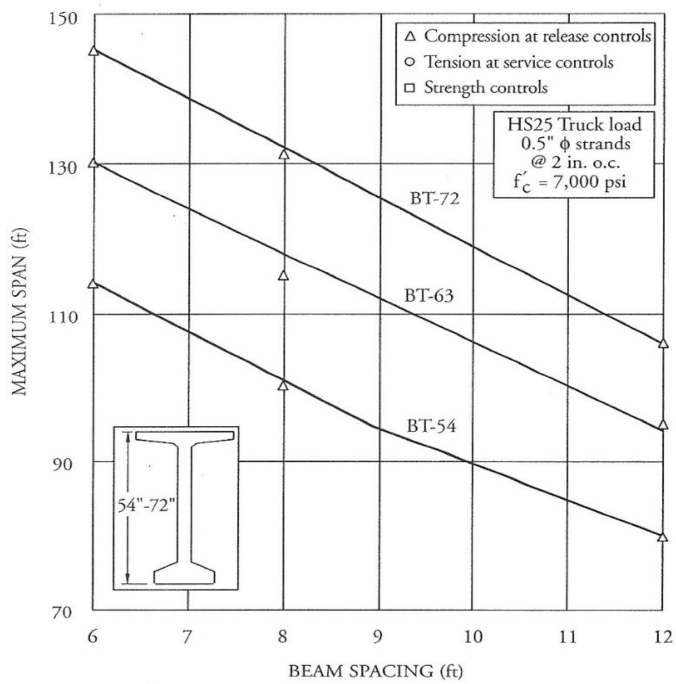

Figure 2.4. PCI-03 first chart type for BT-72 girder section (PCI 2003).

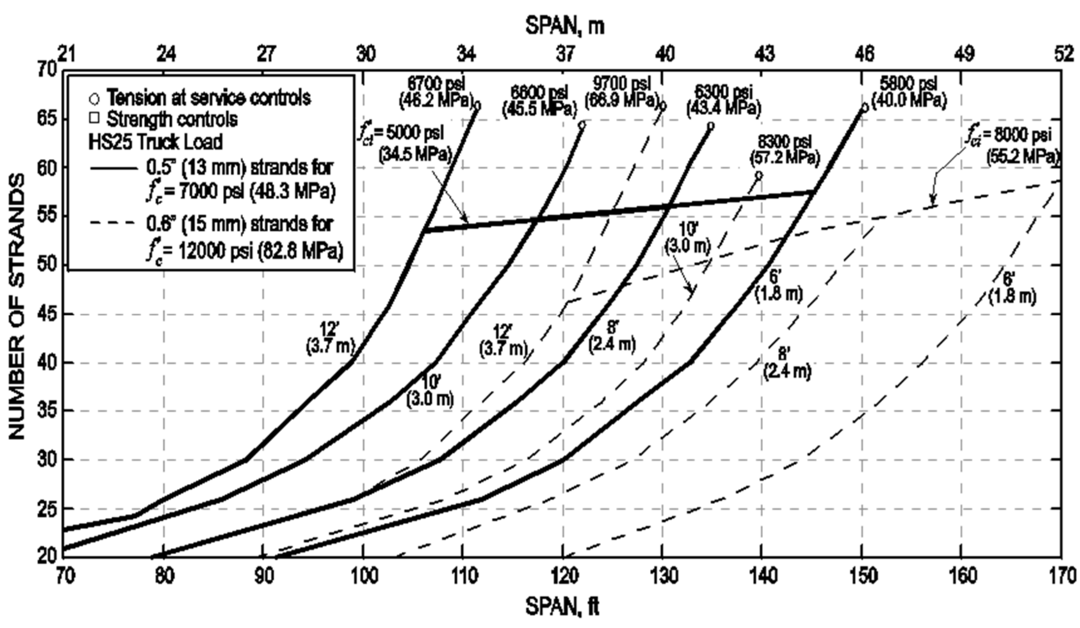

Figure 2.5. PCI-03 second chart type for BT-72 girder section (PCI 2003).

Information from the two sets of charts can be used to obtain a preliminary cost estimate of the superstructure based on the girder and deck requirements and also to determine if local producers are able to fabricate the girder. In addition, handling and transportation of the girder need to be considered in the preliminary bridge design and cost estimate. The girder size, spacing, and/or strand layout may have to be changed to satisfy the budget constraints and/or fabrication restrictions.

As shown in Figure 2.5, the maximum span length may be controlled by the strength or serviceability (tension at service) limit states or allowable stresses at release. An upper bound limit labeled with the specified concrete stress at release, f'_{ci}, indicates where the release stresses are the controlling criteria for the maximum span length. The curves are continued past this line and either tension at service or strength controls (usually tension at service), and the end point of each curve is labeled with the minimum required value of f'_{ci} (not to exceed f'_c). Table 2.3 shows a summary of the benefits and limitations of the PCI-03 preliminary design charts.

Table 2.3. Summary of benefits and limitations of PCI-03 preliminary design charts.

Benefits	Limitations
• Two concrete strengths of f'_c = 7 ksi (48.3 MPa) and f'_c = 12 ksi (82.8 MPa) • Two strands of 0.5 and 0.6-in. (13 and 15 mm) diameter, seven-wire, 270 ksi (1.86 GPa) low relaxation strands • Different girder shapes and sizes	• AASHTO Standard Specifications (2002) • Simple span only • Interior girders only • No distinction between service and strength in charts

2.3 Hanna et al. (2010)

This report provides preliminary design charts for Nebraska University (NU) I-girders based on the AASHTO LRFD Bridge Specifications (2007) and the Nebraska Department of Roads (NDOR) Bridge Operations, Policies, and Procedures (NDOR 2009). Design charts were developed for different girder sizes (from NU900 to NU2000), girder spacings (6 to 12 ft) (1.8 to 3.7 m), and concrete compressive strengths (8 to 15 ksi) (55.2 to 103.4 MPa) using 0.6 and 0.7-in. (15 and 18 mm) diameter strands. The number of prestressing strands was varied from 10 to 60. NU I-girder graphs were developed to cover three sets of configurations including simple span, two-span continuous, and three-span continuous bridge girders. Two types of charts for each set were developed: summary and detailed charts. Summary charts provide the maximum span length for different NU I-girder sections given the concrete strength and girder spacing. Detailed charts provide the required number of strands for a specific NU girder section and concrete strength given the span length and girder spacing. Examples of these two types of charts were described previously in Chapter 1 (see Figures 1.1 and 1.2).

2.3.1 Design Criteria and Assumptions

As mentioned earlier, the design charts were developed based on the AASHTO LRFD Specifications (2007) and the NDOR Manual (2009) for interior girders. Simple span, two-span continuous (with equal spans), and three-span continuous with a 1.25:1 interior to exterior span ratio were considered to develop the design charts. Girder spacings of 6, 8, 10, and 12 ft (1.8, 2.4, 3.0, and 3.7 m) were assumed, similar to those adopted by the PCI Bridge Design Manuals (2003, 2011). Design criteria includes Service III, Strength I (non-composite and composite), release stresses (strength and working stress design methods), negative moment fatigue, and crack control limit states. Nebraska allows the designer to use the strength design approach and/or the working stress method for evaluating the concrete behavior at release and to choose the more feasible option. When the strength design approach is used, some restrictions imposed by the working stress method are eliminated and longer span lengths can be achieved. That is, the release limit state ceases to govern due to the elimination of limits imposed by the working stress method and as a result, Service III controls the span length of the girder as shown in Figure 2.10. For instance, the working stress method limits the top tensile stresses at the ends of the girder to $0.196\sqrt{f'_{ci}}$ in ksi ($0.5\sqrt{f'_{ci}}$ in MPa). If the strength design method is used, this restriction is ignored and consequently the prestressing strands can be released at a lower concrete strength. This reduces the need and the costs associated with accelerated curing and debonding and/or draping of strands at the ends of the girders. According to this paper, the use of the strength design approach at release would allow precast, prestressed girders to be more efficient.

A threaded rod (TR) continuity system was considered to develop design charts for two-and three-span continuous girders. Conventional systems are only continuous for live load whereas the TR system also allows the deck weight to be resisted through continuity. Comparisons of the strength design approach with the working stress method and TR continuity with the conventional system are presented in Section

2.3.2.3. In the next sections, a brief review of the assumptions used in the development of the NU preliminary design charts is provided.

2.3.1.1 Dead and Live Loads

The self-weight of the NU I-girder was computed based on the cross section shown in Figure 2.6. Table 2.4 shows the NU I-girder cross section properties.

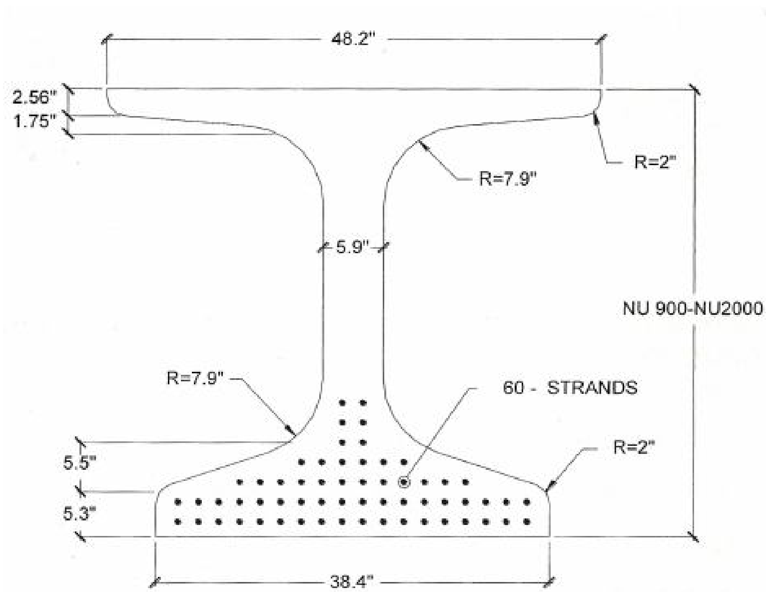

Figure 2.6. NU I-girder cross section with strand template (Hanna et al. 2010).
Note: 1 m = 3.3 ft

Table 2.4. NU I-girder section properties (Hanna et al. 2010).

Section	Height in (mm)	Web Width in (mm)	Top Flange Width in (mm)	Bottom Flange Width in (mm)	A in^2 (mm^2)	Y_b in (mm)	I in^2 ($mm^4 * 10^6$)	W_t Kips/ft KN/m
NU 900	35.4 (900)	5.9 (150)	48.2 (1225)	38.4 (975)	648.1 (418,111)	16.1 (410)	110,262 (45,895)	0.680 (9.85)
NU 1100	43.3 (1100)	5.9 (150)	48.2 (1225)	38.4 (975)	694.6 (448,111)	19.6 (497)	182,279 (75,870)	0.724 (10.56)
NU 1350	53.1 (1350)	5.9 (150)	48.2 (1225)	38.4 (975)	752.7 (485,610)	24.0 (608)	302,334 (126,841)	0.785 (11.44)
NU 1600	63.0 (1600)	5.9 (150)	48.2 (1225)	38.4 (975)	810.8 (523,111)	28.4 (722)	458,482 (190,835)	0.840 (12.33)
NU 1800	70.9 (1800)	5.9 (150)	48.2 (1225)	38.4 (975)	857.3 (553,111)	32.0 (814)	611,328 (254,454)	0.894 (13.03)
NU 2000	78.7 (2000)	5.9 (150)	48.2 (1225)	38.4 (975)	903.8 (583,111)	35.7 (906)	790,592 (329,069)	0.942 (13.74)

Normal weight concrete with a density of 150 pcf (2403 kg/m^3) was used to compute the girder, deck, and haunch weights. The diaphragm weight was assumed as 0.25 k/ft (372 kg/m). A 2-in. (51 mm) asphalt overlay was used to account for the future wearing surface. The dead weight of ten 1 3/8 in. Ø x 50 ft (35 mm Ø x 15 m) threaded rods placed 0.75-in. (19 mm) above the girder top flange in the negative moment sections was used for continuous girders. The HL-93 loading was used to compute the design vehicular live load for interior girders.

2.3.1.2 Deck Properties

Concrete deck thicknesses of 7.5 in. (191 mm) and 8.0 in. (203 mm) were assumed for girder spacings of 6 to 10 ft (1.8 to 3.0 m) and 12 ft (3.7 m), respectively. For girder concrete strengths of f'_c = 8 and 10 ksi (55.2 and 69.0 MPa) and 12 and 15 ksi (82.7 and 103.4 MPa), deck concrete strengths of f'_c = 4 and 5 ksi (27.6 and 34.5

MPa) were assumed, respectively. A 48-in. (1.2 m) wide concrete haunch with a thickness of 1-in. (25.4 mm) was used for simple spans. For continuous spans, haunch thicknesses of 2.5 in. and 3.5 in. (63.5 mm and 89 mm) were used in the positive and negative moment regions, respectively.

2.3.1.3 Girder Properties and Allowable Stresses

The girder section properties are given in Table 2.4. Design charts were developed using 28-day concrete compressive strengths of f'_c = 8, 10, 12, and 15 ksi (55.2, 68.9, 82.7, and 103.4 MPa). Allowable tensile stresses for the concrete at service and release were not explicitly specified in the paper nor the allowable compression stresses at service. Only the allowable compression stresses for the concrete at release were provided as $0.6f'_{ci}$. Concrete strength at release was specified as $0.75f'_c$.

2.3.1.4 Prestressing Strands and Spacing

The strand type was specified as Grade 270, low-relaxation with a modulus of elasticity of E_s = 28,500 ksi (193 kN/mm^2). The yield strength and jacking stress were given as $0.90f_{pu}$ and $0.75f_{pu}$, respectively, where f_{pu} is the tensile strength of the strand. A 0.6-in. (15 mm) diameter strand was used for concrete strengths of f'_c = 8, 10 and 12 ksi (55.2, 68.9, and 82.7 MPa) and a 0.7-in. (18 mm) diameter strand for concrete strengths of f'_c = 12 and 15 ksi (82.7 and 103.4 MPa). The strands were arranged as follows:

- 60 strands – 7 rows (18, 18, 12, 6, 2, 2) @ 2 x 2-in. (25.4 x 25.4 mm) grid spacing;
- straight strands, two point draping allowed at 0.4L; and
- debonding allowed with a maximum of 40% of any row and 25% of total.

2.3.2 Chart Description

As mentioned earlier, two type of charts were developed (summary and detailed). To describe the use of these charts, one example of each is given in the following sub-sections. Note that the charts provide the governing limit state for the design, allowing parameters to be modified to fit local or general design requirements.

2.3.2.1 Summary Charts

This chart type provides the maximum span length when the girder section, concrete strength, and girder spacing are given. These charts were developed for different girder sections from NU 900 to NU 2000 at girder spacings of 6, 8 10 and 12 ft (1.8, 2.4, 3.0 and 3.7 m). Summary charts are useful in the early stages of design because they provide the required girder size and spacing for a given span length and concrete strength. Figure 2.7 shows this type of chart.

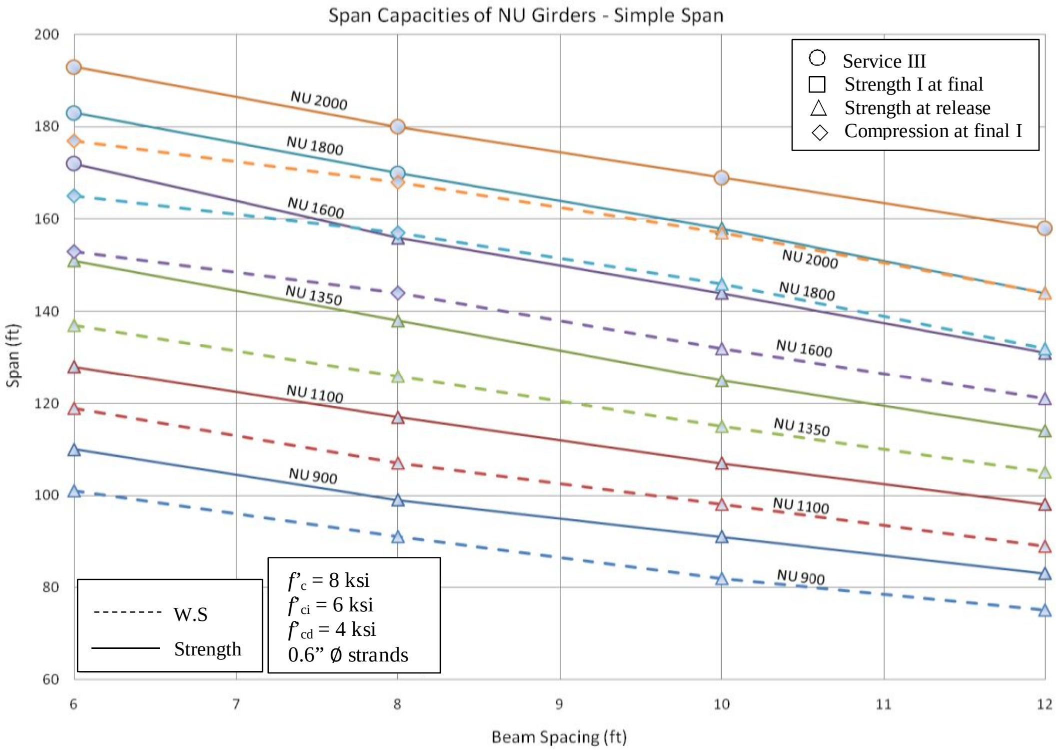

Figure 2.7. Example of summary chart (Hanna et al. 2010). Note: 1 m = 3.3 ft, 1 MPa = 145 psi.

2.3.2.2 Detailed Charts

Detailed charts provide the number of strands given the span length and the girder spacing for a particular girder section and concrete strength. Combinations of the different girder sizes, concrete strengths, and spacings mentioned earlier were used to develop 30 detailed charts. Figure 2.8 shows an example of a detailed chart.

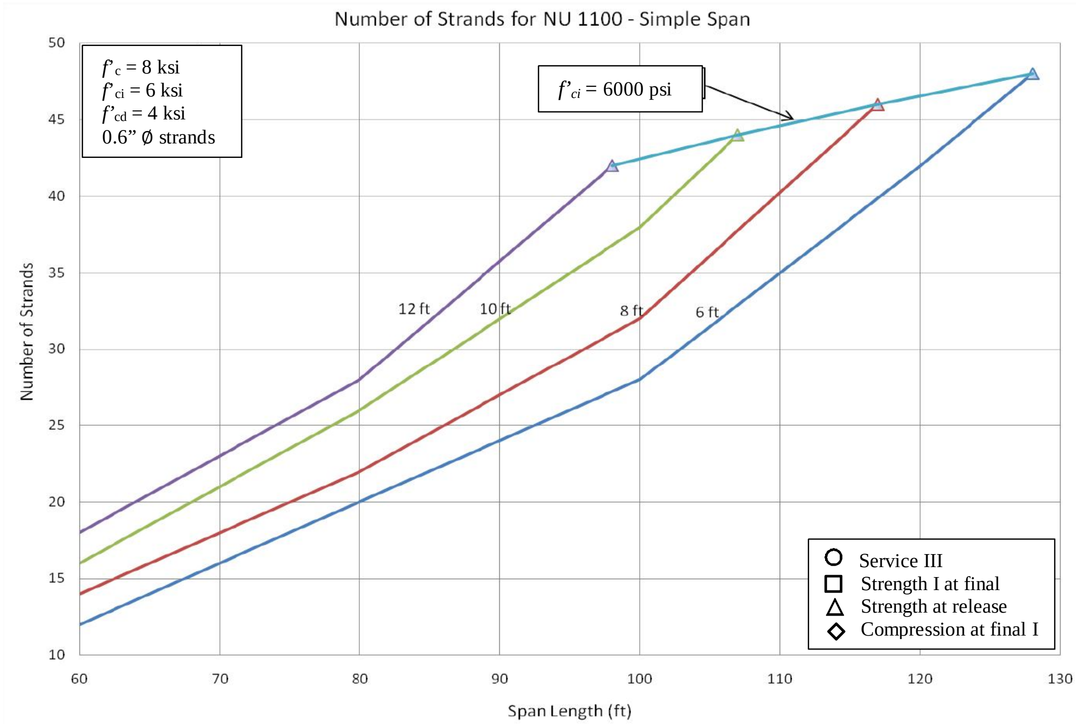

Figure 2.8. Example of detailed chart (Hanna et al. 2010). Note: 1 m = 3.3 ft, 1 MPa = 145 psi.

2.3.2.3 Effect of Design Parameters

In this study, the most important parameters that influenced the design of the NU I-girders were girder type, prestressing strand diameter, concrete strength at release, concrete strength at service, and continuity for multi-span bridges. For simplicity, attention was given to two parameters (concrete strength at release and continuity for multi-span bridges) to describe the design charts in the following sections. As discussed earlier, the strength design approach for concrete strength at release ignores some design requirements imposed by the working stress method, thus resulting in longer span lengths. Figure 2.9 shows a summary chart comparing the strength design approach with the working stress method.

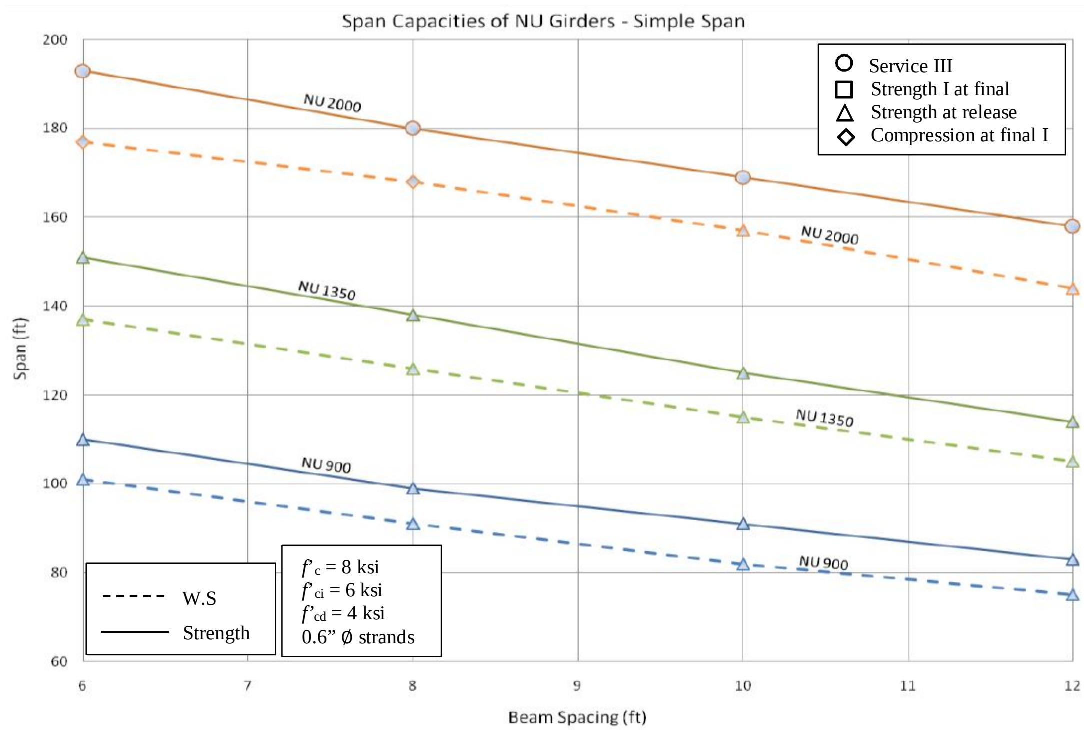

Figure 2.9. Summary chart comparing strength design approach with working stress method (Hanna et al. 2010). Note: 1 m = 3.3 ft, 1 MPa = 145 psi.

It can be estimated from Figure 2.9 that by using the strength design approach, 10% longer span lengths can be achieved. Note that the concrete strength at release is the design limit state that usually controls the maximum span length. The detailed chart given in Figure 2.10 further shows that the use of the strength design approach permits significantly longer span lengths due to the elimination of some restrictions imposed by the working stress method as discussed in Section 2.3.1

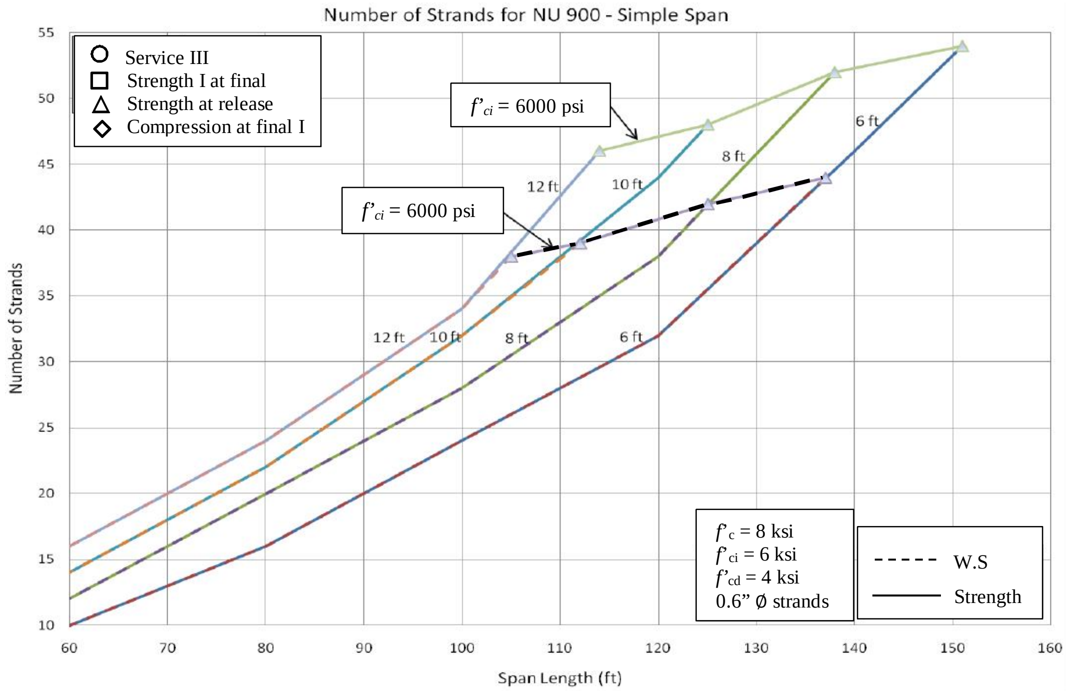

Figure 2.10. Detailed chart comparing strength design method and working stress method (Hanna et al. 2010). Note: 1 m = 3.3 ft, 1 MPa = 145 psi.

The TR continuity system has many advantages versus the conventional system, including but not limited to, longer span lengths, fewer girder lines, and shallower girder depths. One of the major advantages of the TR continuity system is that it makes precast concrete girders continuous for about two-thirds of the total applied load whereas using the conventional system, girders are only continuous mainly for live load. Post-tensioning is not necessary when a TR continuity system is used. Figure 2.11 shows a summary chart comparing the TR and conventional continuity systems.

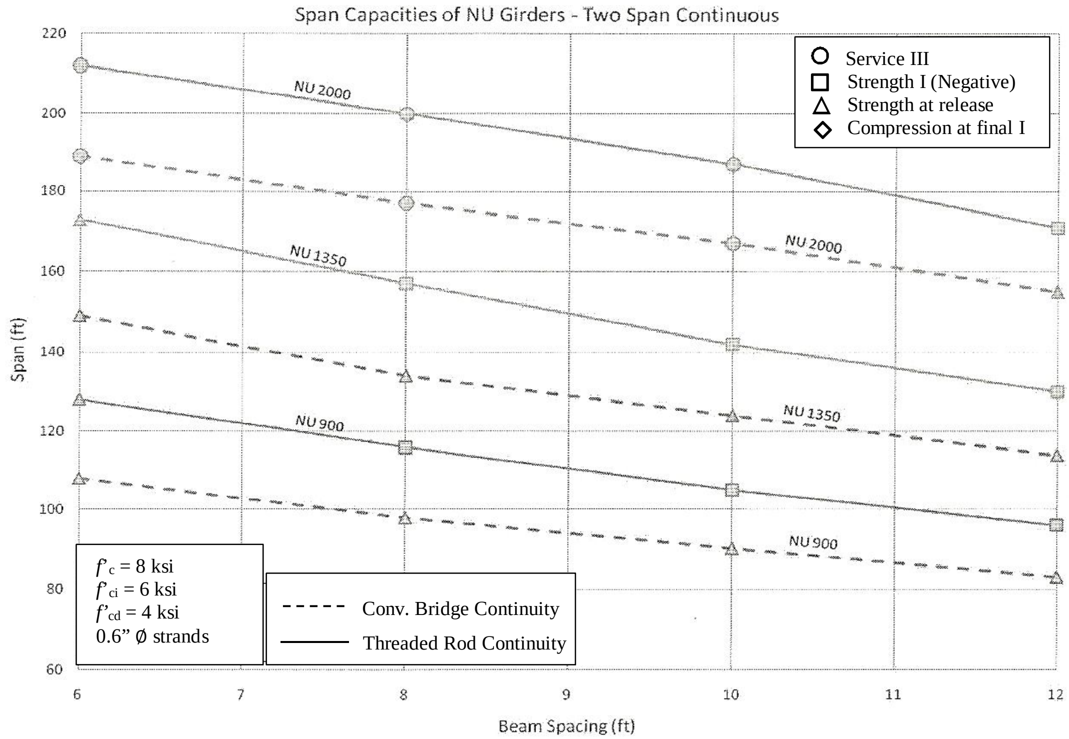

Figure 2.11. Summary chart comparing TR and conventional continuity systems (Hanna et al. 2010). Note: 1 m = 3.3 ft, 1 MPa = 145 psi.

From Figure 2.11, a difference of 10 to 18% in span length is shown for the NU I-girders. For a girder spacing of 6 ft (1.8 m), the TR continuity system designs were mostly governed by the strength at release limit state. However, the Strength I limit state in the negative moment regions governed the majority of the TR designs for wider girder spacings. Larger span lengths than those shown in Figure 2.11 can be attained if the negative moment capacity is increased by adding more threaded rods or increasing the top flange, web, or haunch thickness.

2.4 PCI (2011)

This section covers the preliminary design charts provided in the 3rd Edition of PCI Bridge Design Manual (2011) which were developed to satisfy the strength and serviceability limit states of the AASHTO LRFD Bridge Design Specifications (2010). These charts are hereafter referred to as the PCI-11 preliminary design charts and provide a starting point for girders fabricated using a 28-day concrete compressive strength of f'_c = 8,000 (55.2 MPa) with 0.6-in. (15 mm) diameter strand.

2.4.1 Design Criteria and Assumptions

In the next sections, a brief review of the assumptions used to develop the PCI-11 preliminary design charts is provided.

2.4.1.1 Dead and Live Loads

The PCI-11 preliminary design charts were developed for interior and exterior girders based on the AASHTO LRFD Bridge Design Specifications (2010) using the HL-93 live load for a simple span bridge. This loading consists of a combination of the design truck or design tandem and the design lane load. The HS20 vehicle is the design truck and was also used previously in the AASHTO Standard Specifications (2002). The design tandem consists of a pair of 25.0 kip axles spaced 4.0 ft (1.2 m) apart. The transverse spacing of wheels is 6.0 ft (1.8 m) for both the design truck and design tandem. The lane load consists of a uniform load of 0.64 kip/ft (953.3 kg/m) which is distributed transversely over a 10 ft (3.0 m) width.

The moment live-load distribution factor for interior I-beams is given by Equation 2.1 shown previously. The distribution factor for exterior I-beams without midspan diaphragms for two or more design lanes loaded is given in LRFD Article 4.6.2.2 by the following equation:

$$g = \ e g_{interior} \tag{2.9}$$

where:

$$e = 0.77 + \left(\frac{d_e}{9.1}\right) \geq 1.0 \tag{2.10}$$

and d_e = distance from the center of the exterior beam and the interior edge of the curb or traffic barrier (ft). If rigid midspan diaphragms are provided, the distribution factor for exterior girders based on rigid body motion also applies as given by the following equation (AASHTO 2010):

$$g \geq R = \frac{N_L}{N_b} + \frac{X_{ext} \sum_1^{N_L} e}{\sum_1^{N_b} x^2} \text{ [LRFD Eq. C4.6.2.2.2d-1]} \tag{2.11}$$

where R = reaction on exterior beam in terms of lanes; N_L = number of loaded lanes under consideration; N_b = number of beams; e = eccentricity of a lane from the center of gravity of the pattern of beams (ft); x = horizontal distance from the center of gravity of the pattern of beams to each beam (ft); and x_{ext}= horizontal distance from the center of gravity of the pattern of beams to the exterior beam (ft). Even though different live load distribution factors are used for interior and exterior girders, and different girder section sizes can be determined, LRFD Article 2.5.2.7 requires that the flexural capacity of the exterior girder be at least that of the interior girder.

The live load impact factor, I, used in developing the PCI-11 preliminary design charts based on LRFD is 33% regardless of the girder length (AASHTO 2010). Recall that the AASHTO Standard Specifications (2002) determines the impact factor considering the span length of the girder according to Equation 2.3 given earlier.

The girder, slab, and haunch weights were considered as non-composite dead loads. For composite dead load, values of 0.5 kip/ft (744.8 kg/m) and 0.035 ksf (171 kg/m^2) were assumed to account for the barriers and future wearing surface, respectively. In PCI-03, these composite dead loads were assumed as 15 psf (73.24 kg/m^2) times the girder spacing and 0.025 ksf (122 kg/m^2), respectively.

2.4.1.2 Deck Properties

According to Table 6.5.2.3-1 of the PCI (2011) Manual, a concrete deck thickness of 8 in. (203 mm) was used for 6, 8 and 10 ft (1.8 m, 2.4 m, 3.0 m and 3.7 m) girder spacings and 9 in. (229 mm) for a 12 ft (3.7 m) girder spacing for bulb-tee sections. A ½-in. (13 mm) deduction was made to determine the structural properties and a 28–day concrete compressive strength of f'_c = 4000 psi (28 MPa) was assumed.

2.4.1.3 Girder Properties and Allowable Stresses

The concrete compressive strengths for the girders were assumed as f'_c = 8.0 ksi (55.2 MPa) at service and f'_{ci} = 6.8 ksi (46.9 MPa) at release. In accordance with the AASHTO LRFD Bridge Design Specifications (2010), the allowable tension limits were $7.5\sqrt{f'_{ci}}$ psi ($0.63\sqrt{f'_{ci}}$ MPa) at release and $6\sqrt{f'_c}$ psi ($0.5\sqrt{f'_c}$ MPa) at service while the allowable compression limits were $0.6f'_{ci}$ at release and $0.6f'_c$ at service. Note that the allowable stresses are the same in the AASHTO Standard (2002) and LRFD (2010) Specifications.

2.4.1.4 Prestressing Strands and Spacing

The PCI-11 preliminary design charts were developed using 0.6-in. (13 mm) diameter, seven-wire, 270 ksi (1.86 GPa) low relaxation strands. The center-to-center strand spacing was 2 in. (51 mm) and all strands were assumed to have an initial tension of 202.5 ksi (1.40 GPa) before release. No information was provided as to which method (strand debonding (shielding) and/or harping) was used in the PCI-11 charts to control end stresses. Relative humidity was assumed as 70%. The AASHTO approximate method (given in LRFD Article 5.9.5.3) for long-term losses was used to compute prestress losses in lieu of the detailed time-dependent method (given in LRFD Article 5.9.5.4).

2.4.2 Chart Description

Similar to the PCI-03 preliminary design charts, the PCI-11 charts were developed for different girder shapes that are commonly used including AASHTO box beams, AASHTO-PCI standard bulb-tees, and AASHTO standard I-beams. In addition, the PCI (2011) Manual presents some new girder shapes including, U-beams, non-composite deck bulb-tees, and double-tee stemmed beams known as NEXT beams. Preliminary design charts are provided for two NEXT beam types, Type D and F. The thick top flange (8-in. (203 mm)) of Type D can be used as the structural slab for the bridge. A 3-in. (76 mm) thick asphalt overlay is considered as a future wearing surface in the preliminary design charts. The Type F has a top flange thickness of 4 in. (102 mm) and can be used as a stay-in-place form for an 8-in. (203 mm) thick composite cast-in-place slab. A future wearing surface of asphalt is also considered in the preliminary design charts; however the thickness is not specified. Figure 1.3 given in Chapter 1 shows the Type D and F shapes.

Similar to PCI (2003), two types of preliminary design charts were developed in PCI (2011). The maximum span length versus girder spacing are provided in the first chart type and the second chart type provides the number of prestressing strands versus span length and beam spacing. The PCI-11 charts were developed only for simple spans and interior and exterior girders using a girder concrete strength of f'_c = 8,000 psi (55.2 MPa) and 0.6-in. (15 mm) diameter strands based on the AASHTO LRFD Bridge Design Specifications (2010). No distinction between service and strength was made in the charts. However, distinctions were made in tables. Figures 2.12 and 2.13 show the PCI-11 preliminary design charts for the BT-72 girder section.

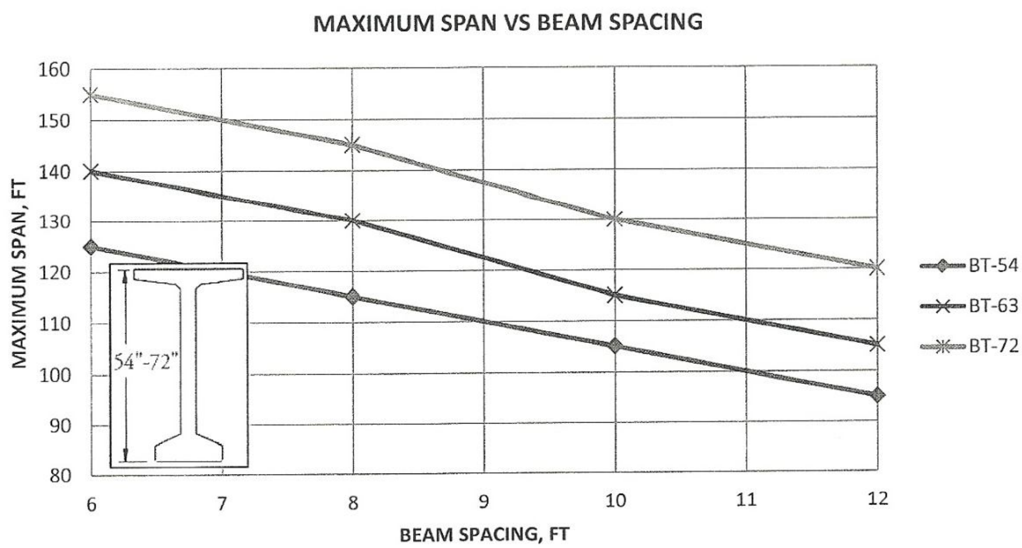

Figure 2.12. PCI-11 maximum span versus beam spacing for BT-72 girder section (PCI 2011).

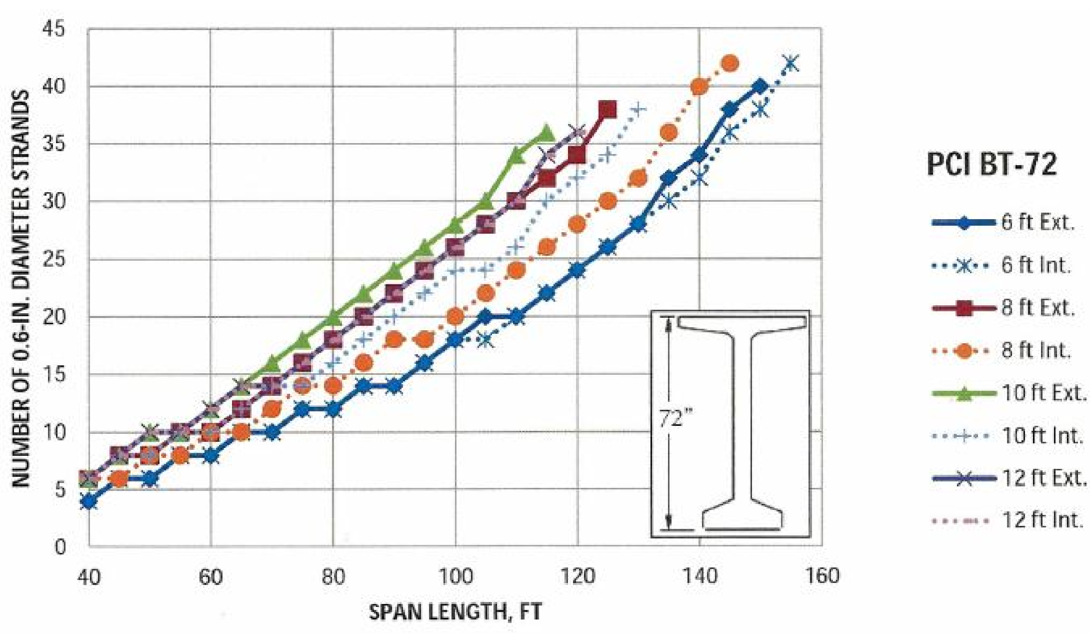

Figure 2.13. PCI-11 number of strands versus span length for BT-72 girder section (PCI 2011).

Except for U-beams (see Figure 1.3 in Chapter 1), girder spacings of 6, 8, 10 and 12 ft (1.8, 2.4, 3 and 3.7 m) were assumed and represent the range used in today's practice. For U-beams, a girder spacing range from 10 to 18 ft (3 to 5.5 m) was selected.

Due to the effect of the different assumptions that vary state from state on the exterior girder design including the actual overhang distance, railing weight, method of load distribution, and other considerations, the PCI-11 preliminary design charts are presented for a typical first interior beam. The first interior beam is more influenced by the assumptions mentioned above. The interior beam charts should be used with precaution along those of the exterior beam to determine the governing member. Table 2.5 shows a summary of the benefits and limitations of the PCI-11 preliminary design charts.

Table 2.5. Summary of benefits and limitations of PCI-11 preliminary design charts.

Benefits	Limitations
• AASHTO LRFD Bridge Design Specifications (2010) • Interior and exterior girders • New girder shapes including the NEXT beam, non-composite deck bulb-tee and U-beams (see Figure 1.3 in Chapter 1)	• Single concrete strength of f'_c = 8,000 psi (55.2 MPa) • Single strand configuration of 0.6-in. (15 mm) diameter, seven-wire, 270 ksi (1.86 GPa) low relaxation strand • Simple span only • No distinction between service and strength in charts

2.5 Jeon et al. (2012)

This paper presents a graphical approach to evaluate the effects of different parameters on the span capability of a bridge girder. The evaluated parameters include: concrete compressive strength, light weight aggregate concrete, prestressing tendons or sheaths (ducts), cross section shape, span continuity, multistage prestressing, decked prestressed concrete girders (i.e., girder and deck are cast simultaneously) and spliced-girder systems. Based on the service and release limit states for fully prestressed components (AASHTO 2010), stress equations were developed and graphed to show the relationship between the number of prestressing tendons and the girder span length. The effects of the parameters given above on the span capability are evaluated using the proposed graphical approach on a prestressed concrete bridge with five girders.

2.5.1 Design Criteria and Assumptions

In the next sections, a review of the assumptions made by Jeon et al. (2012) to develop the design graphs used to evaluate the span ranges of prestressed concrete bridges is provided.

2.5.1.1 Dead and Live Loads

Dead and live loads were determined based on the AASHTO LRFD Bridge Design Specifications (2010). A cross-section of the prestressed concrete girder bridge that was evaluated with five bulb-tee girders is shown in Figure 2.14.

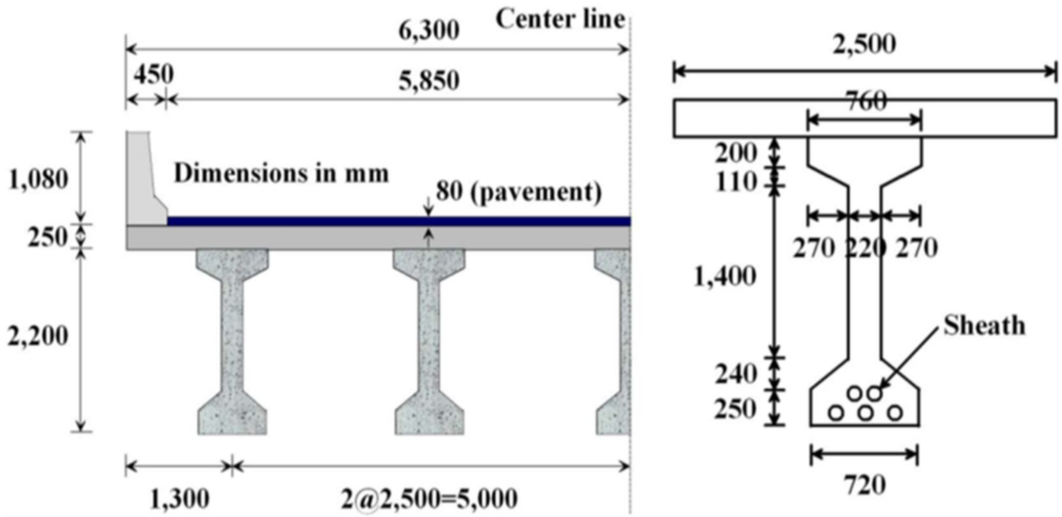

Figure 2.14. Cross-section of the prestressed concrete girder bridge evaluated by Jeon et al. (2012). Note: 1 m = 3.3 ft.

Two cases were considered to evaluate the effect of light weight concrete on the design of an interior girder: (1) light weight concrete used only for the deck and (2) light weight concrete used for both the deck and the girder. Based on Liles and Holland (2010) and Melby et al. (1996), the densities of light weight concrete were taken as 120 pcf (18,829 N/m^3) for the deck and 125 pcf (19,613 N/m^3) for the girder. The density of normal weight concrete was taken as 156 pcf (24,517 N/m^3).

The design live load used was the HL-93. Cross beams with a 0.98 ft (0.3 m) thickness were assumed at the middle of the span, quarter points, and at the supports. A number of finite element analyses of the entire bridge system were performed using ABAQUS to obtain the equivalent distributed live load, w_l, and the equivalent distributed dead load of cross beams, w_c, on each girder. From these analyses, it was found that w_l and w_c on each girder did not exceed 1.37 and 0.137 kip/ft (20 and 2 kN/m), respectively.

2.5.1.2 Deck Properties

A 9.84-in. (250 mm) thick, cast-in-place concrete deck with a 0.5-in. (13 mm) haunch was used and a 8.20 ft (2.5 m) girder spacing. Based on the bridge geometry given in Figure 2.8 and the AASHTO LRFD Bridge Design Specifications (2010), the effective flange width was determined as 8.20 ft (2.5 m). Concrete compressive strengths of f'_c = 3915 psi (27 MPa) for the deck and 5800 psi (40 MPa) for the girder were used as the baseline values in this research. For decked prestressed concrete girders, the concrete strengths of the girder and deck were equal since the two components are monolithic.

2.5.1.3 Girder Properties and Allowable Stresses

Three 28-day concrete compressive strengths for the girders were considered including f'_c = 5.8, 8.7, and 11.6 ksi (40, 60 and 80 MPa). The concrete strength at release was taken as 80% of the 28-day strength. Comparison of the baseline strength of 5.8 ksi (40 MPa) with the higher strengths of 8.7 and 11.6 ksi (60 and 80 MPa) showed that the span lengths were 26 % and 86 % larger, respectively (discussed later). The allowable tensile stresses for the concrete were taken as $3\sqrt{f'_{ci}}$ ksi < 0.2 ksi

($0.25\sqrt{f'_{ci}}$ < 1.4 MPa) at release and $6\sqrt{f'_c}$ ksi (0.5 $\sqrt{f'_{ci}}$ MPa) at service while the allowable compression stresses were taken as $0.6f'_{ci}$ at release and $0.6f'_c$ at service.

2.5.1.4 Prestressing Strands and Spacing

Each sheath was assumed to house twelve 0.5-in. (12.7 mm) strands. Thus, the total area of the strands included in one sheath is A_{ps} = 1.84 in.^{2} (1185 mm^2). The tensile strength of the strand was specified as f_{pu} = 270 ksi (1860 MPa). The average initial, f_{pi}, and effective prestress, f_{pe}, were assumed as 167 ksi (f_{pi} = $0.62f_{pu}$) and 142 ksi (f_{pe} = $0.53f_{pu}$ = $0.85f_{pi}$) (1150 and 980 MPa), respectively. Control of the end stresses, relative humidity values, and methods used to compute prestress losses were not specified in this study.

2.5.2 Chart Description

The graphical approach given in this paper is based on the release and service limit states of AASHTO (2010). Two types of charts are presented as follows: primary prestressing (includes only initial prestressing applied when the girder is fabricated) and multistage prestressing (includes primary and secondary prestressing applied after the deck has been cast and has hardened).

2.5.2.1 Primary Prestressing

The first type of chart corresponds to primary prestressing only and the chart development is as follows. Four stress equations (Equations 2.12 to 2.15 shown in the appendix) are applied, two at the top and bottom fibers at release and service respectively. Substituting the allowable concrete stresses into these expressions gives four curves that represent the relationship between the number of prestressing tendons and the girder span length. Superimposing these curves in a plot gives the feasible design domain represented by the shaded area shown in Figure 2.15.

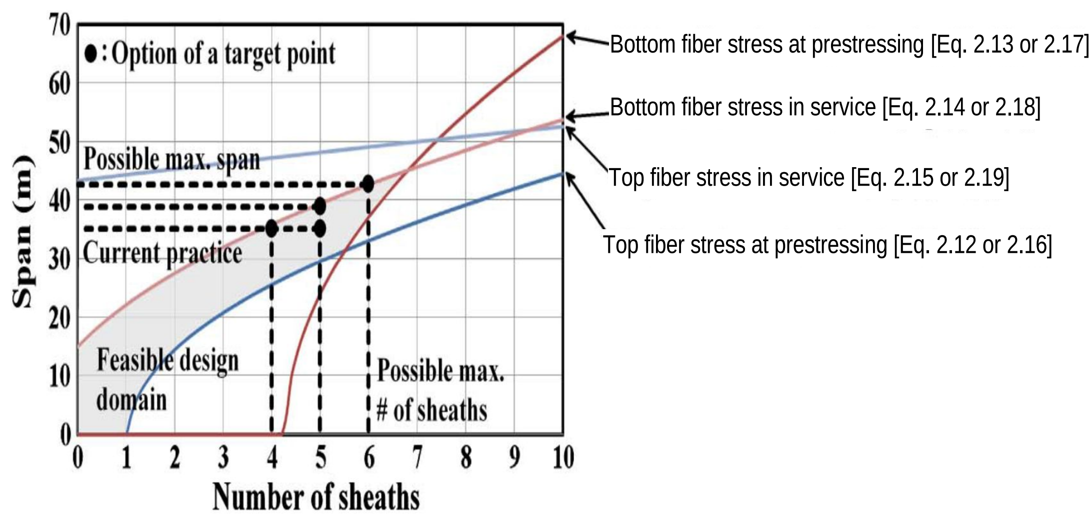

Figure 2.15. Feasible design domain of standard prestressed concrete girder (Jeon et al. 2012). Note 1 m = 3.3 ft.

The girder span length is computed with Equations 2.16 to 2.19 shown in the appendix as previously mentioned. These equations are related to top and bottom stresses at release and service, respectively. To explain the use of this chart, a standard girder with five sheaths (see Figure 2.14) is evaluated which has been used in Korea for highway bridges. Each sheath contains twelve 0.5-in. (12.7 mm) strands. Although a span of 114.8 ft (35 m) can be achieved using only four sheaths or 48 strands, Figure 2.15 shows that five sheaths or 60 strands may be chosen to provide a larger safety factor and remain in the feasible design domain. Note that as the target point moves inward from the outer boundary of the feasible design domain, a higher safety factor is achieved. Figure 2.15 alternatively shows that using five sheaths, a longer span of 128.0 ft (39 m) can be attained. In the figure, the number of sheaths is limited by the curves representing the bottom fiber stresses at service and top and bottom fiber stresses at release of prestressing. Hence, seven sheaths is out of the feasible design domain (shaded area) and six sheaths is the maximum which corresponds to a span length of 141.1 ft (43 m).

The graphical methodology can be used to evaluate the influence of a single parameter or combination of different parameters on the span capability of a bridge girder. For example, Figure 2.16 shows the results using primary prestressing and girder concrete strengths of 5,800, 8,700, and 11,600 psi (40, 60, and 80 MPa); the deck concrete strength was 3,915 psi (27 MPa).

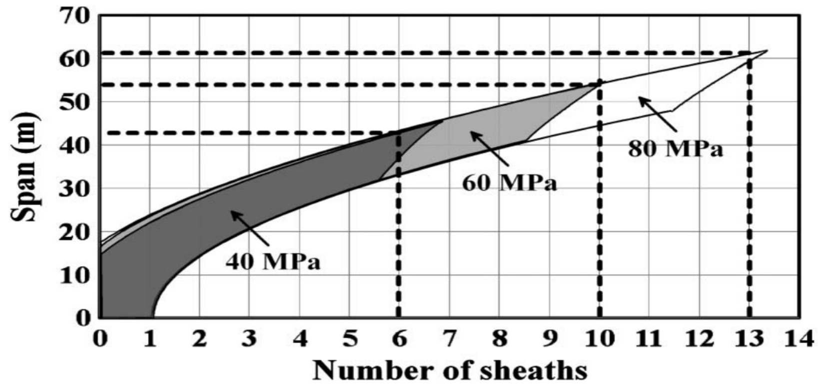

Figure 2.16. Girder design results for high-strength concrete (Jeon et al. 2012).
Note: 1 m = 3.28 ft, 1 MPa = 145 psi.

As the girder concrete strength increases, the curve for the bottom fiber stresses at release of prestressing moves to the right increasing the feasible design domain as shown in Figure 2.16. Recall that the allowable concrete stresses at release were assumed as 80% of the 28-day concrete strength. Maximum span lengths of 141.1, 177.2, and 262.5 ft (43, 54, and 61 m) were attained using concrete strengths of 5800, 8700, and 11,600 psi (40, 60, and 80 MPa), respectively. Note that the curve for the bottom fiber stresses at service did not shift upward as the girder concrete strength increased which was unexpected.

As mentioned earlier, the effect of light weight concrete on the span capability was investigated for two cases. Figure 2.17 shows the design curves for prestressed concrete girders with light weight and normal weight concrete.

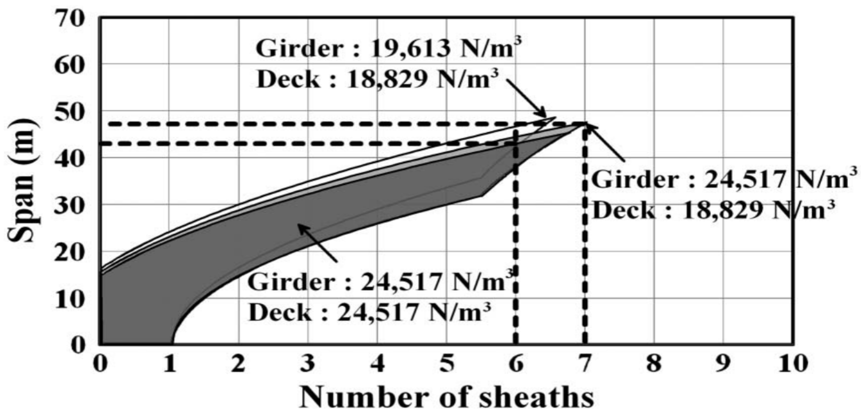

Figure 2.17. Girder design results for light weight and normal weight concrete (Jeon et al. 2012). Note: 1 m = 3.3 ft, 1 kN/m^3 = 6.36 pcf

`

Figure 2.17 shows that when the light weight concrete is used only for the deck, an additional sheath (or 12 strands) is required compared to the case where light weight concrete was used for both components.

Figure 2.18 shows the effect of girder continuity on the girder design for two span continuous girders with primary prestressing. Two cases were studied. In case 1, continuity was achieved when a continuity diaphragm and the deck were cast monolithic. In case 2, girders are made continuous before the deck placement. It was found that the span length increased from 141.0 ft (43 m) to 160.8 ft (49 m) and 187.0 ft (57 m) for cases 1 and 2, respectively.

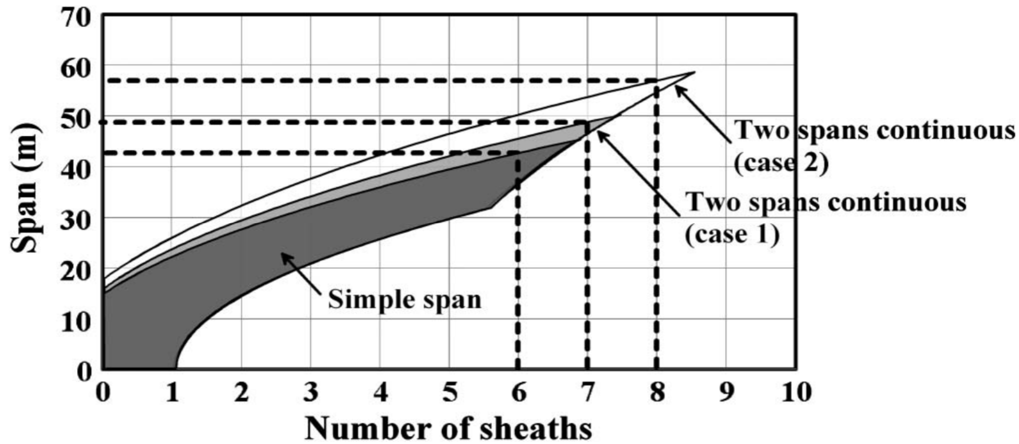

Figure 2.18. Girder design results for simple and continuous spans (Jeon et al. 2011). Note: 1 m = 3.3 ft.

2.5.2.2 Multistage Prestressing

The second type of chart developed by the authors corresponds to multistage prestressing which has been shown to be a very effective strategy to increase the span length of a girder (Han et al. 2003). Two-stage prestressing consists of primary prestressing that is applied at the time the girder is fabricated followed by a second stage of prestressing. The secondary prestressing can be applied either before or after the deck is hardened. The principal difference is that in the latter case, the secondary prestressing is resisted by both the deck and the girder as a composite section.

Figure 2.19 shows the eight curves corresponding to the eight stress criterions (as described in the figure) for two stages of prestressing.

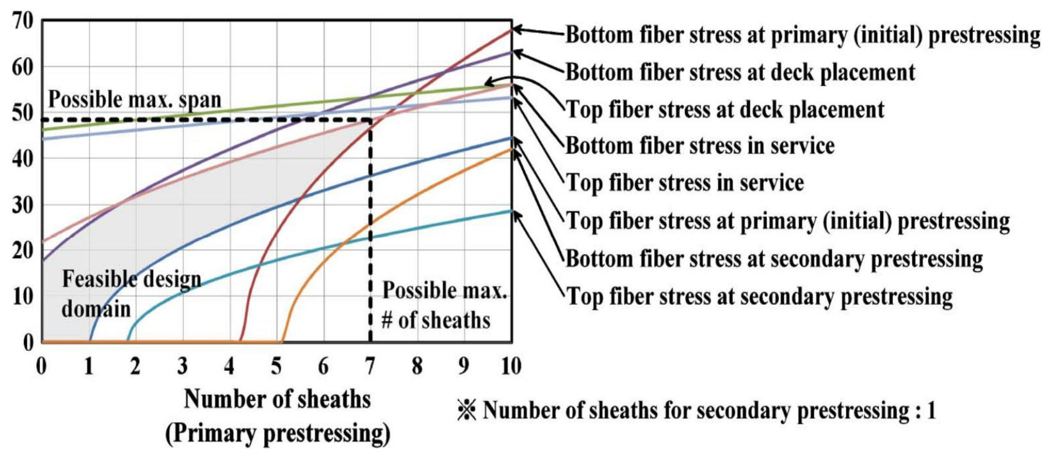

Figure 2.19. Feasible design domain of standard prestressed concrete girder using multistage prestressing (Jeon et al. 2011). Note: 1 m = 3.3 ft.

For the secondary prestressing, one sheath of tendons was assumed. Comparison of Figure 2.19 and Figure 2.15 shows that multistage prestressing results in a larger girder span length than primary prestressing only. This is evident by the upward shift of the curve representing the bottom fiber stress at service. Figure 2.20(a) shows the effect of increasing the number of sheaths for the secondary prestressing before composite action of the deck. As the number of sheaths in the secondary prestressing increases, the span length also increases. Using two and four secondary sheaths, the span length increased to 167.3 and 173.9 ft (51 and 53 m), respectively, from 137.8 ft (42 m).

In certain cases, applying the secondary prestressing before composite action is difficult. The use of precast concrete deck panels (Issa et al. 2007) may be a possible solution to this issue. Using precast panels, the shear pockets are filled with mortar after the secondary prestressing has been applied. Figure 2.20(b) shows the effect of increasing the number of sheaths for secondary prestressing after the concrete deck has hardened.

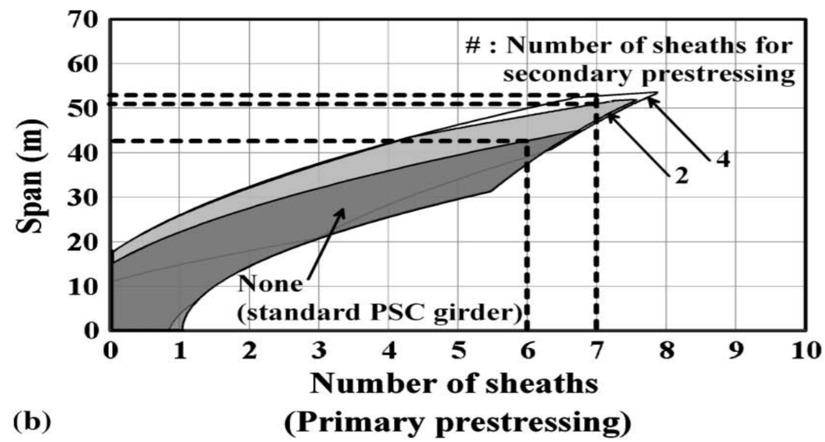

(a)

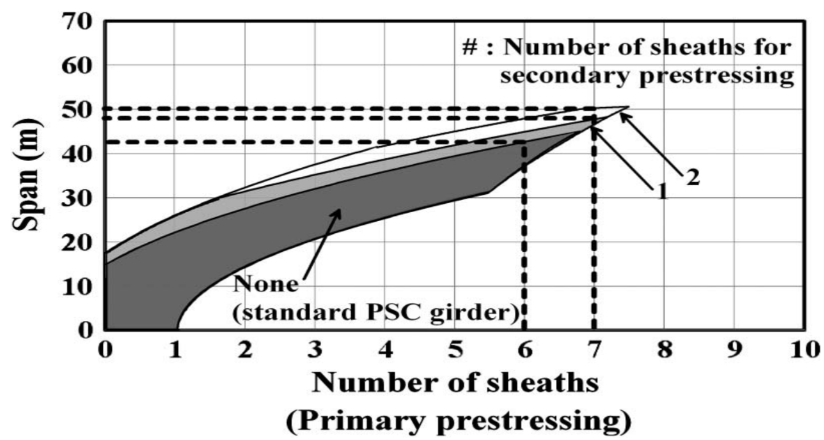

(b)

Figure 2.20. Girder design results using multistage prestressing: a) secondary prestressing before composite action of deck and b) secondary prestressing after composite action of deck (Jeon et al. 2011). Note: 1 m = 3.3 ft.

For this case, the maximum number of sheaths used for the secondary prestressing was two and the maximum span was 164.0 ft (50 m). Comparison of Figures 2.20(a) and 2.20(b) shows that applying the secondary prestressing before the cast-in place deck has hardened is more favorable because the prestressing is applied to a smaller axial concrete compressive area than that after the deck has hardened.

A summary of the maximum span lengths from this study are shown in Figure 2.21. This figure shows that the strategies that had the most significant impact (from largest to smallest) on the span capability were: high-strength concrete; decked prestressed concrete girders; span continuity; multistage prestressing; and light weight concrete. The graphical methodology presented in this study is very helpful because various options can be investigated and ranked according to the span range, thus aiding the designer to optimize the final bridge girder design.

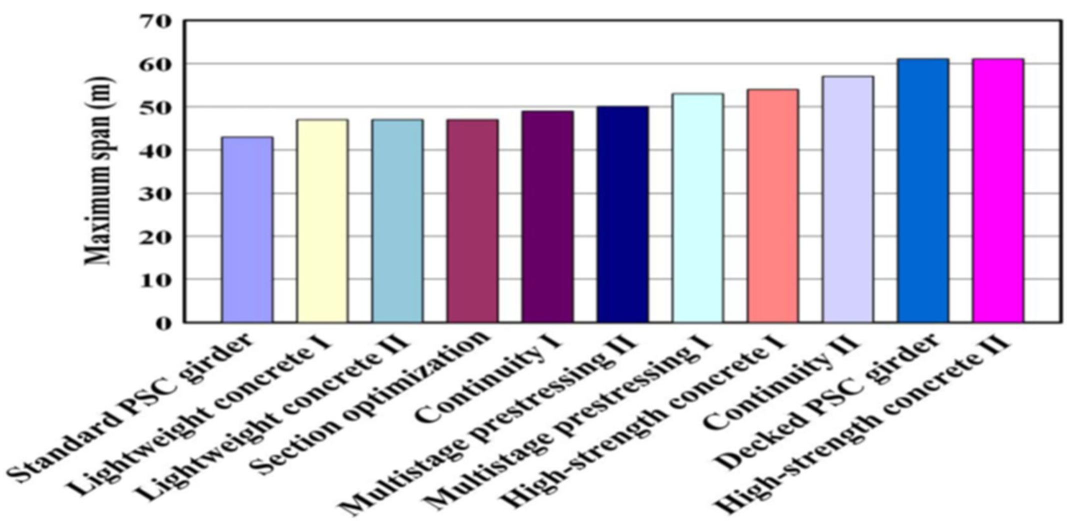

Figure 2.21. Comparison of maximum span lengths for various design strategies (Jeon et al. 2011). Note 1 m = 3.3 ft, 1 MPa = 145 psi.

2.6 Summary of Literature Review

The design criteria and description of preliminary design charts previously developed by other researchers have been discussed and illustrated. Design charts found in this literature provided very useful aids for preliminary bridge girder design. However, there are limitations to the general use of these charts by designers. For example, the PCI-11 preliminary design charts that were developed based on the AASHTO LRFD Bridge Design Specifications (2010) limit the designer to a concrete strength of f'_c = 8,000 psi (55.2 MPa) and 0.6-in. (15 mm) diameter strands. Another limitation is that these charts were developed only for simple spans.

From the literature review, it was found that previous work was made based on methods of analysis with non-closed form solutions or iterative processes that do not allow a designer to evaluate other bridge girder alternatives efficiently. For instance, to determine a feasible design domain for an interior girder, Jeon et al. (2011) first performed a number of finite element analyses using ABAQUS to obtain the equivalent distributed live and dead loads on each girder. This is a significantly time-consuming process. In addition, Fereig (1985) developed a method to determine the required prestressing force for different span lengths based on the CAN3-S6-M78 standard (1978) for design of highway bridges and a linear programming approach. Disadvantages of this method are that the CAN3-S6-M78 standard (1978) is outdated and the linear programming approach requires piecewise linearization to get the solution. It was also observed that the location where strength ceases to govern was not shown in any of the reviewed preliminary design charts. However, making this distinction allows the designer to determine the number of strands and the girder span length where strength ceases to govern and service starts to control. This is important information that the designer can use to choose other alternatives (e.g., partially prestressed girders) which could be considered as an economical option in the final design of the bridge girder.

In this review, recall that design charts for two-and three-span continuous bridges were developed by Hanna et al. (2010) but only for NU I-girders based on the AASHTO LRFD Specifications (2007) and the NDOR Manual (2009) for interior girders. The PCI (2011) Bridge Design Manual does not include preliminary design charts for continuous spans. This is an important design option because the span length can be further increased using span continuity. Longer span bridges are advantageous when traffic and congestion increase in urban areas. Therefore, continuous span girders is an important design alternative that should be included in preliminary design charts to maximize structural performance and optimize the bridge cost when longer spans are required.

Common design policies that are stricter than the AASHTO LRFD Bridge Design Specifications (2010) have been adopted by many state departments of transportation (DOTs) for the design of precast, prestressed concrete I-girder bridges (Brice et al. 2013). These design policies include some design combinations of using gross or transformed section properties, reduced allowable tensile stresses, and a simple-span policy. The use of stricter policies leads to conservative designs compared with bridges designed with the AASHTO LRFD Bridge Design Specifications (2010).

A survey of state departments of transportation was conducted by Brice et al. (2013) to measure the degree to which bridge owners deviate from the minimum requirements given in the AASHTO LRFD Bridge Design Specifications (2010). A total of 38 state DOTs responded to the survey. From this survey, 42% of the states indicated the use of a simple-span policy, 76% responded that bridge design is carried out using gross section properties, and 18% reported that no tension in the precompressed tensile zone at the Service III limit state is used in the design of prestressed concrete girders.

To quantify the effects of common policies on the design of prestressed concrete bridge girders, Brice et al. (2013) performed a base line design study based on the AASHTO LRFD Bridge Design Specifications (2010) using a slab-on-girder system composed of a cast-in place concrete deck on Washington State Department of Transportation (WSDOT) wide-flange series precast concrete girders. Two spans of equal length were considered to analyze prestressed concrete girders that are simple span for girder and deck loads and continuous for superimposed dead and live loads. The bridge owner-adopted policies were compared with the base line design study. As expected, the research showed that using the owner-adopted policy designs led to more robust structures than those using AASHTO LRFD specifications (2010). The study shows the effect of three common owner-adopted design policies (mentioned above) on girder spacing, span capability and prestress requirements. It was reported that girder spacing was the most influenced and span capability the least influenced by the three owner-adopted design policies. Decreasing the allowable tensile stress has the largest effect on girder spacing requirements, meanwhile designing with gross section properties instead of transformed section properties has the least overall effect.

A summary of the literature review is given in Table 2.6. The constant and rapid advancement of bridge technology requires that a versatile and simplified design procedure be developed to evaluate various combinations of different parameters including, but not limited to, concrete girder and deck strengths, girder section and spacing, allowable concrete stresses, stress-strain relationships for concrete and steel, strand sizes, prestress loss equations, and span continuity to provide preliminary design alternatives that allow the designer to achieve a feasible and economical bridge design.

Table 2.6. Summary of the literature review.

Paper Authors	Summary	Benefits	Limitations
Fereig (1985)	A mathematical model based on linear programming was developed to obtain the required prestressing force versus the span length	• Four different CPCI girders were analyzed • Two design controlling conditions for each CPCI section are identified • Different girder spacings	• CAN3-S6-M78 standard (1978) for design of highway bridges • Linear programming approach requires piecewise linearization to get the solution • Single concrete strength of f'_c = 5.08 ksi (35 MPa) • Simple span only • Interior girders only • No distinction between service and strength in charts

Table 2.6. Summary of the literature review (continued).

Paper Authors	Summary	Benefits	Limitations
PCI (2003)	Preliminary design charts were developed to satisfy the strength and serviceability limit states of the AASHTO Standard Specifications (2002)	• Two concrete strengths of f'_c = 7 ksi (48.3 MPa) and f'_c = 12 ksi (82.8 MPa) • Two strands of 0.5 and 0.6-in. (13 and 15 mm) diameter, seven-wire, 270 ksi (1.86 GPa) low relaxation strands • Different girder shapes and girder sizes	• AASHTO Standard Specifications (2002) • Simple span only • Interior girders only • No distinction between service and strength in charts
Hanna et al. (2010)	Preliminary design charts were provided for NU I-girders based on the AASHTO LRFD Bridge Specifications (2007) and NDOR (2009)	• Different girder sizes (from NU900 to NU2000) • Different concrete strengths (8 to 15 ksi)(55.2 to 103.4 MPa) • Two strands of 0.6 and 0.7-in. (15 and 18 mm) diameter, seven-wire, 270 ksi (1.86 GPa) low relaxation strands • Simple, two-span continuous and three-span continuous bridge girders • Threaded rod continuity system allowing the deck weight to be resisted through continuity	• Only NU I-girders • AASHTO LRFD Specifications (2007) and NDOR Manual (2009) • Interior girders only

Table 2.6. Summary of the literature review (continued).

PCI (2011)	Preliminary design charts were developed to satisfy the strength and serviceability limit states of the AASHTO LRFD Bridge Design Specifications (2010)	• AASHTO LRFD Bridge Design Specifications (2010) • Interior and exterior girders • New girder shapes including the NEXT beam, non-composite deck bulb-tee and U-beams (see Figure 1.3 in Chapter 1)	• Single concrete strength of f'_c = 8,000 psi (55.2 MPa) • Single strand configuration of 0.6-in. (15 mm) diameter, seven-wire, 270 ksi (1.86 GPa) low relaxation strand • Simple span only • No distinction between service and strength in charts
Jeon et al. (2012)	Graphical approach to evaluate different parameters on the span capability of a bridge girder	• Two-span continuous • Multistage prestressing • Three concrete strengths of f'_c = 5.8 ksi (40 MPa), f'_c = 8.7 ksi (60 MPa) and f'_c = 11.6 ksi (80 MPa) • Decked prestressed concrete girders	• Finite element analysis using ABAQUS to determine the live and dead load distribution on an interior girder (non-closed form solution) • Interior girders only • Only one girder spacing • No distinction between service and strength in charts

CHAPTER 3

DESCRIPTION OF PRESTRESSED GIRDER MODEL FOR SIMPLE SPANS

This chapter presents the simplified procedure to develop preliminary design charts for simple span, prestressed concrete bulb-tee (BT) girders considering service load stresses, flexural strength and stresses at release. The charts were first developed based on the AASHTO Standard Specifications (2002) and compared with the PCI-03 preliminary design charts (2003) for validation purposes. In Chapter 4, these charts were subsequently adapted to the AASHTO LRFD Bridge Design Specifications (2010) and compared or validated with the PCI-11 charts (2011). A BT-72 girder was considered to illustrate the procedure for computing the maximum span length based on the number of prestressing strands and girder spacing. The prestressed girder model in this study was developed using MATLAB (2011). In the charts, the transition point where strength ceases to govern and service becomes the controlling limit state is identified and shown to provide valuable design information. The design criteria, assumptions, and description of the PCI-03 and PCI-11 design charts were previously given in Chapter 2.

3.1 Design Criteria

3.1.1 Service

For the service limit state, the flexural stresses due to dead load and live load, and the axial/flexural stresses due to prestressing forces at midspan were initially computed according to the AASHTO Standard Specifications (2002). The cross-section properties for a bulb-tee BT-72 shown in Figure 3.1 and Table 3.1 were used.

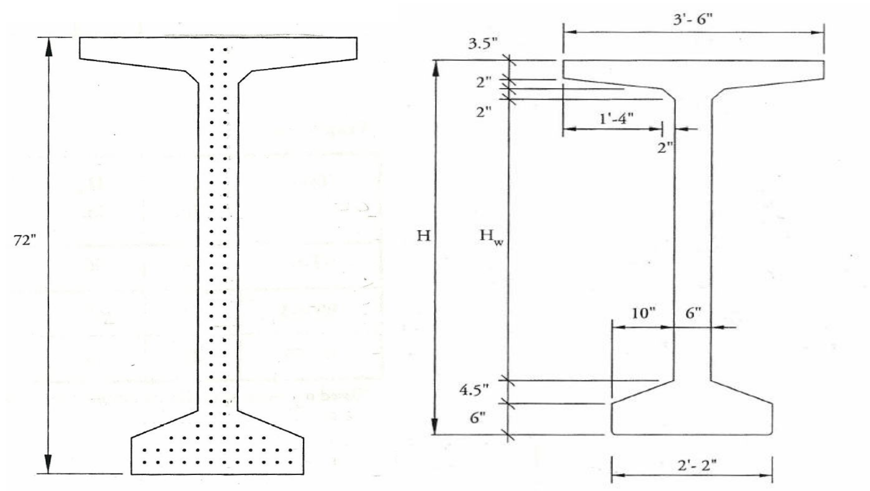

Figure. 3.1. Strand pattern and geometry of AASHTO-PCI Bulb-Tee BT-72.
Note: 1 in. = 25.4 mm

Table 3.1. Mechanical properties of AASHTO-PCI Bulb-Tee BT-72.

Type	H in. (cm)	H_w in. (cm)	Area in.^{2} (cm^2)	Inertia in.^{4} (cm^4)	y_{bottom} in. (cm)	Weight kip/ft (N/cm)	Maximum Span, ft (m)
BT-72	72 (2,195)	54 (1,646)	767 (712,566)	545,894 (471.2x10^9)	37 (1,128)	0.799 (117)	146 (45)

Note that the maximum span listed, 146 ft (45 m), corresponds to a 28-day compressive strength of 9500 psi (66 MPa). The allowable stresses used in the prestressed girder model are summarized in Table 3.2. For HPC and UHPC (i.e., f'_c > 12,000 psi or 82.8 MPa), the allowable tensile stresses at release and service were assumed 33 percent higher than NSC (PCI 2003). That is, the allowable tensile stresses for HPC and UHPC were set at $10\sqrt{f'_{ci}}$ at release and $8\sqrt{f'_c}$ at service, while the allowable compressive stresses were left the same as NSC (i.e., $0.6f'_{ci}$ and $0.6f'_c$). According to Russell and Graybeal (2013), the tensile strength of UHPC varies between $7.8\sqrt{f'_c}$ and $8.3\sqrt{f'_c}$ for steam cured specimens which concurs with the assumed value of $8\sqrt{f'_c}$. For release, the tensile stress limit was assumed 25% higher than service (i.e., $10\sqrt{f'_{ci}}$) in order to agree with the ratio of the stress limits for normal strength concrete (i.e., $6\sqrt{f'_c}$ and $7.5\sqrt{f'_{ci}}$).

Table 3.2. Allowable stresses used in the prestressed girder model.

Type of Concrete	Stress Limits at Service (psi)		Stress Limits at Release (psi)	
	Compression	Tension	Compression	Tension
NSC	$0.6f'_c$	$6\sqrt{f'_c}$	$0.6f'_{ci}$	$7.5\sqrt{f'_{ci}}$
HPC	$0.6f'_c$	$8\sqrt{f'_c}$	$0.6f'_{ci}$	$10\sqrt{f'_{ci}}$
UHPC	$0.6f'_c$	$8\sqrt{f'_c}$	$0.6f'_{ci}$	$10\sqrt{f'_{ci}}$

Note: 1 MPa = 145 psi.

The flow chart shown in Figure 3.2 was followed to compute the maximum span length for the serviceability (concrete tension) limit state.

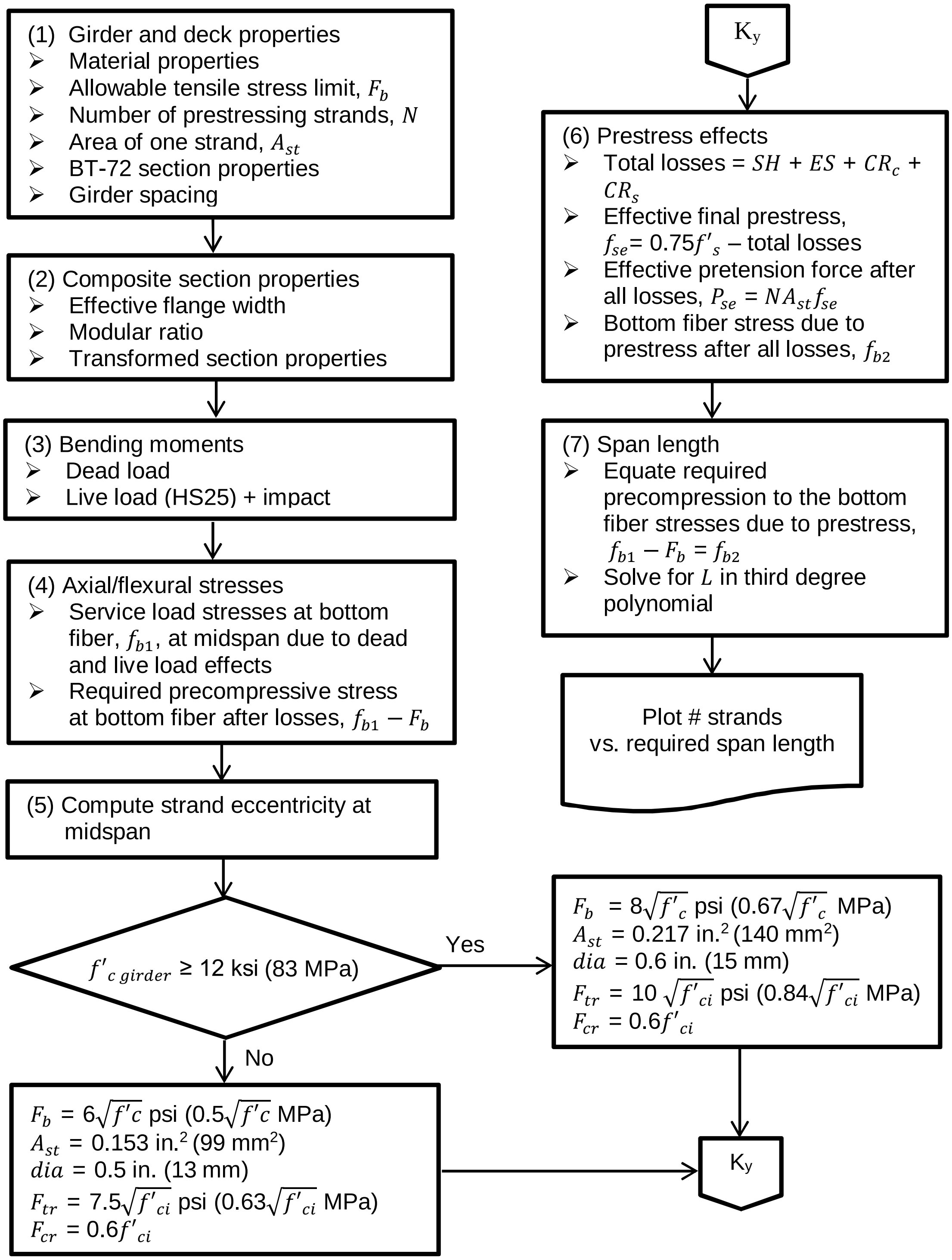

Figure 3.2. Flow chart to compute maximum span length for the service limit state.

In step 1, the girder spacing, BT-72 section properties, and an 8-in. (203 mm) thick concrete deck plus a 0.5-in. (13 mm) haunch were specified. Compressive strengths at 28 days of f'_c = 7,000 psi (48.3 MPa) and 12,000 psi (82.8 MPa) were used for the NSC and HPC girders, respectively. Low relaxation strands with 0.5-in. (13 mm) diameter at 2 in. (51 mm) spacing were used for NSC and 0.6-in. (15 mm) diameter strands were used for HPC. An ultimate stress of f'_s = 270 ksi (1.86 GPa) and initial pretensioning of f_{si} = $0.75f'_s$ were assumed. The allowable tension under service loads (F_b) were specified as discussed earlier. The maximum number of prestressing strands, N, for a BT-72 section was varied from 2 to 70. The maximum number of strands for a BT-72 girder section was assumed to be equal to 70 to agree with most of precast/prestressed concrete current practitioners. The next four steps consisted of the following computations: composite section properties (step 2); bending moments due to dead and live loads (step 3); flexural stresses at the bottom fiber due to dead and live load, f_{b1}, and required precompressive stress, $f_{b1} - F_b$ (step 4); and midspan strand eccentricity (step 5). In step 6, the bottom fiber stress due to prestress after all losses, f_{b2}, was calculated, considering shrinkage of the concrete (SH), elastic shortening (ES), creep of the concrete (CR_c), and relaxation of the steel (CR_s). The bending moment due to live load per lane at midspan was computed as:

$$M_{LL} = \frac{P}{2}\left(\frac{9}{8}L + \frac{21}{2}\right) - 14P \tag{3.1}$$

where P = 40 kips (corresponding to the largest axle load of an HS25 truck). Multiplying M_{LL} by the live load distribution factor, S/5.5, the live load impact factor, $50/(L + 125)$, and a factor of ½ (to account for wheel loading), the midspan moment for live load plus impact was:

$$M_{LL+I} = \left[\frac{9PL^2+1435PL-24500P}{32L+4000}\right]\left(\frac{S}{5.5}\right) \tag{3.2}$$

Finally, in step 7, the required precompression $(f_{b1} - F_b)$ was set equal to f_{b2} resulting in a third degree polynomial which was then solved for the girder length L:

$$f(L) = c_1L^3 + c_2L^2 + c_3L + c_4 \tag{3.3}$$

where c_1, c_2, c_3, and c_4 = constants. Equation 3.3 resulted in three roots, and the final girder length was equal to the maximum positive and non-imaginary root of the polynomial equation. Solving for the girder length L provided the service-based curves in the preliminary design charts.

3.1.2 Strength

The flow chart shown in Figure 3.3 was used to compute the maximum span length for the strength limit state.

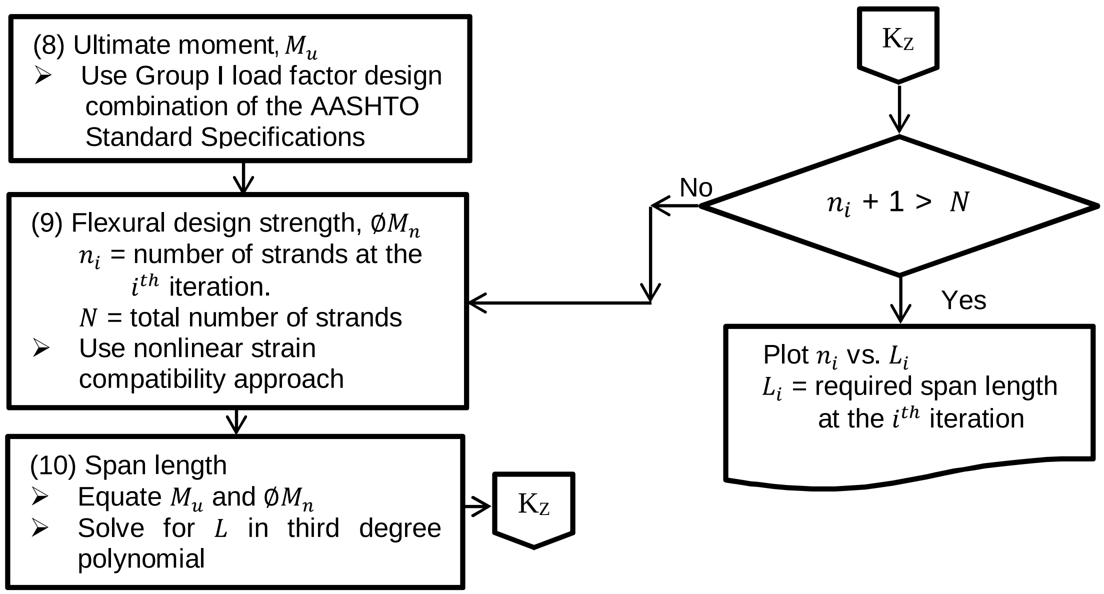

Figure 3.3. Flow chart to compute maximum span length for the strength limit state.

The ultimate moment, M_u, was first determined based on the Group I load factor design combination of the AASHTO Standard Specifications (2002) (step 8 in Figure 3.3) using the dead and live load moments previously determined for service (step 3 in Figure 3.2). The flexural design strength, $\emptyset M_n$, was then determined using the non-linear strain compatibility approach given by Seguirant et al. (2005). General design formulas related to flexural strength assume a parabolic stress-strain relationship for the concrete in compression and ignore the concrete tensile strength. However, for UHPC, the compressive behavior has been shown to be linear and the tensile strength not to be negligible (FHWA 2006). Strain compability provides the means to directly incorporate the concrete stress-strain relationship in compression and tension, which is important for future implementation. For instance, the material model reported by

Gunes et al. (2012) could be used to represent the UHPC stress-strain curve and incorporated into the girder model for future development of UHPC preliminary design charts.

For a given number of strands, $\emptyset M_n$ was computed at midspan (step 9 in Figure 3.3). The nonlinear deck-girder flexural strength model which was used to compute $\emptyset M_n$ is shown in Figure 3.4.

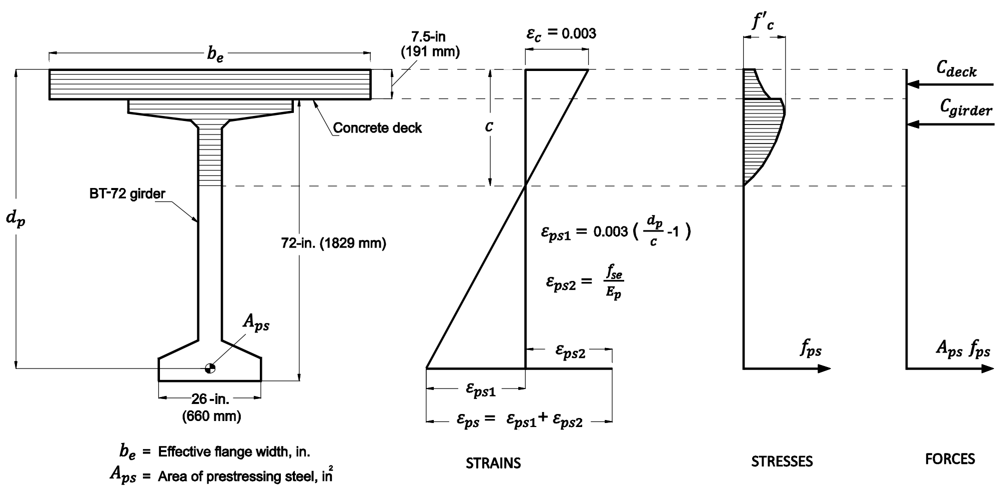

Figure 3.4. Nonlinear composite girder flexural strength model.

The neutral axis depth, *c*, was first assumed and the composite girder section was divided into differential slices. The strains were then computed over the girder height at the center of each slice based on the distance from the neutral axis and the corresponding stresses and forces were determined based on the material properties and geometry of the cross section. A maximum concrete compressive strain of 0.003 was assumed and the non-linear stress-strain relationship from Collins and Mitchell (1991) was used for the deck and girder concrete, as follows:

$$f_c = f'_c \left[\frac{n_s\left(\frac{\varepsilon_{cf}}{\varepsilon'_c}\right)}{n_s - 1 + \left(\frac{\varepsilon_{cf}}{\varepsilon'_c}\right)^{n_s k}} \right] \tag{3.4}$$

where f_c = average compressive stress in concrete slice based on nonlinear behavior (psi); f'_c = specified compressive strength of concrete at 28 days (psi); and ε_{cf} = concrete strain above the neutral axis at the center of each slice. The concrete strain, ε'_c, when f_c reaches f'_c is computed as follows:

$$\varepsilon'_c(1000) = \frac{f'_c}{E_c}\left(\frac{n_s}{n_s - 1}\right) \tag{3.5}$$

The curve fitting factor for nonlinear concrete stress-strain curves, n, the modulus of elasticity of concrete, E_c, and the factor to increase post-peak decay in stress for nonlinear concrete stress-strain curves, k, are computed as follows:

$$n_s = 0.8 + \frac{f'_c}{2500} \tag{3.6}$$

$$E_c = \frac{\left(40{,}000\sqrt{f'_c}+1{,}000{,}000\right)}{1000} \tag{3.7}$$

$$k = 0.67 + \frac{f'_c}{9000}\ \left(\text{if}\left(\frac{\varepsilon_{cf}}{\varepsilon'_c}\right) < 1.0, k = 1.0\right) \tag{3.8}$$

The resulting stress-strain curves from Collins and Mitchell (1991) are plotted in Figure 3.5 for concrete compressive strengths ranging from 5,000 to 15,000 psi (34.5 to 103 MPa).

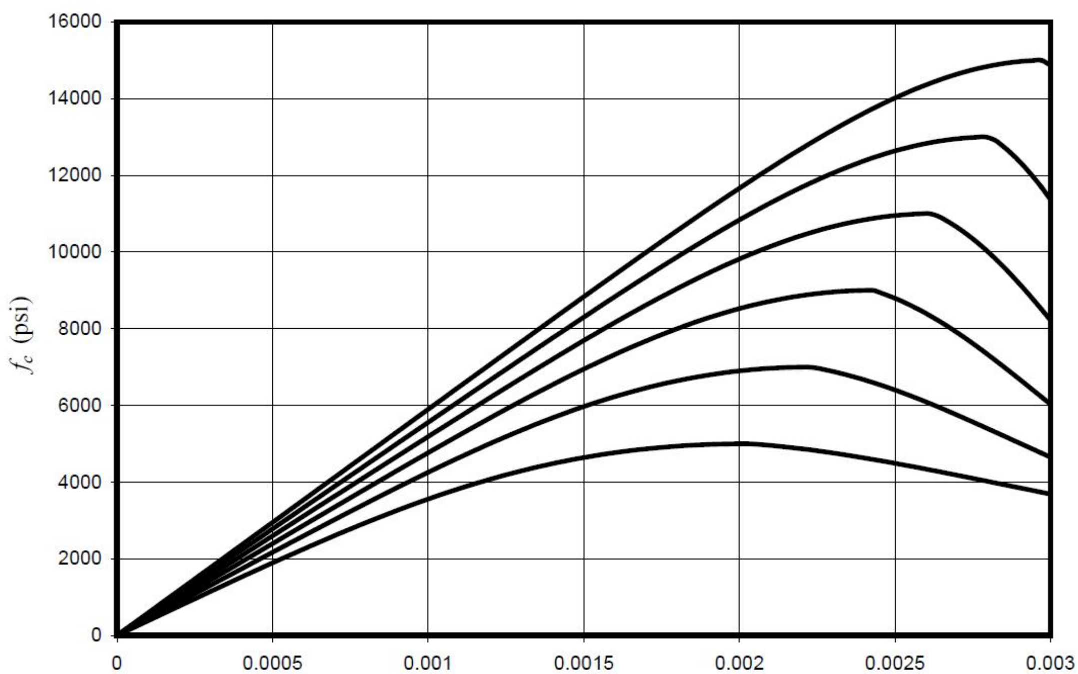

Figure 3.5. Nonlinear concrete compressive stress-strain relationships (Collins and Mitchell 1991). Note 1 psi = $\frac{1}{145}$ MPa

Equation 3.7 was used to determine the modulus of elasticity for the deck and girder concrete. The average stress within each concrete slice above the neutral axis was multiplied by the area of the slice to determine the associated compressive force. Based on the assumed value of c, the strain in the prestressing steel, ε_{ps}, was calculated by (see Figure 3.4):

$$\varepsilon_{ps} = 0.003\left(\frac{d_p}{c} - 1\right) + \frac{f_{se}}{E_p} \tag{3.9}$$

where d_p = distance from extreme compression fiber to extreme tension steel (in.); and E_p = modulus of elasticity of prestressing steel (28,500 ksi (196,500 MPa)) . Where strength controls, Seguirant et al. (2005) recommend that the effective stress in the prestressing steel after losses, f_{se}, be estimated using the following equation (Seguirant et al. 2005):

$$f_{se} = 158 - 0.2[N - 20] \tag{3.10}$$

where N = number of prestressing strands. The use of Equation 3.10 rather than $f_{se} = 0.75f'_s - total\ losses$ (as given in the AASHTO Standard Specifications (2002)) simplified the function that needed to be solved to determine the girder length L. Based on the steel strain, ε_{ps}, the stresses in the steel, f_{ps}, at ultimate moment were computed using the power formula as follows (Devalpura et al. 1992):

$$f_{ps} = \varepsilon_{ps}\left[887 + \frac{27{,}613}{1+(112.4\varepsilon_{ps})^{\frac{1}{7.36}}}\right] \leq 270 \text{ ksi (1862 MPa)} \tag{3.11}$$

The final tension steel forces below the neutral axis were obtained by multiplying the stresses by the strand area, A_{ps}. Force equilibrium was then checked, and if not satisfied, another value for the neutral axis depth c was chosen and the process repeated. Finally, the flexural capacity of the girder was computed by summing moments due to the concrete compressive forces for the deck, C_{deck}, and the girder, C_{girder}, with respect to the centroid of the prestressing steel (see Figure 3.4). The strength reduction factor, $\emptyset$, was computed using the following equation (Seguirant et al. 2005):

$$\emptyset = 0.583 + 0.25\left(\frac{d_p}{c} - 1\right) \quad 0.75 \leq \emptyset \leq 1 \tag{3.12}$$

where d_p = distance from extreme compression fiber to furthest row of tension steel (in.) and c = distance from extreme compression fiber to neutral axis (in.). This equation accounts for the transition zone between tension and compression-controlled members. Similar to service, equating M_u and $\emptyset M_n$ resulted in a third-degree polynomial equation as a function of L for the strength limit state. Again, solving for L provided the strength-based curves in the preliminary design charts.

3.2 Transition Points and Design Regions

Figure 3.6 shows a typical preliminary design chart for the BT-72 girder section developed based on the AASHTO Standard Specifications (2002) and HS25 truck loading. The transition point provides important information for design since it corresponds to the number of strands and span length where the governing limit state changes from strength to service. The transition point is located at the intersection of the strength and service curves (see Figure 3.6) and provides the information needed for a designer to distinguish the zones for fully prestressed (uncracked), partially prestressed, and non-prestressed (cracked) members.

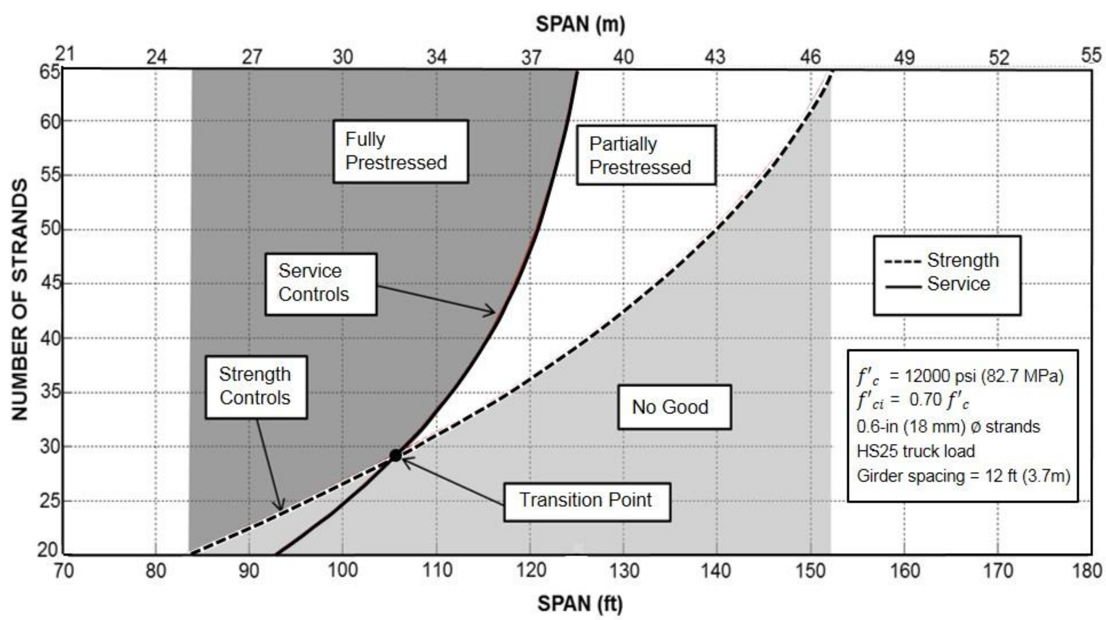

Figure 3.6. Typical preliminary design chart for BT-72 girder showing transition point and prestressed zones.

Currently, the AASHTO LRFD Bridge Design Specifications provides minimal design guidance for partially prestressed members. For instance, Article 5.5.4 of AASHTO LRFD Bridge Design Specifications (2010) provides information regarding the partiall prestress ratio (PPR) for tension-controlled partially prestressed components defined as:

$$PPR = \frac{A_{ps}f_{py}}{A_{ps}f_{py}+A_sf_y} \quad \text{[LRFD Eq. 5.5.4.2.1-4]} \tag{3.13}$$

where A_{ps} = area of prestressing steel (in.^{2}); f_{py} = yield strength of prestressing steel (ksi); f_y = specified yield strength of reinforcing bars (ksi); and A_s = area of nonprestressed tension reinforcement (in.^{2}). Note that no guidance related to this issue was provided in the AASHTO LRFD Bridge Design Specifications (2014). However, this alternative may be more practical for bridge girders, particularly for longer span lengths due to the large number of strands required to obtain a fully prestressed member. Since partially prestressed girders are allowed to experience stresses exceeding the allowable tensile stress, these members may be designed with the number of strands falling within the range above the transition points and between the governing strength and service curves (see Figure 3.6). Hence, the number of strands for partially prestressed girders is less than the number required for the service limit state and larger than the number required for the strength limit state. In general, partially prestessed girders may be considered an economical option for bridge design and the simplified procedure developed in this study provides useful information for selecting the required number of strands particularly for longer span lengths. Design regions that do not meet the strength and service design criteria are shown as “No Good” in Figure 3.6.

3.3 Comparison with PCI-03 Charts

The results obtained from the prestressed girder model were compared with the PCI-03 charts for NSC and HPC for a BT-72 girder section. Figures 3.7 and 3.8 show the NSC and HPC results.

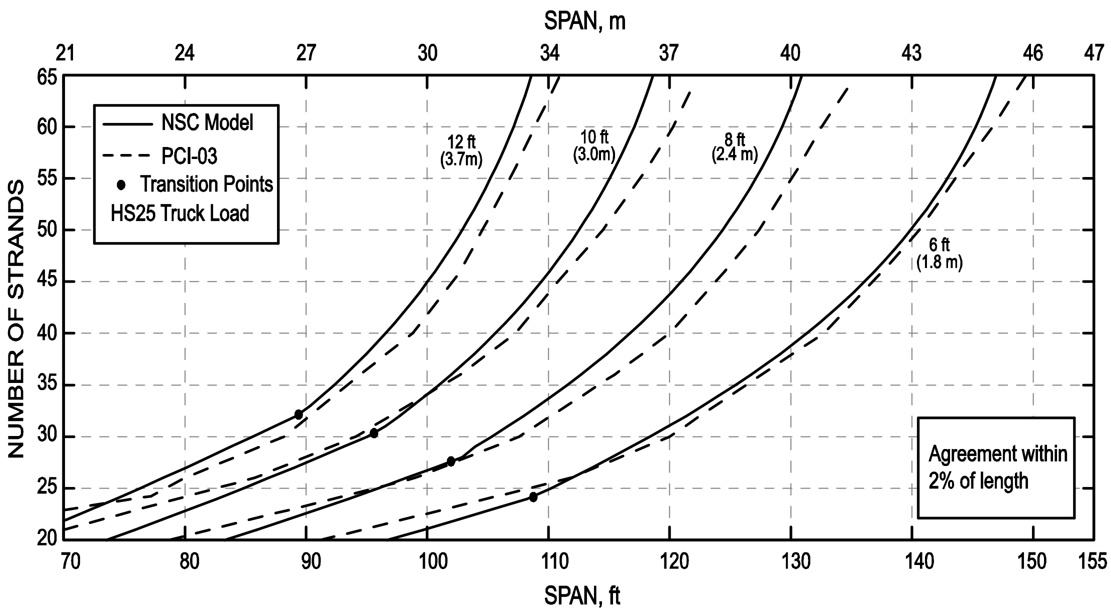

Figure 3.7. Comparison between prestressed girder model and PCI-03 charts using f'_c= 7 ksi (48 MPa) and 0.5 in. (13 mm) diameter strands.

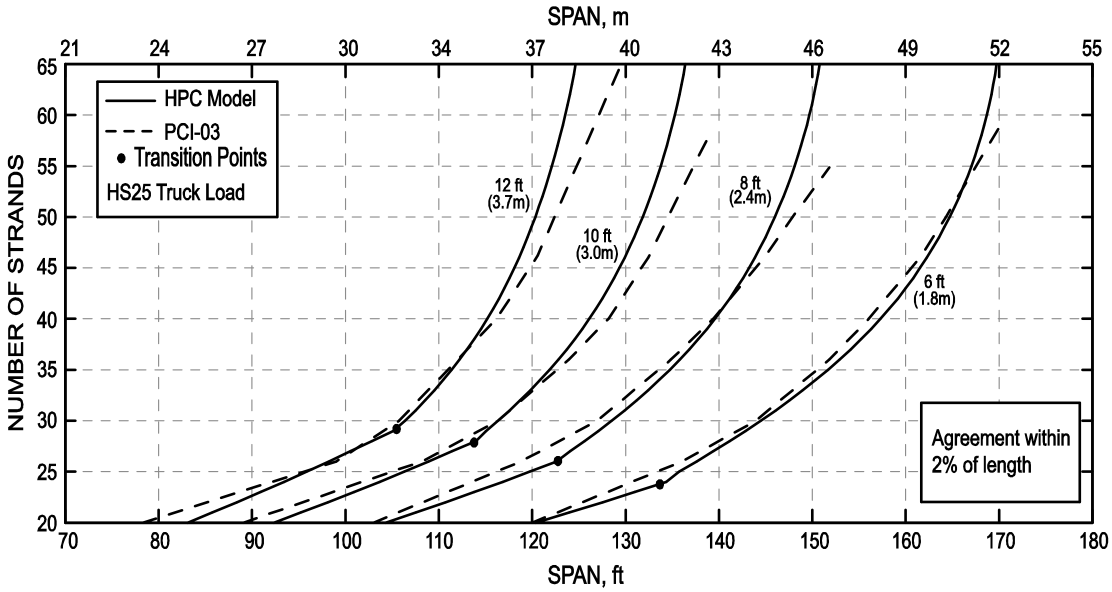

Figure 3.8. Comparison between prestressed girder model and PCI-03 charts using f'_c= 12 ksi (83 MPa) and 0.6 in. (15 mm) diameter strands.

Overall, the average difference between the NSC and HPC models and PCI-03 curves was less than 2% (Marquez et al. 2012). Notice that for a compressive strength of f'_c = 7 ksi (48 MPa), the transition point ranges from 24 to 32 prestressing strands while for 12 ksi (83 MPa) it was 23 to 29 strands for the four girder spacings. Based on these results, the span lengths were governed mostly by service.

Note that the transfer length of the prestressing force will affect the behavior and design of the end zones (Barnes et al. 2003), but will have no impact on the preliminary design charts developed in this study which were based on the final conditions of the structure: service and strength. Cases where stresses at release are the controlling criteria to determine the maximum span length were not considered here but will be discussed later. Having verified the accuracy of the prestressed girder model with the PCI-03 preliminary design charts, the model was subsequently adapted to the LRFD Specifications which is discussed in the next chapter.

CHAPTER 4

ADAPTATION TO LRFD DESIGN CRITERIA

This section explains the changes made to adapt the preliminary design charts originally developed using the AASHTO Standard Specifications (2002) to the LRFD Specifications (2010). Modifications of the prestressed girder model were made to satisfy the LRFD Service III and Strength I limit states. For Service III, the live load effects and prestress losses were adjusted and for Strength I, live load and dead load effects were adjusted according to LRFD design criteria. No changes were made to the flexural strength model since strain compatibility was used and the same allowable stresses were adopted for service since there is no difference between the AASHTO Standard and LRFD Specifications allowable stress requirements.

4.1 Modifications for Service III Limit State

To satisfy the LRFD Service III limit state, bending moments including impact due to HS-20 truck loading were multiplied by an adjustment factor to match bending moments for HL-93 live loading. In addition, prestress losses for the Service III limit state were determined based on the LRFD design criteria.

4.1.1 Live Load Effects

The live load effects (i.e., bending moments including impact) due to HS-20 and HL-93 loading were generated and compared for different girder spacings and span lengths. The live load bending moment plus impact due to HS-20 truck loading was calculated as follows:

$$M_{LL+I(HS-20)} = (M_{LL})\left(\frac{S}{5.5}\right)\frac{1}{2}\left(\frac{50}{L+125}\right) \quad (4.1)$$

where M_{LL}= bending moment per lane at midspan due to HS-20 truck loading from Eq. 3.1 with P = 32 kips; $S/5.5$ = moment distribution factor based on wheel loading; and $50/(L + 125)$ = live load impact factor as before. The midspan bending moment due to HL-93 live loading plus impact was computed as follows:

$$M_{LL+I(HL-93)} = [(M_{LL})1.33 + M_{lane}](mg) \quad (4.2)$$

where 1.33 = live load impact factor; M_{lane} = bending moment at midspan due to lane loading of 0.64 kip/ft; and mg = moment distribution factor under axle loading for an interior girder and multiple design lanes (see Eq. 2.1).

Figure 4.1 shows the bending moments at midspan of a simple-supported beam under HS-20 and HL-93 live loading plus impact based on the AASHTO Standard (2002) and LRFD Specifications (2010), respectively, for 6 and 12 ft (1.8 and 3.7 m) girder spacings. As shown in the figure, bending moments due to HL-93 loading exceed the magnitudes for HS-20 loading as expected. For the smaller girder spacing, the difference between the HL-93 and HS-20 bending moments is larger. The purpose of this analysis was to adapt the live load effects from the AASHTO Standard to LRFD Specifications.

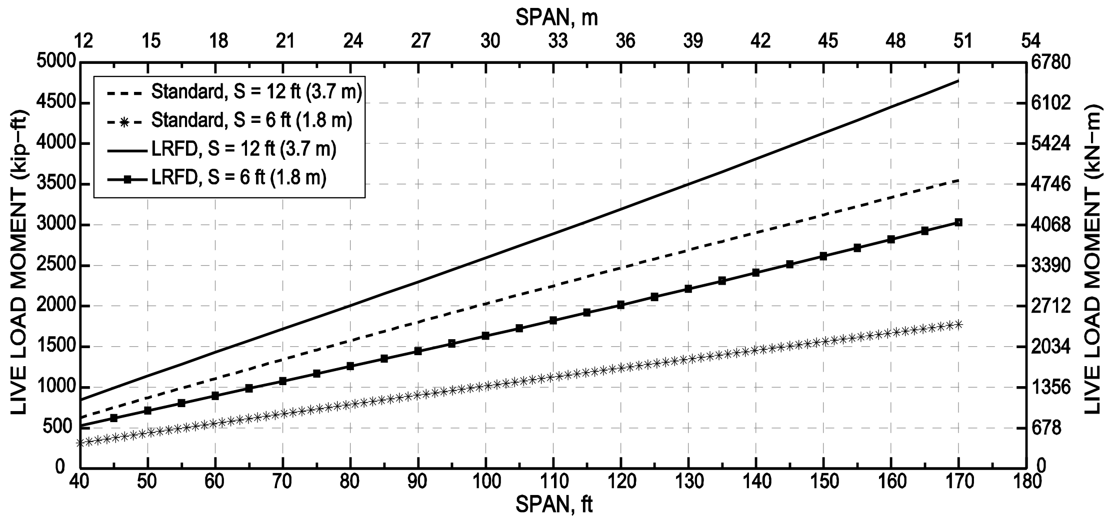

Figure 4.1. Bending moment at midspan of simple supported beam due to HS-20 and HL-93 live loading plus impact.

Accordingly, the girder moments computed for HS-20 truck loading in the prestressed girder model were multiplied by an adjustment factor to match the bending moments for HL-93 live loading. These factors were determined by averaging the ratio of the HL-93 and HS-20 bending moments over the range of span lengths for each girder spacing. Since four girder spacings were considered, four adjustment factors were determined. By multiplying Eq. 4.1 by the adjustment factors, the live load moments closely matched the values from Eq. 4.2. That is:

$$M_{LL+I(HL-93)s} = M_{LL+I(HS-20)} * Adjustment\ Factor \approx M_{LL+I(HL-93)} \tag{4.3}$$

where $M_{LL+I(HL-93)s}$ = simulated bending moment due to HL-93 live loading plus impact. Bending moments for the LRFD Service III limit state, M_{SE}, were then computed as follows:

$$M_{SE} = M_g + M_s + M_b + M_{ws} + \gamma_L M_{LL+I(HL-93)s} \tag{4.4}$$

where M_g = bending moment at midspan due to girder weight; M_s = bending moment due to the slab weight and haunch; M_b = bending moment due to barrier weight; M_{ws} = bending moment due to wearing surface weight; and γ_L = live load factor (equal to 0.8).

For girder spacings of 6, 8, 10, and 12 ft (1.8, 2.4, 3.0, and 3.7 m), factors of 1.642, 1.507, 1.416 and 1.303 were obtained. Averaging the factors for 6 and 8 ft (1.8 and 2.4 m), which are typical bridge girder spacings, and multiplying the average value of 1.575 by the LRFD live load factor of 0.8 gave a value of 1.25. Recall that the original PCI-03 charts used the HS-25 truck loading which is 1.25 times heavier than the HS-20 and approximately equal to the HL-93 live load effects.

4.1.2 Prestress Losses

From a parametric study, it was found that the AASHTO Standard Specifications (2002) tended to overestimate prestress losses, thereby preventing longer span lengths. Figure 4.2 shows this finding. A compressive strength at 28-days of f'_c= 17,500 psi (121 MPa) with 0.7-in. (18 mm) diameter strands and a girder spacing of 6 ft (1.8 m) were selected to develop this graph. Notice that as the number of strands increases, prestress losses also increase preventing longer span lengths.

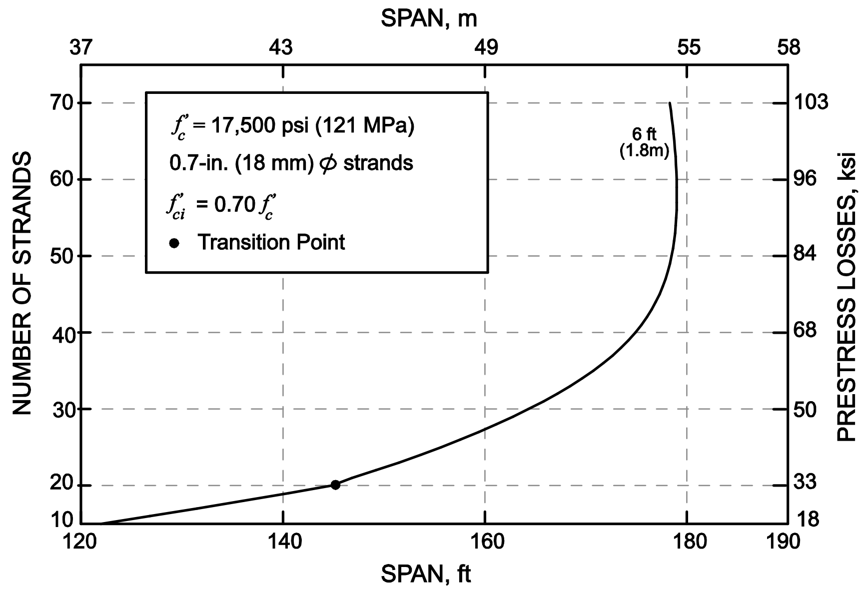

Figure 4.2. Preliminary design chart for UHPC BT-72 girders using f'_c= 17,500 psi (121 MPa) with 0.7-in. (15 mm) diameter strands and a girder spacing of 6 ft (1.8 m).

More evidence of the overestimation of prestress losses based on the AASHTO Standard Specifications (2002) is given in Figure 4.3.

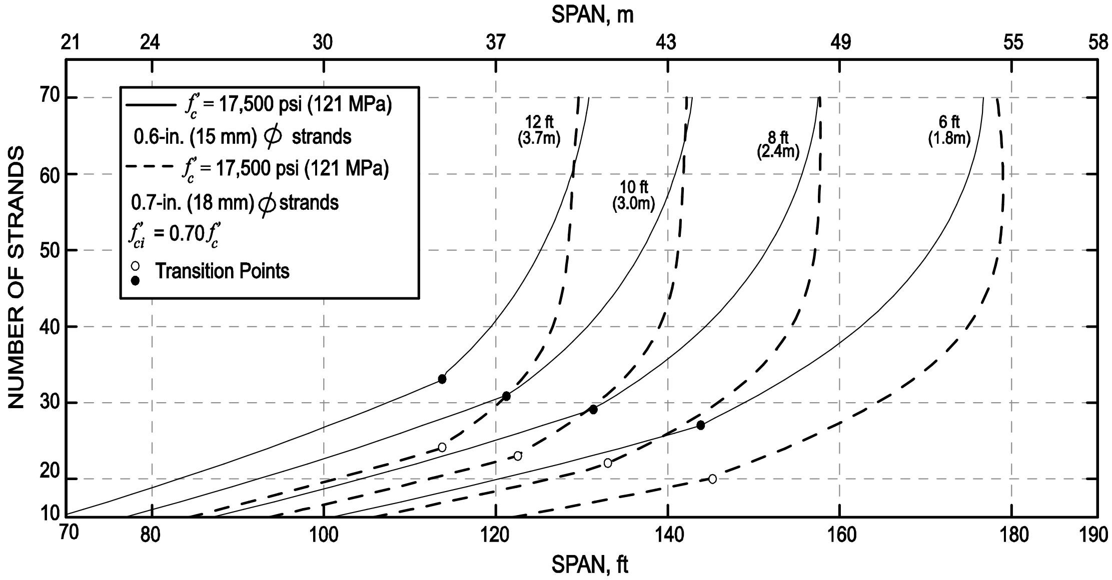

Figure 4.3. Preliminary design chart for UHPC BT-72 girders using f'_c= 17,500 psi (121 MPa) with 0.6-in. (15 mm) and 0.7-in. (18 mm) diameter strands.

A compressive strength at 28-days of f'_c= 17,500 psi (121 MPa) with 0.6-in. (15 mm) and 0.7-in. (18 mm) diameter strands and girder spacings of 12 ft (3.7m), 10 ft (3.0 m), 8 ft (2.4 m) and 6 ft (1.8 m) were selected to develop Figure 4.3. Notice that as the number of strands increased, the different curves corresponding to the four girder spacings reached a maximum span length and become more pronounced as the girder spacing decreased due to the overestimation of prestress losses. This finding agreed with a previous study conducted by Seguirant et al. (1998) which recommended that designers take caution using the AASHTO Standard Specifications (2002) to estimate prestress losses particularly for girders with high pretensioning forces. This is no longer an issue since the preliminary girder design procedure was adapted to the LRFD Specifications (2010). To compute the effective prestressing force, the total prestress losses for the Service III limit state were determined according to LRFD Article 5.9.5.1-1 as follows:

$$\Delta f_{pT} = \Delta f_{pES} + \Delta f_{pLT} \tag{4.5}$$

where Δf_{pES} = instantaneous prestress losses due to elastic shortening and Δf_{pLT} = long term prestress losses due to creep, concrete shrinkage and steel relaxation. The Δf_{pES} and Δf_{pLT} prestress losses were computed according to LRFD Eq. 5.9.5.2.3a-1 and LRFD Eq. 5.9.5.3-1, respectively, as given below (AASHTO 2010):

$$\Delta f_{pES} = \frac{A_{ps} f_{pbt}(I_g + e_m^2 A_g) - e_m M_g A_g}{A_{ps}(I_g + e_m^2 A_g) + \frac{A_g I_g E_{ci}}{E_p}} \quad \text{[LRFD Eq. 5.9.5.2.3a-1]} \tag{4.6}$$

where A_{ps} = area of prestressing steel (in.^{2}); A_g = gross area of non-composite beam section (in.^{2}); E_{ci} = modulus of elasticity of concrete at transfer (ksi); E_p = modulus of elasticity of prestressing tendons (ksi); e_m = average prestressing steel eccentricity at midspan; f_{pbt} = stress in prestressing steel prior to transfer (ksi); I_g = moment of inertia of non-composite beam section (in.^{4}); and M_g = midspan moment due to member self-weight (kip-in). Values of 28,500 ksi (196,552 MPa) and 202 ksi (1393 Mpa) were assumed for E_p and f_{pbt}, respectively. The modulus of elasticity of concrete at transfer, E_{ci}, is determined as $E_{ci} = 33{,}000 K_1 {w_c}^{1.5} \sqrt{f'_{ci}}$ where f'_{ci} = concrete strength at release (ksi). The correction factor for the aggregate source , K_1, was taken as 1.0 and a value of 0.150 kcf was used for the unit weight of concrete, w_c. Long-term prestress losses were estimated as:

$$\Delta f_{pLT} = 10.0\frac{f_{pi}A_{ps}}{A_g}\gamma_h\gamma_{st} + 12.0\gamma_h\gamma_{st} + \Delta f_{pR} \quad \text{[LRFD Eq. 5.9.5.3-1]} \tag{4.7}$$

where f_{pi} = prestressing steel stress immediately prior to transfer (equal to f_{pbt}). The correction factor for relative humidity of the ambient air, γ_h, is computed as $1.7 - 0.01H$ where the average annual ambient humidity, H (%), was assumed to be 70%. The correction factor for concrete strength at time of transfer, γ_{st}, is computed as 5/(1+f'_{ci}). Equations 4.6 and 4.7 are based on research work conducted by Al-Omaishi et al. (2009). To estimate the relaxation loss, Δf_{pR}, a value of 2.4 ksi (16.5 MPa) was assumed for low relaxation strands. The effective prestress force was then calculated as follows:

$$f_{pe} = (f_{pi} - \Delta f_{pT})A_{ps} \tag{4.8}$$

4.2 Modifications for Strength I Limit State

Based on the AASHTO Standard Specifications (2002), dead and live load moments are factored for the Group I load combination as follows:

$$M_u = 1.3\left(M_g + M_s + M_b + M_{ws} + 1.67M_{LL+I(HS-20)}\right) \quad (4.9)$$

where M_u = ultimate bending moment and $M_{LL+I(HS-20)}$ = bending moment plus impact due to HS-20 truck loading. For LRFD, Eq. 4.9 was substituted by the Strength I load combination as follows:

$$M_u = 1.25\left[M_g + M_s + M_b\right] + 1.5M_{ws} + 1.75M_{LL+I(HL-93)s} \quad (4.10)$$

For consistency with the PCI-11 charts, the following changes were also made in the prestressed girder model:

- Barrier weight of 15 psf (73.24 kg/m^2) times girder spacing was changed to 0.25 kip/ft (372.4 kg/m);
- Wearing surface of 0.025 ksf (122 kg/m^2) was changed to 0.035 ksf (171 kg/m^2); and
- Slab thickness of 8 in. (203 mm) for a girder spacing of 12 ft (3.7 m) was changed to 9 in. (229 mm).

4.3 Comparison with PCI-11 Charts

The credibility of the approach presented in this document was evaluated not only based on the comparison between the girder model and the PCI-03 preliminary design charts but also with the PCI-11 charts. Having adapted the girder model to the

LRFD Specifications, an analysis was subsequently performed to compare the results obtained from the simplified procedure with the PCI-11 preliminary design charts which showed an excellent agreement. Figure 4.4 shows the comparison between the prestressed girder model and PCI-11 charts using f'_c= 8 ksi (55.2 MPa) with 0.6-in (15 mm) diameter strands.

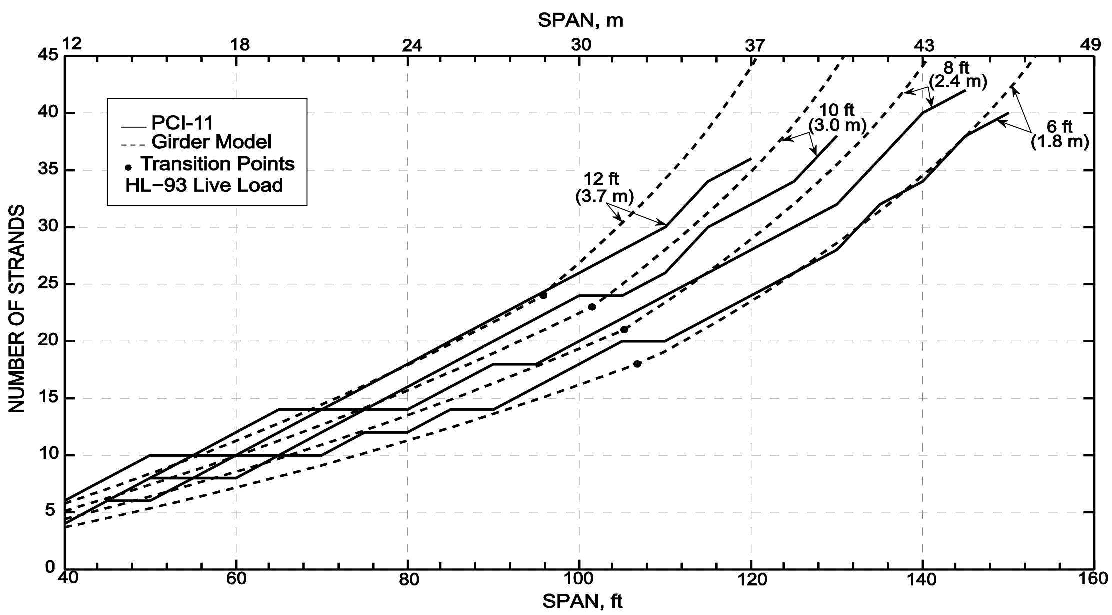

Figure 4.4. Comparison between prestressed girder model and PCI-11 charts using f'_c= 8 ksi (55.2 MPa) and 0.6-in. (15 mm) diameter strands.

Overall, the average percentage difference in length between the girder model and the PCI-11 preliminary design charts was about 4%. Based on the prestressed girder model, transition points were plotted as shown in Figure 4.4, but no distinction between service and strength was made in the PCI-11charts. The impact of continuity and the maximum span lengths governed by stresses at release are not shown in PCI-11 charts; however, these issues will be evaluated later using the girder model.

Recall that the PCI-11 preliminary design charts were developed only for f'_c = 8 ksi (55.2 MPa) and thus, may have limitations for bridge design practice in the U.S. The simplified procedure developed in this research provides the designer the capability to input different design parameters including:

- Concrete girder and deck strengths;
- Constitutive relationships for concrete and steel;
- Girder section and spacing;
- Strand size and prestress loss equations; and
- Allowable concrete stress limits for tension and compression.

The preliminary design charts were developed only for BT-72 girder sections in this dissertation. However, the prestressed girder model can be easily expanded to other girder sections.

4.4 Consideration of Release Stresses

For a given number of strands and span length, concrete stresses at release at the top and bottom fibers of the girder section were computed at two different longitudinal locations for each girder spacing to determine maximum span lengths governed by stresses at release. The first section considered was at the harp point location which is 40% of the beam length from the end of the beam. The second section was located at midspan.

Figure 4.5 shows an upper bound limit labeled with the specified concrete strength at release, f'_{ci} = 6.8 ksi (47 MPa), indicating cases where the controlling criteria for the maximum span length is compressive or tensile stresses at release. This chart was developed using a value of f'_c= 8 ksi (55.2 MPa) with 0.6-in. (15 mm) diameter strands.

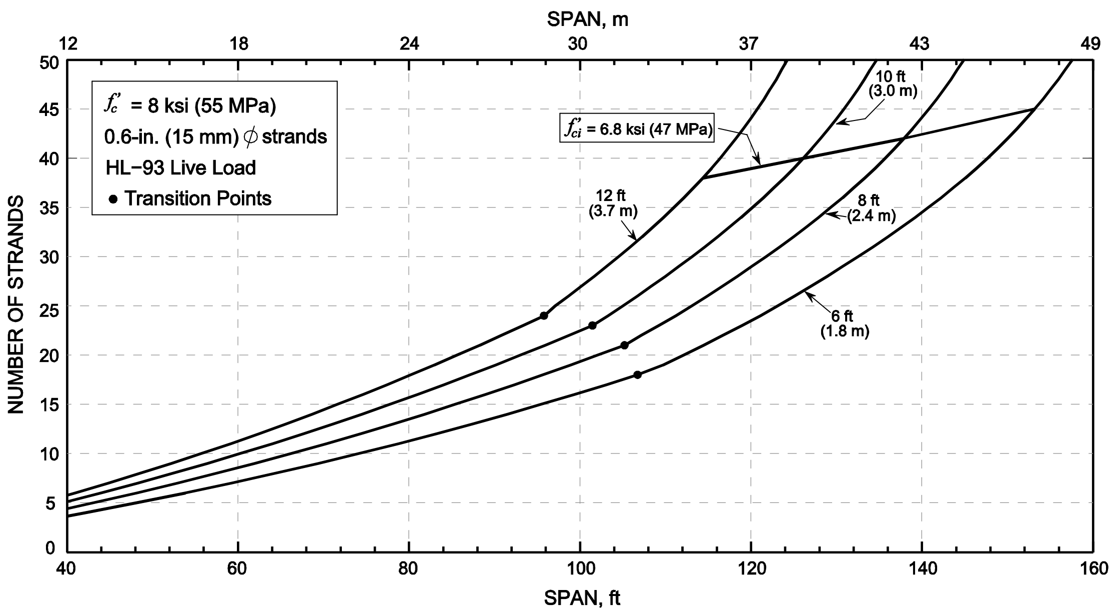

Figure 4.5. Preliminary design chart using f'_c= 8 ksi (55.2 MPa) and 0.6-in. (15 mm) diameter strands with f'_{ci} = 6.8 ksi (47 MPa).

If a larger value of f'_{ci} is used but not exceeding f'_c, the upper bound labeled as f'_{ci} = 6.8 ksi (47 MPa) in Figure 4.5 moves upwards. As an example, the effect of increasing the strength at release from f'_{ci} = 6.8 ksi (47 MPa) to 7.8 ksi (54 MPa) was investigated as shown in Figure 4.6. A compressive strength at 28-days of f'_c= 8 ksi (55.2 MPa) with 0.6-in. (15 mm) diameter strands were used to develop this chart.

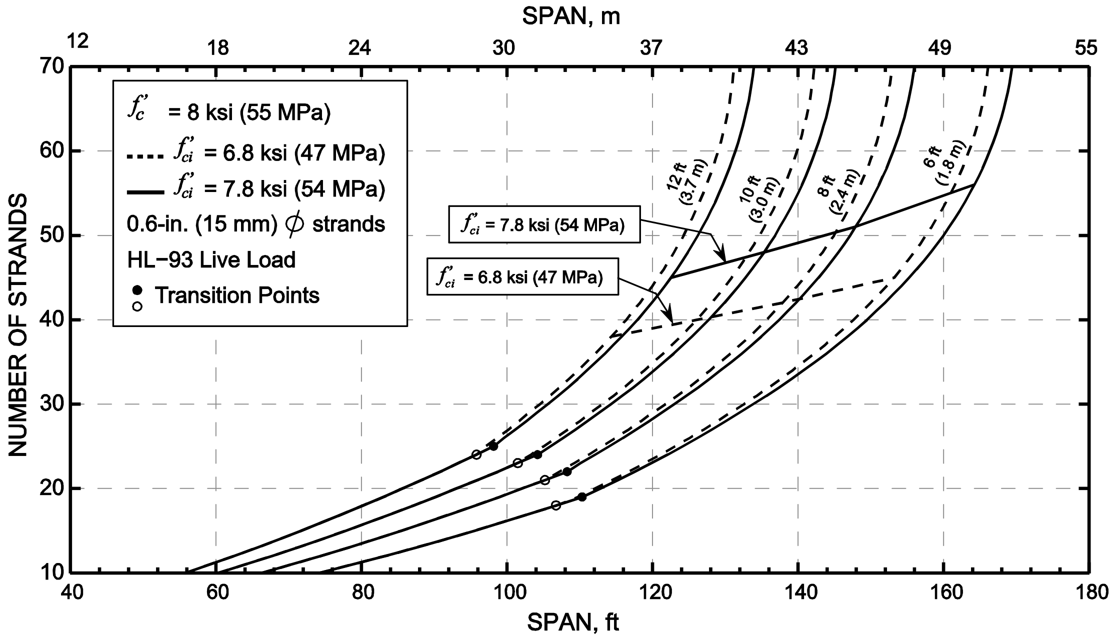

Figure 4.6. Effect of increasing strength at release from f'_{ci} = 6.8 ksi (47 MPa) to 7.8 ksi (54 MPa) with f'_c= 8 ksi (55.2 MPa) and 0.6-in. (15 mm) diameter strands.

As shown in the figure, the span lengths controlled by release at f'_{ci} = 6.8 ksi (47 MPa) increased by 8, 9, 10 and 11 ft (2.4, 2.7, 3.0, and 3.4 m) for 12, 10, 8, and 6 ft (3.7, 3.0, 2.4 and 1.8 m) girder spacings, respectively. In addition, the number of prestressing strands increased by 7 to 11 for the four girder spacings. Figure 4.6 also shows that span lengths controlled by service (span lengths above the transition points) for f'_{ci} = 6.8 ksi (47 MPa) increased slightly by about 1.53%. This is attributed to the fact that instantaneous prestress losses due to elastic shortening decreased leading to the longer span lengths. Instantaneous prestress losses, Δf_{pES} , decreased because the modulus of elasticity of concrete at transfer, E_{ci}, increased due to the 1 ksi (6.9 MPa) increase of f'_{ci} (see Eq. 4.6). Below the transition points (where strength controls) there was no change in span length because the 28-day concrete compressive strength was not modified and f'_{ci} has negligible influence on the strength limit state. Finally, it can also be noticed that for a compressive strength at release of 6.8 ksi (47 MPa), the transition point ranges from 18 to 24 prestressing strands while for 7.8 ksi (54 MPa) it was 19 to 25 strands for the four girder spacings. Based on this data, the strength limit state governs only for a low number of strands as shown before.

To attain larger span lengths than those for f'_{ci} = 7.8 ksi (55 MPa), a higher target f'_{ci} value can be computed as follows. For a given number of prestressing strands, span length and girder spacing, the required concrete strength at release can be determined by equating the largest value between the top and bottom release stresses computed at the harp points and midspan locations to the allowable stresses at release and solving for f'_{ci}. It is important to note that increasing f'_{ci} will affect production schedules due to the time increase in curing process and consequently, the bridge cost.

4.5 Extension to Two-Span Continuous Bridges

4.5.1 Analytical Approach

Equal spans of length L as shown in Figure 4.7 were considered to develop preliminary design charts for two-span continuous bridges. Figure 4.7 shows a typical configuration of simple span versus two-span continuous bridge considering dead and live load distribution and bending moment curves. Simple spans carry the girder weight (w_g), slab and haunch weights ($w_s + w_h$), barriers and wearing surface loads ($w_b + w_{ws}$), and HL-93 live loading (HS-20 design truck + lane loading) placed as shown in

Figure 4.7 to get maximum bending moments. Two-span continuous girders are typically constructed simple for dead load and continuous for live load.

Based on qualitative influence lines and bending moment diagrams for two-span continuous beams, it was assumed that the maximum bending moments due to live and superimposed dead loads (i.e., HL-93 loading and $(w_b + w_{ws})$ occur at $\frac{2}{5}L$ from an exterior support as shown in Figure 4.7.

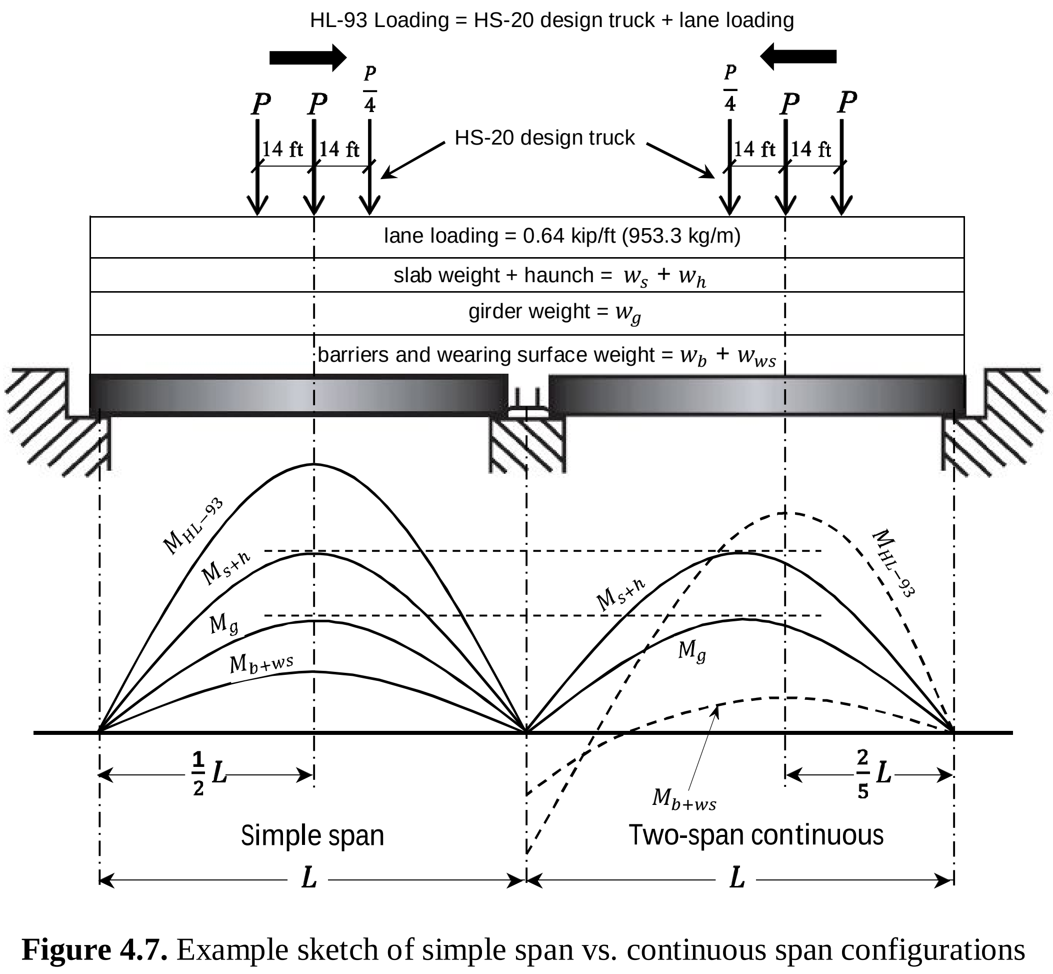

Figure 4.7. Example sketch of simple span vs. continuous span configurations
Note: P = 32 kips (142.34 kN).

For two-span continuous bridges, the girder, slab and haunch weights (w_g, w_s and w_h) are placed on the girders when the slab and haunch concrete has not yet harden and consequently, continuity has not been achieved. Therefore, for two-span continuous girders, bending moment diagrams due to the girder, slab and haunch weights (M_g and M_{s+h}) are the same as those for simple spans as shown in Figure 4.7. However, after the slab concrete has hardened, the girder section is composite and the girders are continuous. After continuity has been achieved, live and superimposed dead loads are placed on the two-span continuous girders resulting in bending moment values (M_{HL-93} and M_{b+ws}) smaller than those for simple span girders as shown in Figure 4.7. To analyze a two-span continuous girder, it is important to note that even though maximum positive moments occur at different locations (before and after the concrete hardens), live and dead load moments are assumed to be maximum at $\frac{2}{5}L$ from an exterior support.

Bending moments due to live and superimposed dead loads were determined as follows. Figure 4.8 shows the typical configuration of a two-span beam loaded with the HS-20 design truck and lane loading of 0.64 kip/ft (953.3 kg/m) that was used to compute the maximum live load effects.

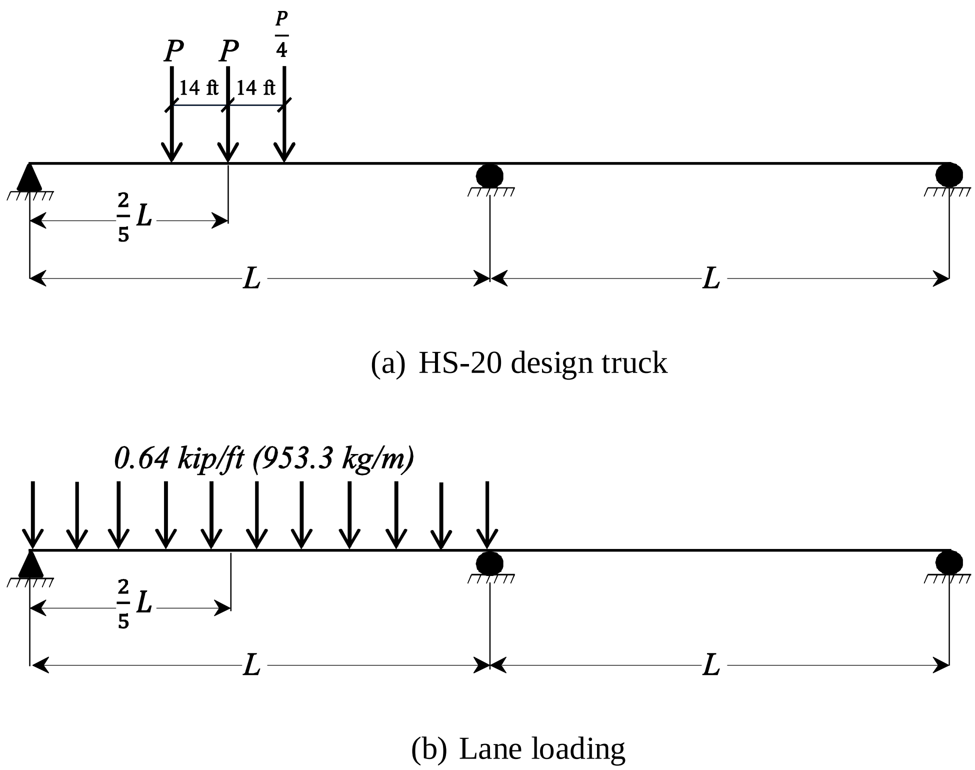

Figure 4.8. Typical configuration of two-span beam loaded with a) HS-20 truck loading and b) lane loading of 0.64 kip/ft (953.3 kg/m) used to compute maximum positive moments. Note: P = 32 kips (142.34 kN).

Bending moments due to the HS-20 design truck and lane loading of 0.64 kip/ft (953.3 kg/m) for a two-span continuous system were determined at $\frac{2}{5}L$ from the exterior support (see Figure 4.7) as follows:

$$M_{HS-20(two-span)} = \frac{P(1161L^3 - 23135L^2 + 73500L - 514500)}{2500L^2} \quad (4.11)$$

$$M_{lane(two-span)} = \frac{19wL^2}{200} \quad (4.12)$$

Equations 4.11 and 4.12 were determined using MATLAB (2011) and the live loads shown in Figure 4.8.

Bending moments due to non-composite dead loads (i.e., beam, deck and haunch weight) and superimposed dead loads (i.e., barriers and future wearing surface) were computed at $\frac{2}{5}L$ from an exterior support using simple and two-span continuous bending moment equations as follows:

$$M_{g\ (simple-span)} = \frac{3}{25} w_g L^2 \tag{4.13}$$

$$M_{s+h\ (simple\ span)} = \frac{3}{25}\ (w_s + w_h) L^2 \tag{4.14}$$

$$M_{b\ (two-span)} = \frac{7}{100} w_b L^2 \tag{4.15}$$

$$M_{ws\ (two-span)} = \frac{7}{100} w_{ws} L^2 \tag{4.16}$$

where $M_{g\ (simple-span)}$ = simple-span bending moment due to girder weight (w_g); $M_{s\ (simple\ span)}$ = simple-span bending moment due to the slab weight (w_s) and haunch (w_h); $M_{b\ (two-span)}$ = two-span bending moment due to barrier weight (w_b); and $M_{ws\ (two-span)}$ = two-span bending due to wearing surface weight (w_{ws}). Equations 4.13 and 4.14 were derived using basic static equations. Equations 4.15 and 4.16 were determined using the reaction supports for a 2-equal span continuous beam of length L given by Leet et al. (2008) and basic static equations. Equations 4.11 to 4.16 are the basis to compute the live and dead bending moments to develop preliminary design charts for two-span continuous bridges.

4.5.2. Design Criteria

Design criteria followed to develop the LRFD preliminary design charts for simple-span, prestressed concrete bulb-tee (BT) girders considering service load stresses, flexural strength and stresses at release was extended to two-span girder continuous bridges. Modifications for service and strength are given below.

4.5.2.1 Service

Equations 4.11 and 4.12 were used to compute M_{LL} and M_{lane}, respectively, and were substituted into Equations 4.1 and 4.2 to compute bending moments plus impact due to HS-20 and HL-93 live loading for two-span continuous systems. Bending moments at $\frac{2}{5}L$ from an exterior support due to HS-20 and HL-93 live loading plus impact were then plotted as shown in Figure 4.9.

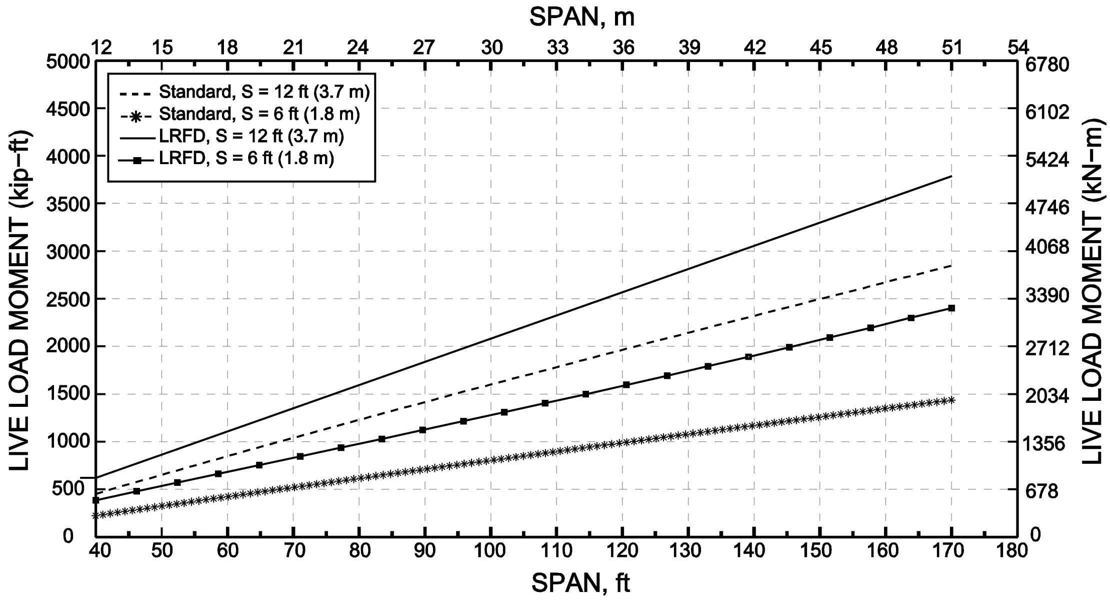

Figure 4.9. Bending moment at $\frac{2}{5}L$ from an exterior support of two-span beam due to HS-20 and HL-93 live loading plus impact.

For girder spacings of 6, 8, 10, and 12 ft (1.8, 2.4, 3.0, and 3.7 m), new adjustment factors of 1.653, 1.518, 1.425 and 1.309 were determined respectively. Adjustment factors increased slightly by an average of 0.62% compared to those obtained for simple-span girders. Substituting the new adjustment factors and bending moments plus impact due to HS-20 for two-span continuous bridges into Equation 4.3, bending moments for HL-93 live loading were simulated. Bending moments for the LRFD Service III limit state, M_{SE}, were then computed by substituting Equations 4.13 through 4.16 and the simulated bending moment due to HL-93 live loading plus impact for two-span continuous bridges into Equation 4.4.

The flow chart shown in Figure 3.2 was followed to compute the maximum span length for the service limit state and the prestress losses were determined according to LRFD Article 5.9.5.1-1 (see Equations 4.5 to 4.7). Equation 4.8 was used to compute the effective prestress force. The flexural service load stress at the bottom fiber due to live and dead loads, f_{b1}, was computed based on the dead load moments from Equations 4.13 through 4.16 and simulated bending moment due to HL-93 live loading plus impact for two-span continuous behavior. The bottom fiber stress due to prestress after all losses, f_{b2}, was calculated considering f_{pe} from Equation 4.8. As before, a third degree polynomial resulted from equating the required precompression $(f_{b1} - F_b)$ to f_{b2}. Solving for the girder length L provided the service-based curves in the preliminary design charts for two-span continuous bridges.

4.5.2.2 Strength

The flow chart shown in Figure 3.3 was followed to compute the maximum span length for the strength limit state. Equations 4.13 through 4.16 and simulated bending moments due to HL-93 live loading plus impact for two-span continuous behavior were substituted into Equation 4.10 to determine the ultimate bending moment, M_u. As before, for a given number of strands, the flexural design strength, $\emptyset M_n$, was computed using the strain compability approach. Again, equating M_u and $\emptyset M_n$ resulted in a third-degree polynomial equation as a function of L. Solving for L provided the strength-based curves in the preliminary design charts for two-span continuous bridges.

4.5.2.3 Release

Similarly to simple spans, maximum span lengths governed by stresses at release were determined for two-span continuous girders. As before, stresses at release were computed at harped and midspan locations using simple span bending moments due to self-weight and pretension force after allowing for elastic shortening. Maximum span lengths governed by stresses at release are indicated as shown in Figure 4.10.

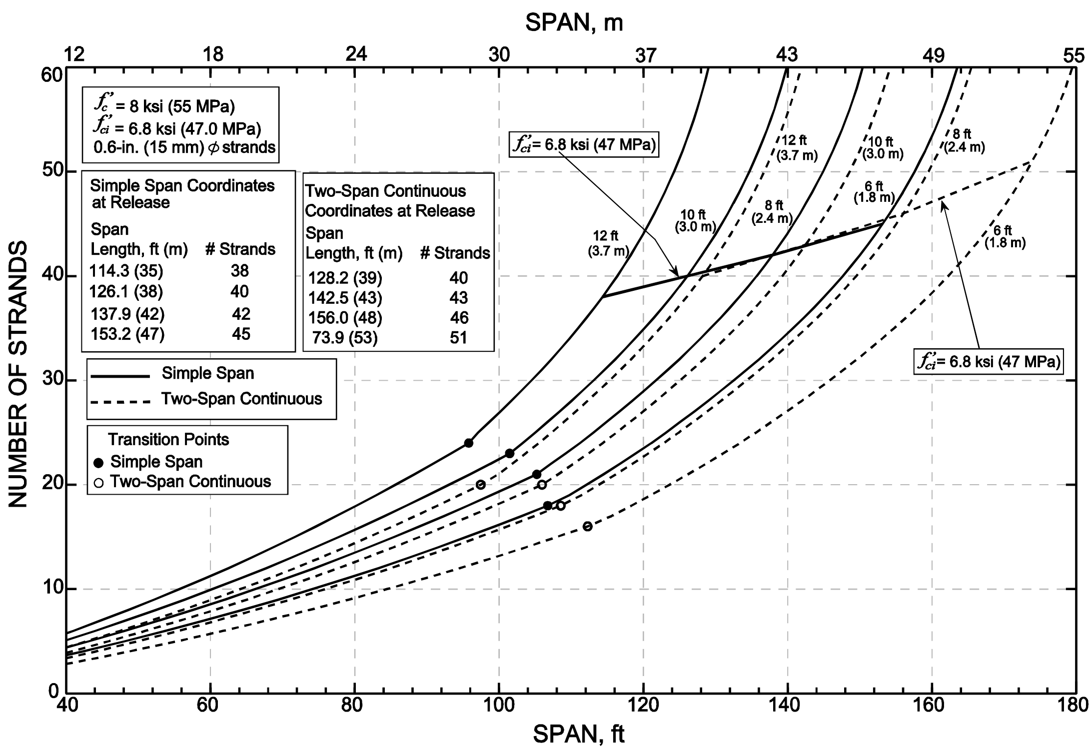

Figure 4.10. Maximum span lengths governed by stresses at release for simple and two-span continuous girders using f'_c= 8 ksi (55.2 MPa) and 0.6-in. (15 mm) diameter strands with f'_{ci} = 6.8 ksi (47 MPa).

In Figure 4.10, the maximum span lengths governed by stresses at release are indicated by an upper bound limit labeled with the specified concrete strength at release, f'_{ci} = 6.8 ksi (47 MPa) for simple and two-span continuous girders. Note that a solid line represents the maximum span lengths for simple spans and continues as a dashed line representing the maximum span lengths for two-span continuous systems at release. At girder spacings of 6, 8 and 10 ft (1.8, 2.4 and 3.0 m) these two lines overlap each other as if only one line were plotted because stresses at release are computed considering only moments due to self-weight and pretension forces after allowing for elastic shortening and continuity at the supports is not considered. As the girder spacing decreases, maximum span lengths governed by stresses at release increase (the upper bound limit increases) and the controlling service range becomes larger. The impact of continuity using higher concrete strengths and larger strand diameters with considerations of release stresses is discussed in the next chapter.

CHAPTER 5

IMPACT OF CONCRETE STRENGTH, STRAND SIZE, AND SPAN CONTINUITY

Using the simplified LRFD procedure, preliminary design charts were developed as shown in Figures 1.1 and 1.2 (Chapter 1) for simple span bridges to investigate the impact of concrete strength and strand size on prestressed concrete girder design (including span length capability, number of prestressing strands, and girder spacings). Concrete compressive strengths at 28 days of f'_c= 7 ksi (48 MPa) for NSC, 12 ksi (83 MPa) for HPC, and 20 ksi (138 MPa) for UHPC were considered. In addition, prestressing strands of 0.5-in. (13 mm), 0.6-in. (15 mm), and 0.7-in. (18 mm) diameters were used.

To study the impact of span continuity and strand size, preliminary design charts were developed for simple span and two-span continuous bridges. Concrete strengths of 8, 12 and 20 ksi (55, 83, and 138 MPa) with prestressing strands of 0.6-in. (15 mm) and 0.7-in. (18 mm) diameters were assumed. Some states in the U.S have adopted a simple span policy instead of a continuous bridge policy based on the AASTHO LRFD Bridge Design Specifications (2010). The implications of this policy will be discussed in this chapter.

According to PCI (2003) only a very limited number of precast producers in the country are likely to have a prestressing bed capacity capable of 90 strands. To develop the preliminary design charts there was no attempt to determine whether or not the number of strands was feasible. Accordingly, this should be verified with the bed capacity of local producers. The maximum number of strands for a BT-72 girder section was assumed to be equal to 70 which is typical of current precast/prestressed concrete producers.

In the charts, the transition point where strength ceases to govern and service becomes the controlling limit state is explained and shown to provide valuable design information. In addition, the maximum span lengths governed by stresses at release are presented and discussed in this chapter. Practical limitations on span length based on fabrication, transportation and erection are discussed to show the potential impact of using the maximum attainable girder span lengths.

5.1. Impact of Concrete Strength and Strand Size

With the prestressed girder model adapted to the AASHTO LRFD design criteria, and the results in agreement with the 2011 PCI Bridge Design Manual, new preliminary design charts were confidently generated for a BT-72 girder. Figures 5.1 through 5.3 show the charts for different combinations of f'_c equal to 12 and 20 ksi (82.8 and 137.9 MPa) and strand diameters of 0.6 and 0.7 in. (15 and 18 mm). The transition point where the span length changes from being controlled by the LRFD Strength I to Service III limit state is marked by a dark circle in the figures.

In Figure 5.1, compressive strengths of 12 ksi (82.8 MPa) and 20 ksi (137.9 MPa) with a 0.6-in (15 mm) diameter strand were used. The figure shows that the change in concrete strength had no effect on the span length for the strength limit state (situated below the transition point) since the tensile strength of the concrete was ignored after cracking (also for UHPC). Furthermore, as the girder spacing increases, the number of strands at the transition point increases, signifying that the strand layout is governed more by the strength limit state. The transition point ranges between 25 and 31 strands for f'_c = 12 ksi (82.8 MPa) and between 32 and 44 strands for f'_c = 20 ksi (137.9 MPa). Above the transition point, the span lengths are governed by the service limit state. Also note that the number of strands at the transition points increases as the concrete compressive strength increases. This is because the allowable tensile stress of the concrete increases as the concrete compressive strength increases. For instance, at 8 ft (2.4 m) girder spacing, the number of strands at the transition point increased from 28 strands with f'_c = 12 ksi (82.8 MPa) to 37 strands with f'_c = 20 ksi (137.9 MPa).

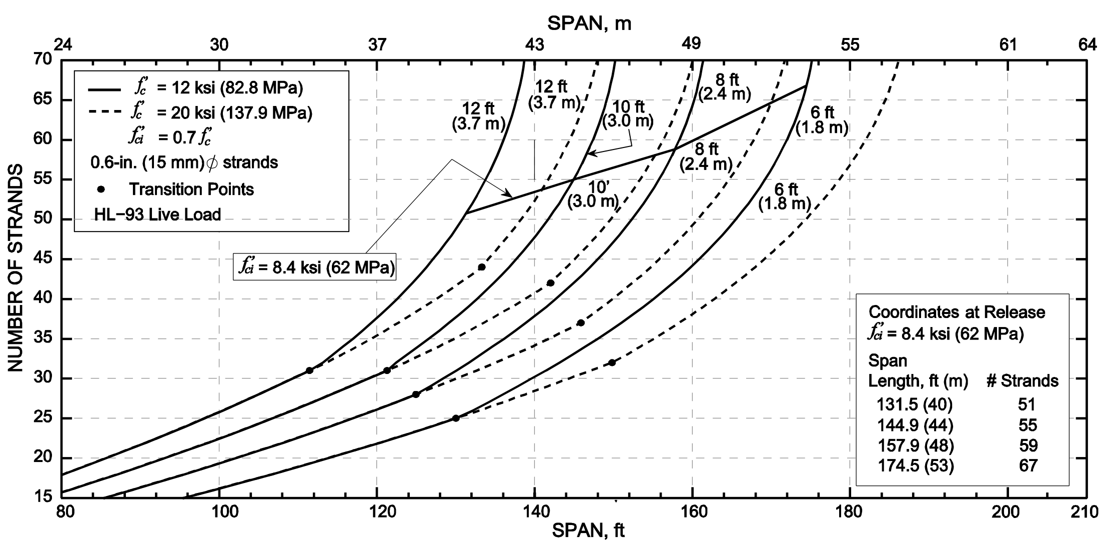

Figure 5.1. Preliminary design chart for BT-72 girder using f'_c = 12 ksi (82.8 MPa) and 20 ksi (137.9 MPa) with 0.6-in. (15 mm) diameter strands.

Setting the number of prestressing strands constant above the transition point, longer span lengths can theoretically be achieved when the concrete compressive strength is increased. Considering 40 strands and an increase in compressive strength from 12 ksi (82.8 MPa) to 20 ksi (137.9 MPa), the theoretically possible span length increased by an average of 4.7% in Figure 5.1. In a like manner, for a given span length above the transition point, the number of prestressing strands decreases as the compressive strength increases. At a span length of 130 ft (39.6 m), for example, the average decrease in the number of strands was 8.2%. It is important to note that relatively small changes occurred since the strand diameter was not increased (only the concrete compressive strength was increased).

Note that maximum span lengths governed by stresses at release are indicated by an upper bound labeled as f'_{ci} = 8.4 ksi (62 MPa). Coordinates at release are also provided in Figure 5.1. For instance, for a concrete strength of 12 ksi (82.8 MPa) and a girder spacing of 8 ft (2.4 m) the maximum span length attained at release is 157.9 ft (48 m) and the required number of prestressing strands is 59. For a concrete strength of 20 ksi (137.9 MPa) stresses at release no longer control the maximum span lengths but rather stresses at service.

Figure 5.2 shows the impact of using different strand diameters with no change in compressive strength. A 28-day compressive strength of f'_{c} = 12 ksi (82.8 MPa) with 0.6-in. (15 mm) and 0.7-in. (18 mm) strands were used to develop this graph. As shown in the figure, the effect of using a larger strand diameter was more significant than increasing the concrete compressive strength since the change in span length and number of strands was much greater.

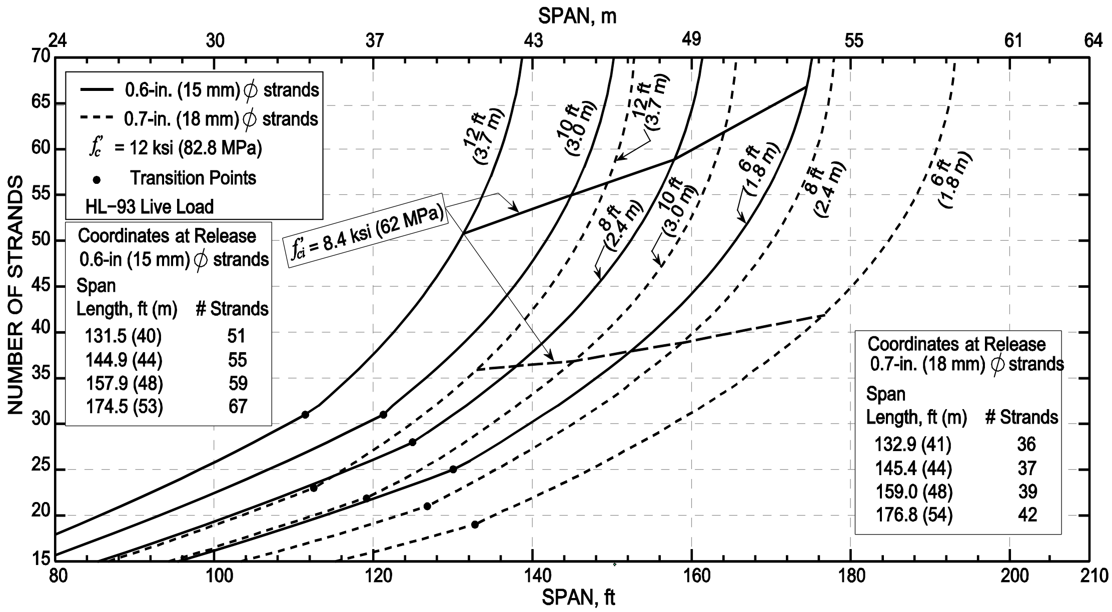

Figure 5.2. Preliminary design chart for BT-72 girder using f'_c = 12 ksi (82.8 MPa) with 0.6-in. (15 mm) and 0.7-in. (18 mm) diameter strands.

For instance, at 40 strands, the potential span length increased by approximately 17 ft (5.2 m) due to the increase in strand diameter, whereas the 8 ksi (55.2 MPa) increase in compressive strength resulted in only a 6.5 ft (2.0 m) longer span as shown in Figure 5.1. In other words, at 40 strands the span length increased by 260% more due to the increase in strand diameter than due to the increase in concrete strength. Furthermore, the number of strands decreases more significantly as the strand diameter increases. For example, at a 10 ft (3.0 m) girder spacing and span length of 120 ft (36.6 m), the number of prestressing strands decreased from 30 to 22 (75%) when the strand diameter was changed from 0.6-in. (15 mm) to 0.7-in. (18 mm).

Figure 5.1 shows that above the transition points and for a concrete strength of 20 ksi (137.9 MPa) service governs meanwhile for 0.7-in. (18 mm) diameter strands maximum span lengths are governed by stresses at release as shown in Figure 5.2. For instance, Figure 5.1 shows that for a girder spacing of 8 ft (2.4 m) and a concrete strength of 20 ksi (137.9 MPa) with 0.6-in. (15 mm) diameter strands the maximum potential span length is governed by service and is equal to 171.7 ft (52.3 m) meanwhile Figure 5.2 shows that for the same girder spacing with a concrete strength of 12 ksi (82.8 MPa) and 0.7-in. (18 mm) diameter strands the maximum span length governed by stresses at release is equal to 159 ft (48 m). Finally, Figure 5.2 shows that increasing the diameter strand from 0.6-in. (15 mm) to 0.7-in. (18 mm), the maximum span lengths governed by stresses at release increased slightly by an average of 0.9 % (from 152.2 ft (46.4 m) to 153.5 (46.8 m)). Meanwhile, the number of strands was reduced significantly by an average of 48.7 % (from 58 to 39 strands). Although the increase in span length is not substantial, the number of prestressing strands reduced significantly which results in a decrease in material and labor costs.

Figure 5.3 shows the impact of increasing the concrete strength and the strand diameter. This graph was developed with compressive strengths of f'_c = 12 ksi (82.8 MPa) and 20 ksi (137.9 MPa) with 0.6-in. (15 mm) and 0.7-in. (18 mm) strands, respectively. The figure shows that the increase of both properties was much more significant than the individual increase of either the concrete strength or strand diameter.

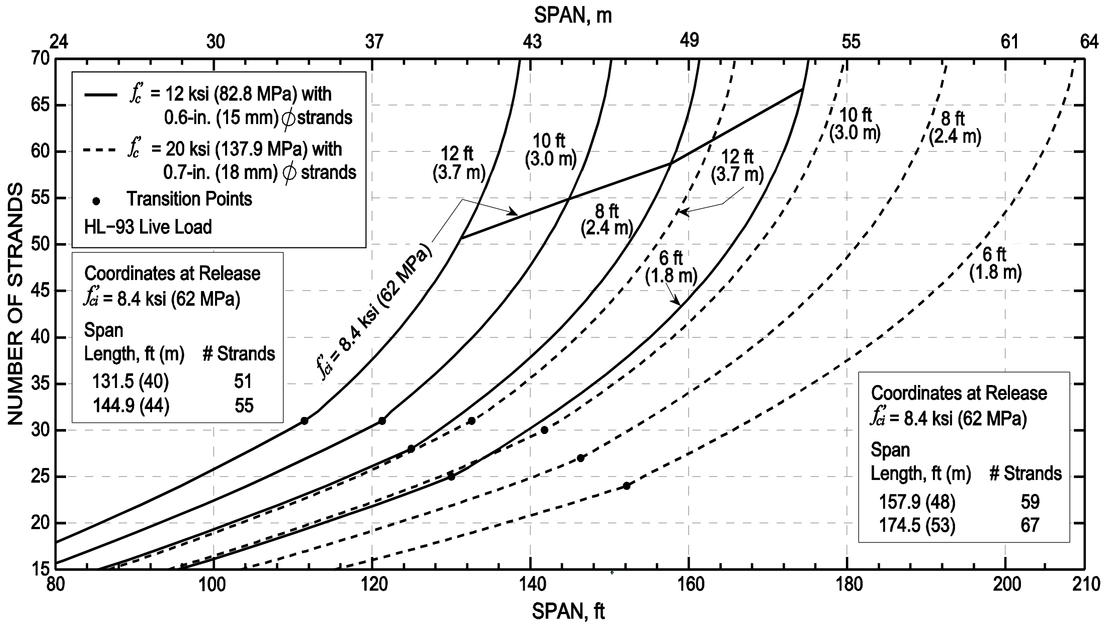

Figure 5.3. Preliminary design chart for BT-72 girder using f'_c= 12 ksi (82.8 MPa) with 0.6-in. (15 mm) diameter strands and f'_c= 20 ksi (137.9 MPa) with 0.7-in. (18 mm) diameter strands.

At 40 strands, the potential span length increased by approximately 26.2 ft (8 m), whereas increasing either the compressive strength from 12 to 20 ksi (82.8 to 137.9 MPa) or the strand diameter from 0.6-in. (15 mm) to 0.7-in. (18 mm) resulted in 6.5 ft (2 m) or 17 ft (5.2 m) longer spans as shown before in Figures 5.1 and 5.2, respectively. In Figure 5.3, above the transition points and for a concrete strength of f'_c= 12 ksi (82.8 MPa) release controls and for f'_c= 20 ksi (137.9 MPa) service controls. Note that maximum span lengths governed by stresses at release are indicated by an upper bound labeled as f'_{ci} = 8.4 ksi (62 MPa) and coordinates at release are provided as shown in Figure 5.3.

Figure 5.4 shows the impact of using NSC, HPC, and UHPC with 0.5-in. (13 mm), 0.6-in. (15 mm) and 0.7-in. (18 mm) strands, respectively, for a girder spacing of 8 ft (2.4 m). Transition points (marked by a dark circle) show that the maximum span lengths are governed mainly by the service limit state.

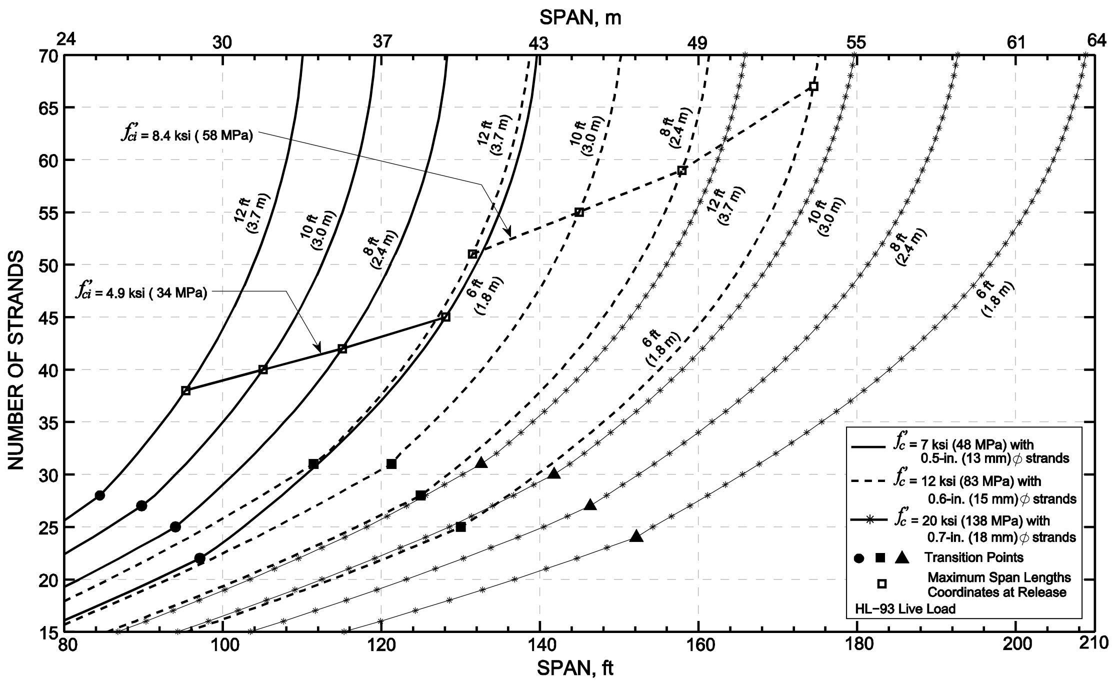

Figure 5.4. Preliminary design chart for BT-72 girders using NSC, HPC, and UHPC.

As shown in the figure, an 8 ksi (55.2 MPa) increase in concrete strength and another strand change of 0.1 in. (2.54 mm) diameter resulted in approximately the same increase in potential span length as when the concrete strength was changed from 7 to 12 ksi (48.3 to 82.8 MPa) and the strand diameter was changed from 0.5 to 0.6-in. (13 to 15 mm). In other words, the increase in span lengths from HPC to UHPC are comparable to those obtained from NSC to HPC. Note that above the transition points, and for NSC and HPC, maximum span lengths are governed by stresses at release. Meanwhile, for UHPC, service controls. Above the transition points, as the concrete strength increases and the girder spacing decreases, stresses at release cease to govern maximum span lengths and service becomes the controlling criterion. Figures 5.1 through 5.4 illustrate the different options available to the designer to conduct a preliminary investigation of the pros and cons of using different combinations of concrete strengths and strand diameters for a BT-72 girder.

5.2. Impact of Continuity

Using the two-span continuous and simple span prestressed girder models, new preliminary design charts were generated for a BT-72 girder to evaluate the impact of continuity on prestressed concrete bridge design (e.g., span lengths, prestressing strands, and girder spacings). Figures 5.5 and 5.7 were developed for simple and two-span continuous girders; different combinations of f'_c equal to 12 and 20 ksi (82.8 and 137.9 MPa) and strand diameters of 0.6 and 0.7 in. (15 and 18 mm) were used. In Figure 5.5, changing from a simple to two-span continuous layout, the span length increased by an average of 10.8, 11.9, 12.5, and 13.2% for girder spacings of 12, 10, 8, and 6 ft (3.7, 3.0, 2.4, and 1.8 m), respectively. As shown in the figure, as the girder spacing decreases, the potential span length increases by approximately the same amount for both the simple span and two-span continuous configuration. For example, considering 40 strands and a decrease in girder spacing from 10 ft (3.7 m) to 8 ft (3.0 m), the span length increased by 8 ft (2.4 m) for simple span layout, and 8.4 ft (2.6 m) for two-span continuous layout.

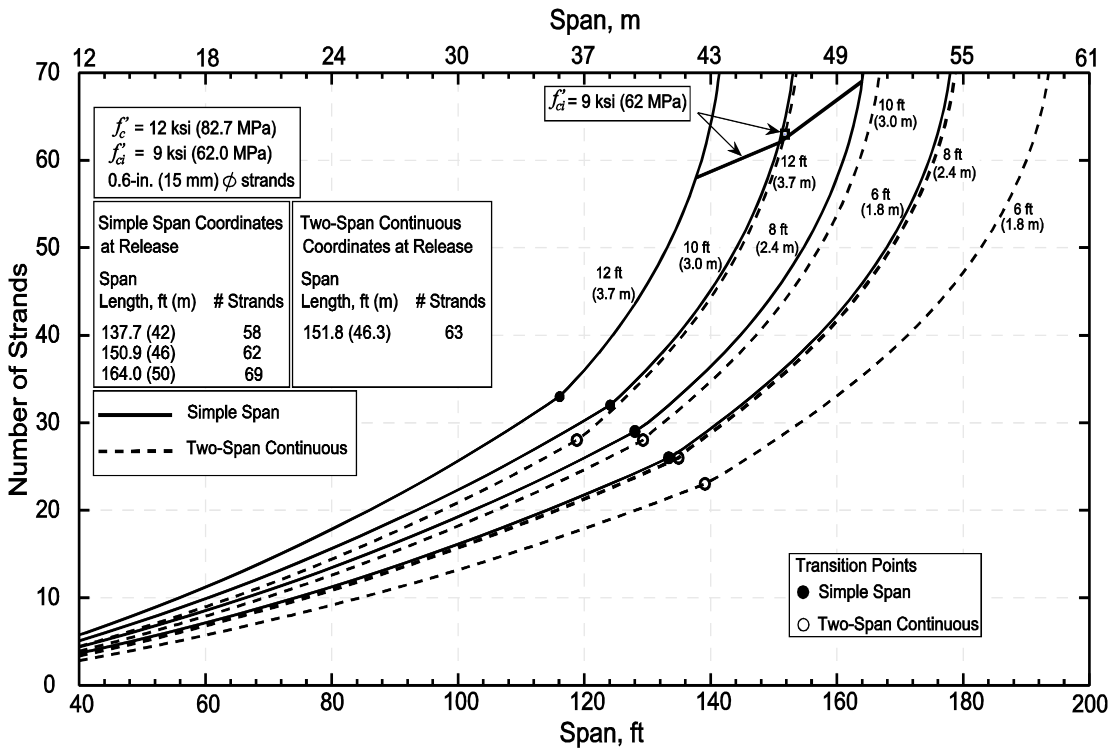

Figure 5.5. Preliminary design chart using f'_C = 12 ksi (82.8 MPa) with strand diameter of 0.6-in. (15 mm) for simple and two-span continuous girder layouts.

Transition points are marked by dark and white circles for simple and two-span continuous layouts, respectively. For a given girder spacing, the number of strands at the transition points is lower for two-span continuous than for simple span, signifying that service governs more for continuous span. In Figure 5.5, an upper bound labeled as f'_{ci} = 9.0 ksi (47 MPa) indicates the maximum span lengths that are governed by stresses at release. As the girder spacing decreases, the upper bound labeled as f'_{ci} = 9.0 ksi (47 MPa) increases meaning that the release limit state ceases to govern maximum span lengths and service becomes the controlling criterion. Simple span and two-span continuous coordinates at release are shown in Figure 5.5. For example, the maximum potential span length governed by stresses at release at a girder spacing of 8 ft (2.4 m) for simple span is 164 ft (50 m) and the number of strands is 69. For a two-span continuous and a girder spacing of 10 ft (3.0 m) the maximum span at release is 151.8 ft (46.3 m). Note that for a girder spacing of 6 ft (1.8 m) for simple span and 6, 8 and 10 ft (1.8, 2.4 and 3 m) for two-span continuous, stresses at release no longer control girder span lengths but service.

To determine whether top or bottom stresses control at release, release stresses at harp points and midspan were plotted versus the span length of the girder as shown in Figures 5.6 and 5.7.

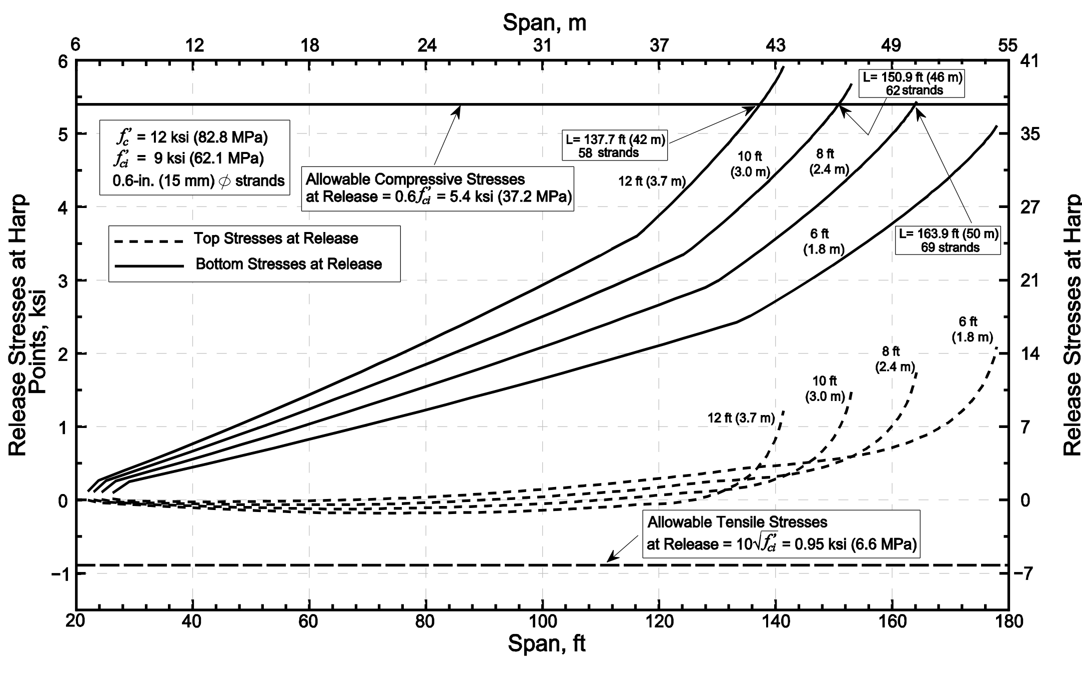

Figure 5.6. Top and bottom release stresses at harp points of simple span girder.

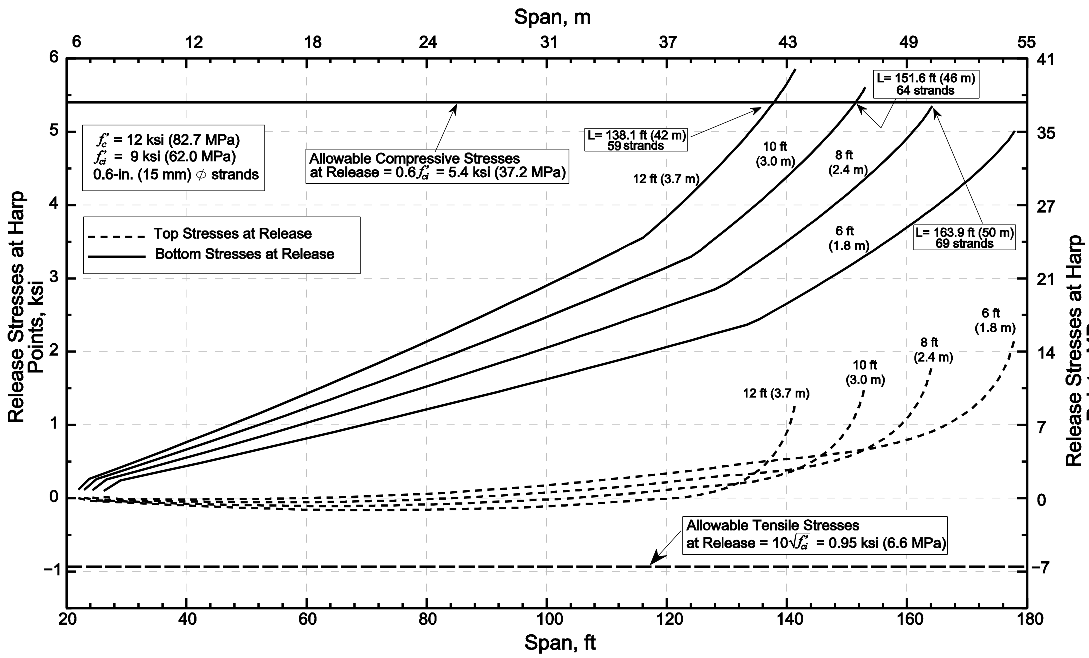

Figure 5.7. Top and bottom release stresses at midspan of simple span girder.

The behavior and design of the end zones will be affected by the transfer length of the prestressing force (Barnes et al., 2003), but will have no impact on the preliminary design charts developed in this study which were based on the final conditions of the structure: service and strength.

Figures 5.6 and 5.7 show that the bottom compressive stresses are larger than the top stresses (tension or compression) at release and consequently, govern the maximum possible span lengths. In addition, Figures 5.6 and 5.7 show that release stresses at the harp points are slightly larger than those at midpan for any girder spacing and therefore, the harp points are the governing locations. For instance, for a given span length of 120 ft (36.6 m) bottom release stresses at harp points are 3.9, 3.2, 2.7, and 2.1 ksi (26.9, 22.1, 18.6 and 14.5 MPa) for girder spacings of 12, 10, 8, and 6 ft (3.7, 3.0, 2.4, and 1.8 m), respectively, meanwhile at midspan are 3.8, 3.1, 2.6, and 2.0 ksi (26.2, 21.4, 17.9, 13.8 MPa) for the same girder spacings, respectively. Furthermore, Figures 5.6 and 5.7 show that as the girder spacing decreases, the potential span length increases and the bottom and top stresses at release decrease and increase, respectively, due to the bending moment increase from the self-weight of the girder.

Figure 5.8 shows the impact of continuity based on concrete compressive strength of 20 ksi (82.8 MPa) and 0.7-in. (15 mm) diameter strand for simple and two-span continuous layouts.

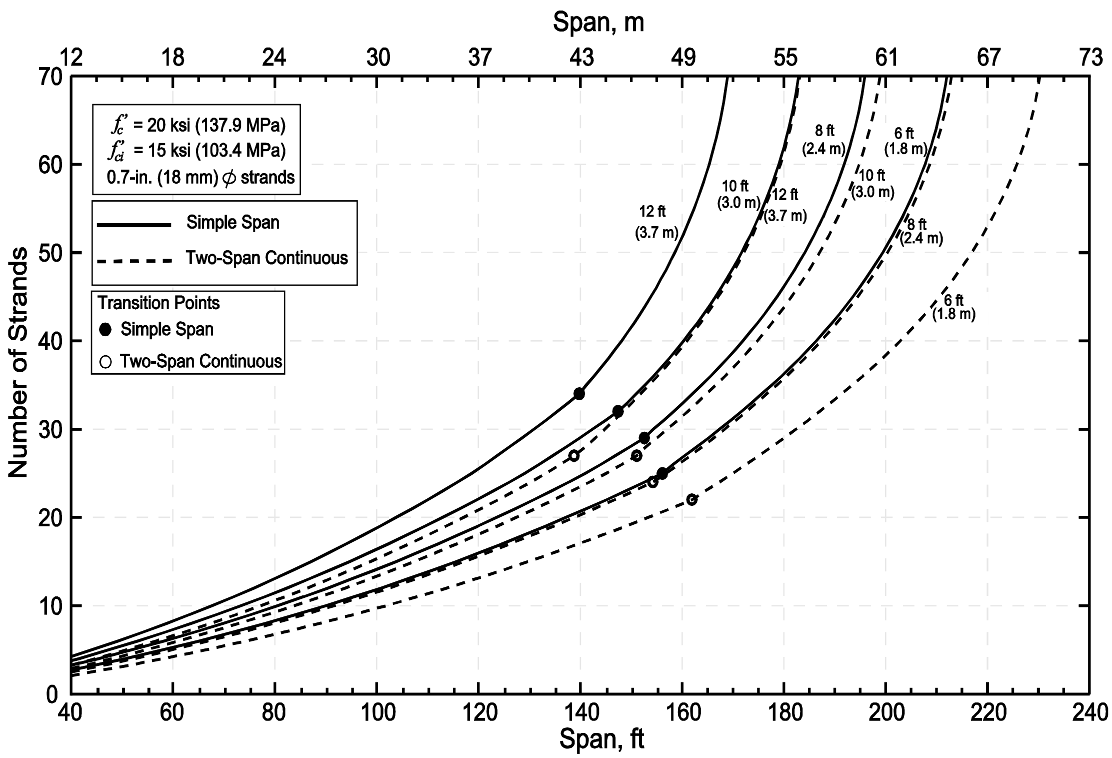

Figure 5.8. Preliminary design chart using f'_c = 20 ksi (137.9 MPa) with a strand diameter of 0.7-in. (18 mm) for simple and two-span continuous layouts.

For girder spacings of 12, 10, 8, and 6 ft (3.7, 3.0, 2.4, and 1.8 m), the potential span length increased by an average of 10.7, 10.9, 10.6 and 10.2%, respectively, due to span continuity. As before, reducing the girder spacing by 2 ft (0.6 m) for a simple span layout, results in approximately the same increase in potential span length as the two-span continuous layout. Transition points show that service governs more the two-span than the simple span layout. As shown in Figure 5.8, maximum span lengths are no longer governed by stresses at release but by the service limit state. The longest span length reached 230.3 ft (70.2 m) for a girder spacing of 6 ft (1.8 m). However, according to Hueste et al. (2012), span lengths above 150 ft (46 m) are not feasible due to weight and length restrictions during girder transportation. Practical implications are further discussed in the next section.

5.3. Practical Implications

Using maximum span lengths and girder spacings from Figure 4.10 (Chapter 4), 5.5 and 5.8, the chart shown in Figure 5.9 was developed. Figure 5.9 shows the maximum attainable span length versus girder spacing for a BT-72 girder for concrete strengths of 8, 12, and 20 ksi (55, 83, and 138 MPa) with 0.6 and 0.7-in. (15 and 18 mm) diameter strands for simple and two-span continuous layouts. For consistency with the PCI-11 charts, the concrete strength at release, f'_{ci}, was assumed as 85% of f'_c for a concrete strength of 8 ksi (55 MPa). For concrete strengths larger than 8 ksi (55 MPa), a value of 75 % of f'_c was assumed. The allowable tensile and compressive stresses at release are shown in Figures 5.6 and 5.7.

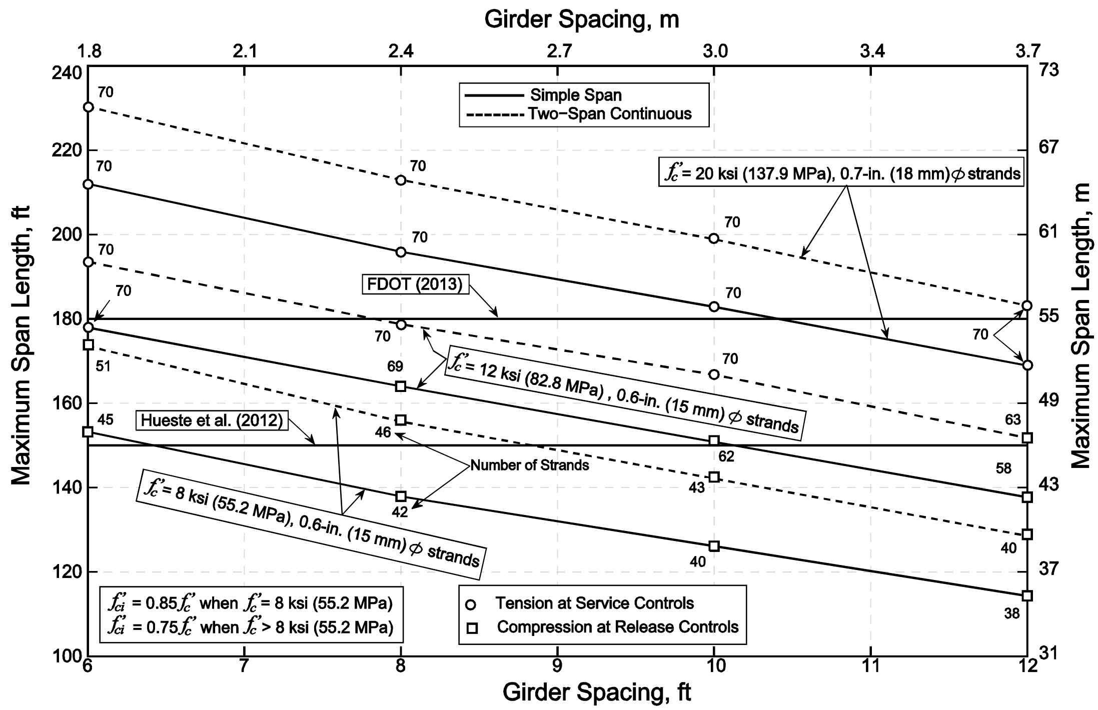

Figure 5.9. Maximum span length versus girder spacing for BT-72 girder using f'_c = 8, 12, and 20 ksi (55, 83, and 138 MPa) with 0.6 and 0.7-in. (15 and 18 mm) diameter strands for simple and two span continuous layouts.

For a given girder spacing, concrete strength, and strand diameter, the maximum attainable span length can be estimated from Figure 5.9 for simple and two-span continuous layouts. The governing limit state and number of strands are provided at girder spacings of 6, 8, 10, and 12 ft (1.8, 2.4, 3.0 and 3.7 m) in the figure. It is shown that bottom compressive stresses at release govern for span lengths less than 180 ft (55 m), except at girder spacings of 6 ft (1.8) for simple span with a concrete strength of 12 ksi (83 MPa) and 8 and 10 ft (2.4 and 3.0 m) for two-span continuous. That is, using HPC with 0.6-in. (15 mm) diameter strands, compressive stresses at release mostly govern for span lengths smaller than 180 ft (55 m) for simple and two-span continuous layouts; for span lengths larger than 180 ft (55 m), tension at service controls. Note that for simple and two-span continuous layouts service controls when the number of prestressing strands reaches 70 at any girder spacing and with concrete strengths of at least f'_c = 12 ksi (83 MPa).

Using a concrete strength of f'_c = 20 ksi (137.9 MPa) and a girder spacing of 6 ft (1.8 m), maximum span lengths of 212 and 230.3 ft (64.6 and 70.2 m) result for simple and two-span continuous layouts, respectively, from Figure 5.9. However, the use of longer full-span girders has limitations based on fabrication, transportation, and erection that must be considered. For instance, Hueste et al. (2012) states that span lengths above 150 ft (46 m) are not feasible due to weight and length restrictions during girder transportation. However, precast beams 210 ft (64 m) in length and more than 150 tons in weight have been allowed in Pennsylvania, Washington, Nebraska and Florida (PCI 2011). Prestressed concrete girders longer than 200 ft (61 m) can be constructed but according to the Florida Department of Transportation (FDOT 2013) the maximum transportable girder length is approximately 180 ft (54.9 m). Nevertheless, longer span lengths for prestressed simple supported concrete girders may be achieved using a new splicing technique (FDOT 2013). The Florida I-beam ninety six (FIB96), for example, can attain a maximum length of 208 ft (63.4 m) using a concrete strength of 8.5 ksi (58.6 MPa) and 215 ft (65.5 m) using 10 ksi (68.9 MPa) concrete. The girder length restriction of 180 ft (54.9 m) from FDOT is represented by a horizontal line in Figure 5.9 labeled as “FDOT (2013)”. Based on this girder length restriction and considering a concrete strength of f'_c = 20 ksi (138 MPa) with 0.7-in.

(18 mm) diameter strands, the maximum span lengths are not feasible at any girder spacing for a two-span continuous layout and at girder spacings smaller than 10.3 ft (3.1 m) for simple spans.

The span-to-depth ratio is an important bridge parameter that should be considered to design prestressed concrete bridges because it influences the structural behavior, cost efficiency, and aesthetics of the structure (Hueste et al. 2012). Traditional minimum depths for constants depth superstructures are given in Table 2.5.2.6.3-1 of the AASHTO LRFD Specifications (2010) as shown in Table 5.1.

Table 5.1. Traditional minimum depths for constant depth superstructures (adapted from AASHTO 2010).

Superstructure		**Minimum Depth (Including Deck)** When variable depth members are used, values may be adjusted to account for changes in relative stiffness of positive and negative moment sections	
Material	**Type**	**Simple Spans**	**Continuous Spans**
Reinforced Concrete	Slabs with main reinforcement parallel to traffic	$\frac{1.2(\ \ +10)}{30}$	$\frac{\ \ +10}{30} \geq 0.54$ ft
	T-Beams	$0.070L$	$0.065L$
	Box Beams	$0.060L$	$0.055L$
	Pedestrian Structure Beams	$0.035L$	$0.033L$
Prestressed Concrete	Slabs	$0.030L \geq 6.5$ in.	$0.027L \geq 6.5$ in.
	CIP Box Beams	$0.045L$	$0.040L$
	Precast I-Beams	$0.045L$	$0.040L$
	Pedestrian Structure Beams	$0.033L$	$0.030L$
	Adjacent Box Beams	$0.030L$	$0.025L$

Table 5.1. Traditional minimum depths for constants depth superstructures (adapted from AASHTO 2010) (continued).

Superstructure		Minimum Depth (Including Deck) When variable depth members are used, values may be adjusted to account for changes in relative stiffness of positive and negative moment sections	
Material	**Type**	**Simple Spans**	**Continuous Spans**
Steel	Overall Depth of Composite I-Beam	0.040L	0.032L
	Depth of I-Beam Portion of Composite I-Beam	0.033L	0.027L
	Trusses	0.100L	0.100L

Barker and Puckett (2007) state that values given in this table are traditional ratios used to guarantee that vibration and deflection would not be a problem. Research conducted by Poon (2009) at the University of Toronto indicated that values given in Table 2.5.2.6.3-1 of the AASHTO LRFD Specifications (2010) give an optimal solution in terms of cost efficiency and aesthetics. According to Leonhardt (1982), the concrete volume is reduced, and the prestressing requirements are increased when a high ratio (i.e., slender girder) is used. For precast I-beam simple span and continuous span layouts, respectively, values of 0.045L and 0.040L (L = girder length) are given in Table 2.5.2.6.3-1 of AASHTO LRFD Specifications (2010). Hence, based on these span-to-depth ratios, the maximum span lengths for a BT-72 girder section for simple-span and two-span continuous layouts are 133.3 ft (40.6 m) and 150 ft (45.7 m), respectively.

The girder length restriction of 150 ft (46 m) from Hueste et al. (2012) is represented by a horizontal line in Figure 5.9 labeled as “Hueste et al. (2012)”. Based on this girder length restriction and considering a concrete strength of f'_c = 8 ksi (55 MPa) with 0.6-in. (15 mm) diameter strands, the maximum span lengths are not feasible at girder spacings smaller than 6.4 ft (1.95 m) for simple spans and for girder spacings smaller than 8.8 ft (2.7 m) for two-span continuous layouts as shown in Figure 5.9. For concrete strengths of f'_c = 12 ksi (83 Mpa) with 0.6-in. (15 mm) diameter strands, maximum span lengths are not feasible for girder spacings smaller than 10.1 ft (3.1 m) for simple spans and at any girder spacing for two-span continuous layouts. Maximum span lengths are not feasible for concrete strengths equal to or greater than 20 ksi (138 MPa) with 0.7-in. (18 mm) at any girder spacing.

According to Brice et al. (2013), real bridge cost savings result from extending spans (reducing the number of piers) and/or reducing the girder lines. As shown in Figure 5.9, changing from a simple to two-span continuous layout, the span length increases by an average of 12.9, 11.6, and 12.5% for concrete strengths of 8, 12 and 20 ksi (55, 83, and 138 MPa), respectively. In addition, the span length increases by an average of 42.9% using span continuity and increasing the concrete strength from 8 to 20 ksi (55 to 138 MPa). Article 5.14.1.4 of the AASHTO LRFD Bridge Design Specifications (2010) provide the requirements for simple-span concrete bridge girders made continuous. Currently, some states in the U.S. do not design continuous span girders but rather have adopted a simple-span design policy.

To evaluate the degree of which bridge owner's may deviate from the minimum requirements given in the LRFD specifications, a survey of state departments of transportation (DOTs)) was conducted by Brice et al. (2013). A total of 38 state DOTs responded to the survey and 42% indicated the adoption of a simple-span policy including Arizona, Colorado, Idaho, Kansas, Louisiana, Minnesota, New York, North Carolina, Oklahoma, Pennsylvania, and Texas. Alternatively, the states of Washington, Michigan, Pennsylvania, and South Carolina design for the more critical of a fully effective continuity connection and simple span. The survey ultimately showed that using the owner-adopted design policy led to stouter structures than those designed using the AASHTO LRFD specifications (2010).

Normally, the overall cost of a bridge is not significantly influenced by the number of prestressing strands except it may exceed the capacity of local precast producers (Brice et al. 2013). From Figure 5.9, it is evident that the number of strands increases as the concrete strength increases and the girder spacing decreases. The maximum number strands assumed for a BT-72 girder is 70; however, it must be determined if the required number of strands is compatible with the prestressing bed capacity of local producers.

Section 2.5.2.6 of the AASHTO LRFD Specifications (2010) states that deformations in bridges including live load deflections and span-to-depth ratios should be limited to avoid undesirable structural behavior or psychological effects. Live load deformation effects and span-to-depth ratio criteria was adopted to limit deterioration of wearing surfaces and local cracking of concrete deck slabs that could adversely affect serviceability and durability. According to the AASHTO LRFD Specifications (2010) Article 2.5.2.6.2 limits the maximum deflection due to live load and impact as follows:

- Vehicular load, general = Span/800
- Vehicular and/or pedestrian loads = Span/1000

No explanations or detailed justifications for these limits are provided in the AASHTO LRFD Design Specifications (2010) articles and/or commentary (Hueste et al. 2012). Deflections due to prestressing force at transfer (camber), dead loads, live loads and impact, were not considered in the development of preliminary design charts in this dissertation. However, these deflections should be considered for the final design of the bridge. In summary, girder length restrictions due to fabrication, transportation, and erection, span-to-depth ratios, number of strands, and the continuous span design policy are issues that significantly influence a preliminary prestressed concrete bridge design and should be considered carefully to optimize the final design of the bridge.

CHAPTER 6

SUMMARY, CONCLUSIONS, AND FUTURE WORK

6.1 Summary

This dissertation provides a simplified method to develop preliminary design charts for prestressed concrete bulb-tee girders considering service load stress limits, flexural strength, and stresses at release. A BT-72 girder was considered to illustrate the procedure for computing the maximum span length based on the number of prestressing strands and girder spacing. The charts were first developed based on the AASHTO Standard Specifications (2002) and compared with the PCI-03 preliminary design charts (2003) for validation purposes. These charts were subsequently adapted to the AASHTO LRFD Bridge Design Specifications (2010) and further confirmed with the PCI-11 charts (2011).

Modifications of the prestressed girder model were made to satisfy the LRFD Service III and Strength I limit states. For Service III, the live load effects and prestress losses were adjusted and for Strength I, live load and dead load effects were adjusted according to LRFD design criteria.

Prestress losses were computed considering shrinkage of the concrete, elastic shortening, creep of the concrete, and relaxation of the steel. The simplified method presented in this study resulted in third-degree polynomial functions whose solutions provided the girder span lengths for a given number of strands and girder spacing based on the release, service, and strength limit states.

Using the simplified LRFD procedure, preliminary design charts were developed for simple span bridges to investigate the impact of concrete strength and strand size on prestressed concrete girder design (including span length capability, number of prestressing strands, and girder spacings). Concrete compressive strengths at 28 days of f'_c= 7 ksi (48 MPa) for NSC, 12 ksi (83 MPa) for HPC, and 20 ksi (138 MPa) for UHPC were considered. In addition, prestressing strands of 0.5-in. (13 mm), 0.6-in. (15 mm), and 0.7-in. (18 mm) diameters were used.

To study the impact of span continuity and strand size, preliminary design charts were developed for simple span and two- span continuous bridges. Concrete strengths of 8, 12 and 20 ksi (55, 83, and 138 MPa) with prestressing strands of 0.6-in. (15 mm) and 0.7-in. (18 mm) diameters were assumed. In the charts, the transition point where strength ceased to govern and service became the controlling limit state is explained and shown to provide valuable design information. Maximum span lengths governed by stresses at release and service were determined to show the maximum attainable span length versus girder spacing for concrete strengths of 8, 12, and 20 ksi (55, 83, and 138 MPa) with 0.6 and 0.7-in. (15 and 18 mm) diameter strands for simple and two-span continuous layouts. Practical limitations on span length based on fabrication, transportation, erection, span-to-depth ratio criteria, and deflections due to live and dead load were discussed to show their influence on the maximum attainable span length given in the preliminary design charts developed in this dissertation.

6.2 Conclusions

The simplified procedure given in this dissertation is a unique contribution to the prestressed concrete bridge profession because it offers a closed-form solution for preliminary girder design. Spreadsheets or commercial software may alternatively be used, however, these tools may require the designer to solve for the span length iteratively to obtain discrete solutions for different combinations of the number of strands and girder spacing.

Many factors can affect preliminary girder design including: regional and/or state polices for calculating prestress losses; types of beam sections (AASHTO, Bulb-tee, I girders); section analysis using different properties (gross, net, transformed); and methods for dead and live load distribution analyses. Such factors can be easily incorporated into the prestressed girder model developed herein that correspond to the design policies adopted by the bridge owner. The development of the preliminary design charts for a BT-72 prestressed concrete girder section presented herein has led to the following findings:

(1) The girder model was formulated and adapted from the AASHTO Standard to the LRFD Specifications and provides the designer more options to consider including different combinations of concrete strengths and strand diameters instead of being limited to a given concrete strength.

(2) The use of the "transition point" was introduced which corresponds to the number of strands and span lengths where the governing limit state changes

from strength to service. The point is located at the intersection of the strength and service curves, and provides the information needed for a designer to distinguish the zones between fully prestressed (uncracked), partially prestressed, and non-prestressed (cracked) members. The transition points between the strength and service limit states for the prestressed girder model showed that the span lengths were governed mostly by service. At this time, the AASHTO LRFD Bridge Design Specifications provides minimal design guidance for partially prestressed members. However, this alternative may be more practical for bridge girders, particularly for longer span lengths due to the large number of strands required to obtain a fully prestressed member.

(3) New LRFD preliminary design charts were generated for a BT-72 girder using normal strength concrete (NSC), high performance concrete (HPC), and ultra-high performance concrete (UHPC). Based on the excellent agreement (within 2% and 4%) between the preliminary design charts developed in this study and those given in the PCI Bridge Design Manuals (2003, 2011), the new LRFD charts were shown to be accurate for the design assumptions made. The charts provide initial results for comparing the potential span length capability of UHPC girders with NSC and HPC.

(4) This dissertation illustrates the increases in span lengths caused by implementation of 0.7 in. (18 mm) diameter strand and UHPC which many state DOTs are considering for future prestressed concrete bridge design. According to Morcous et al. (2011), 0.7-in. (18 mm) diameter strands can be used without

major changes to current production practices and/or the design criteria given in the LRFD specifications.

(5) The preliminary design charts demonstrate the impact of using UHPC and/or larger strand size and/or two-span continuous layouts. Increasing the concrete compressive strength or the strand diameter or using two-span continuous for a given number of strands and girder spacing resulted in an increase of the span length. The effect of using two-span continuous with the combination of UHPC and a larger strand diameter was clearly shown to be much more significant than just increasing the concrete compressive strength or the strand diameter or using two-span continuous layouts. However, the use of longer full-span girders has girder length restrictions due to fabrication, transportation, erection, span-to-depth ratios, and live and dead load deflections that influence a preliminary prestressed concrete bridge design and consequently, should be considered carefully for the final design of the bridge. For instance, Hueste et al. (2012) states that span lengths above 150 ft (46 m) are not feasible due to weight and length restrictions during girder transportation.

The use of UHPC results in more slender girders than current practice which may lead to transportation and erection challenges that may be assessed based on the span lengths given in the new LRFD charts.

However, there are UHPC design alternatives other than increasing the span length that can be considered to reduce material cost and avoid transportation limitations by truck such as increasing the girder spacing (to reduce the number of beam lines) and/or reducing the girder depth.

6.3 Future Work

To further investigate the structural behavior and economic impact on the superstructure of prestressed concrete bridges using the simplified method developed herein, the following recommendations are made based off the findings of the research presented in this dissertation:

(1) The simplified method developed herein is subject to the following limitations: (1) BT-72 sections and (2) interior girders. The new LRFD charts were generated based on allowable tension and flexural strength using the same assumptions as the PCI Bridge Design Manuals (2003, 2010). Future implementation of the simplified procedure requires that Articles of the LRFD specifications related to prestress losses, allowable stresses, material properties, and flexural resistance be updated as research becomes available for concrete strengths larger than the current upper limits of 10 ksi (69 MPa) and 15 ksi (103 MPa), in particular for UHPC.

(2) Camber, dead and live load deflections were not considered to develop the preliminary design charts for concrete prestressed concrete bridge girders presented herein. To improve the designer options to look at different

combinations of concrete strengths and strand diameters, camber, dead and live load deflections should be considered in the simplified method presented in this dissertation.

(3) States such as Washington, Texas, Nebraska, Utah, Florida, Pennsylvania, and the New England states have developed their own girder shapes based on typical AASHTO-PCI bulb-tee sections, AASHTO I-beams, and multi-web stemmed beams given in the PCI Bridge Design Manuals (2003, 2011). It is recommended to implement these girder shapes to the simplified method to expand the designer options and optimize the final design and cost of the superstructure of prestressed concrete bridges.

(4) The AASHTO LRFD Bridge Design Specifications (2010) provides minimal design guidance for partially prestressed members and no guidance related to this issue was provided in the AASHTO LRFD Bridge Design Specifications (2014). Partial prestress girders may be an economical option for bridge design and a more practical alternative for bridge girders, particularly for longer span lengths due to the large number of strands required to obtain a fully prestressed member. Hence, recommendations for partially prestressed members should be developed to optimize the final design of the prestressed concrete bridge girders.

REFERENCES

Abdel-Karim, A., and Tadros M.K., 1995, "State-of-the-Art of Precast/Prestressed Concrete Spliced I-Girder Bridges". *Precast/Prestressed Concrete Institute*, Chicago, IL, 143 pages.

Al-Omaishi N., Tadros MK. and Seguirant SJ., 2009, "Estimating prestress loss in pretensioned, high-strength concrete members", PCI Journal, Vol.54, No. 4, pp. 132-159.

American Association of State Highway and Transportation Officials (AASHTO), 2002, *Standard Specifications for Highway Bridges,* Seventeenth Edition, Washington, D.C.

American Association of State Highway and Transportation Officials (AASHTO), 2007, "AASHTO LRFD Bridge Design Specifications", 4th Edition, Washington, DC.

American Association of State Highway and Transportation Officials (AASHTO), 2010, LRFD Bridge Design Specifications, Fifth Edition, Washington, D.C.

American Association of State Highway and Transportation Officials (AASHTO), 2014, LRFD Bridge Design Specifications, Sixth Edition, Washington, D.C.

American Concrete Institute (ACI). ACI Concrete Terminology, 2013.

Bache, H.H., 1981, "Densified cement/ultra-fine particle-based materials", *Second International Conference on Super-plasticizers*, Ontario, Canada, CBL RAPPORT NR. 40, Technical Report

Barnes RW, Grove JW., and Burns NH., 2003, "Experimental assessment of factors affecting transfer length.", ACI Structural Journal, Vol. 100, No. 6, pp. 740-748.

Barker, R.M. and J.A. Puckett 2007, "Design of Highway Bridges: An LRFD Approach.", Second Edition, John Wiley & Sons, Inc.

Canadian Standards Association, 1978, Design of highway bridges. Standard CAN3-S6-M78.

Castrodale R.W., and White and C.D, 2004, "Extending Span Ranges of Precast Prestressed Concrete Girders", *Transportation Research Board*, *National Cooperative Highway Research Program,* Report No. 517, 603 pages.

Collins, M.P. and Mitchell, D., 1991, “Prestressed Concrete Structures”, Prentice-Hall, Inc., A Division of Simon & Schuster, Englewood Cliffs, NJ, pp. 61-65.

Dassault Systèmes Simulia Corporation, 2009. ABAQUS 6.9-analysis user’s manual, Providence, RI.

Devalapura, R.K., and Tadros, M.K., September-October 1992, “Critical Assessment of ACI 318 Eq. (18-3) for Prestressing Steel Stress at Ultimate Flexure.” ACI Structural Journal, Vol. 89, No. 5, pp. 538-546.

Federal Highway Administration (FHWA), August 2006, “Material Property Characterization of Ultra–High Performance Concrete”, Publication FHWA-HRT-06-103, McLean, VA, pp. 145-161.

Fereig, S.M., 1985, “Preliminary design of standard CPCI prestressed bridge girders by linear programming”, *Canadian Journal of Civil Engineering,* Vol. 12, Issue 1, pp. 213-225.

Ferguson, T.S., “Linear Programming, A Concise Introduction”, 1998, University of California, Department of Mathematics, http://www.math.ucla.edu/~tom/LP.pdf

Florida Department of Transportation Research (FDOT), December 2013, “Long Spans with Transportable Precast Prestressed Girders”, UF Project No. 000829523, FDOT Contract No. BDK75 977-30.

Graybeal, B., 2009, “UHPC Making Strides”, *Public Roads*, Federal Highway Administration, McLean, VA, Vol. 72, No. 4, pp. 17-21.

Graybeal, B., March 2011, “Ultra-High Performance Concrete”. *Technical Note No. FHWA-HRT-11-38,* Federal Highway Administration, McLean, VA, pp. 1-8.

Gunes O., Yesilmen S., 2012, Gunes B., and Ulm F.J., “Use of UHPC in Bridge Structures: Material Modeling and Design”, *Advances in Materials Science and Egineering: 1-12.*

Han, M.Y., Hwang, E.S., and Lee, C.D., 2003, “Prestressed concrete girder with multistage prestressing concept”, *ACI Structural Journal*, 100(6), pp. 723–731.

Hanna, K.E, Morcous, G., and Tadros, M.K., July 2010, “Design Aids of NUI-Girder Bridges”, *Nebraska Department of Roads (NDOR),* Project Number: P322.

Hueste, M.B., Mander J.B., and Parkar A.S., June 2012, "Continuous Prestressed Concrete Girder Bridges", Report No. FHWA/TX-12/0-6651-1, *Texas Department of Transportation Research and Technology Implementation Office,* Vol. 1.

Issa, M. A., Anderson, R., Domagalski, T., 2007, Asfour, S., and Islam, M. S., "Full-scale testing of prefabricated full-depth precast concrete bridge deck panel system", ACI Structural Journal., 104(3), pp. 324–332.

Jeon, S-J., Choi, M-S., and Kim, Y-J., 2012, "A Graphical Assessment for Span Ranges of Prestress Concrete Girder Bridge", *Journal of Bridge Engineering*, Vol. 17, pp. 343-352.

Leet, K.M., Uang, C-M., and Gilbert, A.M., 2008, "Fundamental of Structural Analysis", Third Edition, McGraw-Hill Companies, Inc., New York, NY, pp. 434-435.

Leonhardt, F., 1982, "Bridges: Aesthetics and Design", First Edition, Deutsche Verlags-Anstalt, Stuttgart, Germany.

Liles, P., and Holland, R. B., 2010, "High strength lightweight concrete for use in precast, prestressed concrete bridge girders in Georgia", HPC Bridge Views, 61, pp. 1–3.

Marquez, J., Jauregui D.V., Weldon B.D., and Newtson C., 2012, "Development of Preliminary Design Charts for Prestressed UHPC Bridge Girders", CD-ROM, PCI (Precast/Prestressed Concrete Institute) and National Bridge Conference in Nashville, Tennessee.

Melby, K., Jordet, E. A., and Hansvold, C., 1996, "Long-span bridges in Norway constructed in high-strength LWA concrete", Eng. Struct., 18(11), pp. 845–849.

Meyer, KarlF., and Lawrence F.K, 2002, "Lightweight Concrete Reduces Weight and Increase Span Length of Pretensioned Concrete Bridge Girders", Precast/Prestressed Concrete Institute, Chicago, IL., Vol. 47, No. 1 (January-February), pp. 68-75.

Morcous, G., Hanna, K., and Tadros, M.K., Fall 2011, "Use of 0.7-in.-diameter strands in pretensioned bridge girders", PCI Journal, pp. 65-82.

Nebraska Department of Roads (NDOR) Bridge Operations, Policies, and Procedures (BOPP), 2009.

New Mexico Department of Transportation (NMDOT), April 2013, *Bridge Procedures and Design Guide*, Santa Fe, NM.

Philips, D.T., Ravindran, A., and Solberg, J. 1976, “Operations research: principles and practice”, *John Wiley and Sons*, New York, NY.

Poon, Sandy Shuk-Yan 2009, “Optimization of Span-to-Depth Ratios in High-Strength Concrete Girder Bridges”, M.A.Sc Thesis, University of Toronto, Canada, 146 pages.

Portland Cement Association (PCA) engineering bulletin *High-Strength Concrete* (EB114T) and edited for *Concrete Technology Today*, 1994

Precast/Prestressed Concrete Institute (PCI), 2003, *PCI Bridge Design Manual*, Second Edition, Chicago, IL.

Precast/Prestressed Concrete Institute (PCI), 2011, *PCI Bridge Design Manual*, Third Edition, Chicago, IL.

Ramirez J., Olek J., Rolle E., and Malone B., 2000, “Performance of Bridge Decks and Girders with Lightweight Aggregate Concrete”, *Final Report No. FHWA/IN/JTRP-98/17*, Vol. 1, Indiana Department of Transportation, Purdue University.

Richard, P., and Cheyrezy, M., 1995, “Composite of Reactive Powder Concrete”, *Cement and Concrete Research*, V.25, No. 4, pp.1501-1511.

Russell, H.G. and Graybeal B.A., June 2013, “Ultra-high Performance Concrete: A State-of-the-Art Report for the Bridge Community”, Publication No. FHWA-HRT-13-060.

Seguirant, S.J., July-August 1998, “New Deep WSDOT Standard Sections Extend Spans of Prestressed Concrete Girders.” PCI Journal, pp. 92-105.

Seguirant, S.J., Brice, R. and Khaleghi, B., January-February 2005, “Flexural Strength of Reinforced and Prestressed Concrete T-Beams”, PCI Journal, Vol. 50, No. 1, pp. 44-68.

The MathWorks, Inc., MATLAB and Simulink © 1984-2011

Vadivelu, J., and Z. Ma., 2008, “Potential Impact of 0.7-inch Strands on Precast/Prestressed Concrete Bridge I-Girders: Spacing of Large Diameter Strands”, PCI National Bridge Conference, CD-ROM.

APPENDIX

A.1 Equations 2.12 to 2.19 were used by Jeon et al., 2012 to plot the feasible design domain represented by the shaded area shown in Figure 2.15 (Chapter 2). Equations 2.12 to 2.15 are applied to compute top and bottom stresses at release and service, respectively. Equations 2.16 to 2.19 were derived from Equations 2.12 to 2.15 to compute the girder span length given in Figure 2.15 (Chapter 2).

$$f_{ct} = \frac{P_i}{A_c} - \frac{P_i e_p}{I_c} y_t + \frac{M_{d1}}{I_c} y_t > f_{ci,g,ta} \tag{2.12}$$

$$f_{cb} = \frac{P_i}{A_c} + \frac{P_i e_p}{I_c} y_b - \frac{M_{d1}}{I_c} y_b < f_{ci,g,ca} \tag{2.13}$$

$$f_{ct} = \frac{P_e}{A_c} - \frac{P_e e_p}{I_c} y_t + \frac{M_{d1} + M_{d2}}{I_c} y_t + \frac{M_l}{I_c^*} y_{t,g}^* < f_{c,g,ca} \tag{2.14}$$

$$f_{cb} = \frac{P_e}{A_c} + \frac{P_e e_p}{I_c} y_b - \frac{M_{d1} + M_{d2}}{I_c} y_b - \frac{M_l}{I_c^*} y_b^* > f_{c,g,ta} \tag{2.15}$$

$$l < \sqrt{\frac{n_1 A_{ps} f_{pe}\left(\frac{e_{p,1} y_t}{I_c} - \frac{1}{A_c}\right) + a_4 f'_{c,g}}{\frac{\left[b_1 \gamma_c A_c + b_2\left(\gamma_{c,d} A_d + w_c\right)\right] y_t}{I_c}}} \tag{2.16}$$

$$l < \sqrt{\frac{n_1 A_{ps} f_{pe}\left(\frac{e_{p,1} y_b}{I_c}+\frac{1}{A_c}\right)+a_3 f'_{c,g}}{\frac{\left[b_1 \gamma_c A_c+b_2\left(\gamma_{c,d} A_d+w_c\right)\right] y_b}{I_c}}} \tag{2.17}$$

$$l < \sqrt{\frac{n_1 A_{ps} f_{pe}\left(\frac{e_{p,1} y_t}{I_c}-\frac{1}{A_c}\right)+n_2 A_{ps} f_{pi}\left(\frac{e_{p,2} y_t}{I_c}-\frac{1}{A_c}\right)-a_3 f'_{c,g}}{\frac{\left[b_1 \gamma_c A_c+b_2\left(\gamma_{c,d} A_d+w_c\right)\right] y_t}{I_c}}} \tag{2.18}$$

$$l < \sqrt{\frac{n_1 A_{ps} f_{pe}\left(\frac{e_{p,1} y_b}{I_c}+\frac{1}{A_c}\right)+n_2 A_{ps} f_{pi}\left(\frac{e_{p,2} y_b}{I_c}+\frac{1}{A_c}\right)-a_4 f'_{c,g}}{\frac{\left[b_1 \gamma_c A_c+b_2\left(\gamma_{c,d} A_d+w_c\right)\right] y_b}{I_c}}} \tag{2.19}$$

where:

f_{ct} = top concrete fiber stresses

f_{cb} = bottom concrete fiber stresses

P_i = $nA_{ps}f_{pi}$ = average prestressing force at release

P_e = $nA_{ps}f_{pe}$ = average effective prestressing force

f_{pi} = average prestress at release

f_{pe} = average effective prestress

n = number of sheaths (ducts)

A_{ps} = total área of the strands included in one sheath = 1.84 in.^{2} (1185 mm^2)

e_p = average eccentricity of the strands

I_c = non-composite moment of inertia of girder

I_c^*	= composite moment of inertia of girder
y_b	= non-composite distance from neutral axis to the extreme compression fiber
y_b^*	= composite distance from neutral axis to the extreme compression fiber
y_t	= non-composite distance from neutral axis to the to the extreme tensile fiber
$y^*_{t,g}$	= composite distance from neutral axis to the to the extreme tensile fiber
M_{d1}	= bending moment by the self-weight of a girder
M_{d2}	= bending moment by the self-weight of a deck with the contribution of cross beams (diaphragms) included
M_l	= bending moment by live load with the self-weight of pavement and railing Included
$f_{ci,g,ta} = a_1\sqrt{f'_{ci,g}}$	= allowable tensile concrete girder stress at release as a function of the concrete compressive stress at release, $f'_{ci,g}$
$f_{ci,g,ca} = a_2 f'_{ci,g}$	= allowable compressive concrete girder stress at release as a function of the concrete compressive stress at release, $f'_{ci,g}$
$f_{c,g,ta} = a_3\sqrt{f'_{c,g}}$	= allowable tensile concrete girder stress at service as a function of the concrete compressive stress at service, $f'_{c,g}$
$f_{ci,g,ca} = a_4 f'_{c,g}$	= allowable compressive concrete girder stress at service as a function of the concrete compressive stress at service, $f'_{c,g}$
a_1, a_2, a_3, a_4	= concrete compressive stresses coefficients > 0
b_1, b_2, b_3	= moment coefficients which represent the maximum positive moment occurring in the span, are 0.125 for a simple span and have a lower value for a continuous span

γ_c = unit weight of the girder

$\gamma_{c,d}$ = unit weight of the deck

A_c = concrete area of non-composite section

A_d = area of the deck

l = span length

w_c, w_l = equivalent distributed load due to cross beams and live load, respectively, applied to one girder

A.2 MATLAB Code

```
% A Simplified Method to Develop LRFD Preliminary Design Charts for
Prestressed Concrete Bridges.

% Service Limit State
%Data:
%Cast-in place Slab:
%Structural thickness (in):
%ts = 7.5;
%Concrete strength at 28 dias, f'c(psi):
fcs = 4000;
%Haunch thickness (in):
Ht = 0.5;
%Precast beams: AASHTO-PCI BT-72 Bulb-Tee :
%Concrete strength at release, f'ci (psi):
fci = input ('Beam Concrete strength at release, (psi)= ?');
%Concrete strength at 28 dias (service), f'c:
fcb = input ('Beam Concrete strength at service, (psi)= ?');
%Concrete unit weigth (pcf):
Wc = 150;
%Distance center to center of beams (ft):
%for J = 1 :100
%BS = input('Beam Spacing Vector = [s1,s2,...n] = ? (ft)');
%ts = input('deck thickness Vector = [t1,t2,...n] = ? (in)');
%F = input('Factors to adapt STANDARD to LRFD charts = [f1,f2,...n] = ?');
%R = input('Is there any error ? (y/n) = ','s');
%if  R == 'n'
%break
%else
%clear BS
%end
%end
%Nstr = input('Maximum number of strands to be considered = (a pair
number) ?');
BS = [ 12 10 8 6];
ts = [8.5 7.5 7.5 7.5];
F = [ 1.302927 1.416086 1.50673056 1.642456658];
```

```
Nstr = 70;
LE = length(BS);
AS = input('Do you want to keep previous plot(s)? (y/n) = ','s');
if AS == 'y'
hold on
else
hold off
end
Mu = cell(LE,1);
cont1 = 0;
cont2 = 0;
SFL = cell(Nstr,1);
ROOT = zeros(Nstr, LE);
Yst = zeros(Nstr, 1);
ROOT3 = zeros(Nstr,1);
Pse2 = cell(Nstr,LE);
Psi2 = cell (Nstr,LE);
Psi3 = zeros(Nstr,LE);
Mgt3 = zeros(Nstr,LE);
Mgt4 = zeros(Nstr,LE);
MB = cell(LE,1);
MWS = cell(LE,1);
ML = cell(LE,1);
MG = cell(LE,1);
MS = cell(LE,1);
STG = zeros(LE,1);
SBC = zeros(LE,1);
LRTCH = zeros(Nstr,LE);
LRTTH = zeros(Nstr,LE);
LRBCH = zeros(Nstr,LE);
LRBTH = zeros(Nstr,LE);
LRTCM = zeros(Nstr,LE);
LRTTM = zeros(Nstr,LE);
LRBCM = zeros(Nstr,LE);
LRBTM = zeros(Nstr,LE);
FINN = zeros(Nstr,LE);
ftrH12 = zeros(Nstr,1);
ftrH10 = zeros(Nstr,1);
```

```
ftrH08 = zeros(Nstr,1);
ftrH06 = zeros(Nstr,1);
fbrH12 = zeros(Nstr,1);
fbrH10 = zeros(Nstr,1);
fbrH08 = zeros(Nstr,1);
fbrH06 = zeros(Nstr,1);
ftrM12 = zeros(Nstr,1);
ftrM10 = zeros(Nstr,1);
ftrM08 = zeros(Nstr,1);
ftrM06 = zeros(Nstr,1);
fbrM12 = zeros(Nstr,1);
fbrM10 = zeros(Nstr,1);
fbrM08 = zeros(Nstr,1);
fbrM06 = zeros(Nstr,1);
for V =1 : LE
%Pretensioning Strands: seven wire, low relaxation:
%Area of one strand (in2):
%Ast = 0.153 or Ast = .217 depending of the type of concrete used
% Ast = 0.153 in2 for Normal concrete strength
% Ast = 0.217 in2 for High concrete strength
%Ultimate Stress, f's(ksi):
fs = 270;
%Yield Strength, fy = 0.9*f's (ksi):
Fyp = .9*fs
%Initial Pretensioning, Fsi = 0,75*f's(ksi):
Fsi = 0.75*fs
%Modulus of Elasticity, Es (ksi):
Est = 28500;
% Design Parameters According to PCI-11: Section 6.5.2
% Future wearing surface = 35 psf
% Barriers weight = 0.25 Kip/ft
Wws = 35*BS(1,V)/1000;
%Barrier and railing weight : 0.25 kip/ft
Wb = 0.25;
% Cross Section Properties for a Typical Interior Beam:
%Non-Composite Section:
%A = Area of cross section of precast beam (in2):
A = 767;
```

```
%h = overall depth of precast beam (in) =
h = 72;
%I = moment of Inertia about the centroid of the non-composite precast beam
(in4):
I = 545894;
Ig = I;
%Yb = Distance from centroid to the extreme bottom fiber of the non-
composite precast beam (in):
Yb = 36.6;
%Ybh = Distance from centroid of the hauncch to the extreme bottom fiber of
the non-composite precast beam (in)
Ybh = 72.25
%Ybsl = Distance from centroid of the slab to the extreme bottom fiber of the
non-composite precast beam (in)
Ybsl = 76.25
%Yt = Distance from centroid to the extreme top fiber of the non-composite
precast beam (in):
Yt = 35.4;
%Sb = Section Modulus for the extreme bottom fiber of non-composite
precast beam = I/Yb (in3)
Sb = I/Yb
%St  = Section Modulus for the extreme top fiber of the non-composite
precast beam = I/Yt (in3):
St = I/Yt
%Modulus of Elasticity for the cast-in-place slab (psi):
Ecs = ((Wc)^1.5)*33*sqrt(fcs)/1000
%Modulus of Elasticity for the beam at release (psi) :
Eci = ((Wc)^1.5)*33*sqrt(fci)/1000
%Modulus of Elasticity for the beam at service loads (psi) :
Ecb = ((Wc)^1.5)*33*sqrt(fcb)/1000
%Composite Section
%Efective web width (bew):
%Effective web width of the precast beam is the lesser of
%a.)be1 =Top flange width (in)
be1 = 42;
%b.)be2 = 6*(tflange,max) + web width + 2*fillets (in)
%Maximum Flange Thickness Tfl (in) :
Tfl = 5.5;
```

```
%Web width Ww (in)
Ww = 6;
%Fillets: Fill (in)
Fill = 2;
%be2 = 6*(5.5)+ 6 + 2*(2)
be2 = 6*(Tfl)+ 6 + 2*Fill;
if be1 <= be2
bew = be1;
else
bew = be2;
end
%The effective flange width (be) is the lesser of:
%a.)1/4 span length; (not applicable for bulb tee (BT-72)since min L=70 ft)
%b.) Distance center to center of beams
bef1 = BS(1,V)*12;
%c.)12(effective slab thickness) plus effective beam web with:
bef2 = 12*ts(1,V) + bew;
if bef1 < bef2
be = bef1;
else
be = bef2;
end
%Modular ratio between slab and beam materials
%n = Ec(slab)/Ec(beam)
n= Ecs/Ecb;
%Transformed Section Properties:
%Transformed Flange width = n(effective flange width):
TFW = n*be;
% Transformed Flange area = n(effective flange width)(ts):
TFA = n*be*ts(1,V);
%Transformed haunch width:
THW = n*be1;
%Transformed Area of the haunch:
THA = n*be1*Ht;
 % Properties of Composite Section:
%Total Area of the composite section = Beam + Haunch + Slab
Ac = A + THA + TFA;
%hc = Total height of composite section :
```

```
hc = 80;
%Ybc = Distance from the centroid of the composite section to extreme
bottom fiber of the precaste beam (in):
Ybc = (A*Yb + THA*Ybh + TFA*Ybsl)/Ac;
%Ic = Moment of Inertia of the composite section (in4)
format ('long')
Ic = (I + A*(Ybc-Yb)^2)+ (((1/12)*THW*Ht^3)+THA*(Ybc-Ybh)^2 ) +
(((1/12)*TFW*(ts(1,V))^3)+ TFA*(Ybc-Ybsl)^2);
%Ytg  = distance from the centroid of the composite section to extreme top
fiber of the precaste beam:
Ytg = h-Ybc;
%Ytc = Distance from the centoid of the composite section to extreme top
fiber of the slab:
Ytc = hc-Ybc;
%Sbc = composite section modulus for extreme bottom fiber of the precast
beam = Ic / Ybc:
Sbc = Ic/Ybc;
%Stg = composite section modulus for top fiber of the precast beam =   Ic /
Ytg:
Stg = Ic/Ytg;
%Stc = composite section modulus for top fiber of the slab
Stc = Ic/(n*Ytc);
Dead Loads:
%Wg = Beam weight kip/ft:
Wg = 0.799;
% 8 in slab weight:
Ws = (Wc/1000)*((ts(1,V) + 0.5)/12)*BS(1,V);
%Haunch weight:
Wh = (Ht/12)*(be1/12)*(Wc/1000);
% LIVE LOAD : Consider HS25 Truck = 1.25 x Standard HS20 Truck (Used
in many states)
%P = 32*1.25;
P = 32;
% Mc = Flexural Moment due to HS25 Truck at the middle of the Span L
syms L
Mc = (P/2)*(((9/8)*L)+(42/4))-14*P;
% Df = Distribution Factor
Df = (BS(1,V)/5.5)*(1/2);
```

```
% IM = Impact Factor
IM = (50/(L+125))+ 1;
% MLL = Flexural Moment due to Live Load plus Impact
MLL = ((P/2)*(((9/8)*L)+42/4)-
14*P)*((BS(1,V)/5.5)*(1/2))*(1+(50/(L+125)))*F(1,V)
ME = subs(MLL, L, 120)
%Ybs = Distance from center of gravity of the strand to the bottom fiber of
the beam
% eccentricity at midspan : Ybs
% Data for Strands Arrangement according to AASHTO/PCI Standard
PRODUCTS
AA=[1 12 12; 2 12 24; 3 8 32; 4 4 36; 5 2 38; 6 2 40; 7 2 42; 8 2 44; 9 2 46;
10 2 48; 11 2 50;
12 2 52; 13 2 54; 14 2 56; 15 2 58; 16 2 60; 17 2 62; 18 2 64; 19 2 66; 20 2
68; 21 2 70;
22 2 72; 23 2 74; 24 2 76; 25 2 78; 26 2 80; 27 2 82; 28 2 84; 29 2 86; 30 2
88; 31 2 90;
32 2 92; 33 2 94; 34 2 96; 35 2 Nstr];
%Coputing Strand eceentricity at midspan :
Ybs = zeros(Nstr,1);
for J = 1:12
Ybs(J) = 2;
end
for J = 13 : 24
Ybs(J) = (12*2 + (J-12)*4)/J;
end
for J= 25: 32
Ybs(J) = (12*2 + 12*4 + (J-24)*6)/J;
end
for J = 33 : 36
Ybs(J) = (12*2 + 12*4 + 8*6 +(J-32)*8)/J;
end
con = 0;
K1 = 36;
K = 5;
KON = Ybs(J);
for J = 37 : Nstr
Ybs(J) = (KON*(K1) + (J-K1)*K*2)/J;
```

```
con = con+1;
if con >=2
K1=K1+con;
K=K+1;
KON = Ybs(J);
con = 0;
end
end
% ec = Strand eccentricity with respect to the centroid of the
% non-precast beam = Yb-Ybs
ec = zeros(Nstr,1);
for R = 1 : Nstr
ec(R) = Yb-Ybs(R);
end
%disp('The strand eccentricity for 44 strands is: ec = (in)')
%disp(ec(44))
% Compute Bottom tensile stress due to apllied load, considering:
% fb = (Mg+Ms)/Sb     +    (Mb+ Mws + MLL+I)/Sbc
% Compute Mg: Unfactored bending Moment due to beam self-weight,ft-kip
Mg = Wg*L^2/8;
% Compute Ms : Unfactored bending Moment due to slab and haunch
weights:
Ms = ((Ws + Wh)/2)*(L^2/4);
% Compute Mb : Unfactored bending Moment due to Barriers:
Mb = Wb*L^2/8;
% Compute Mws: Unfactored bending Moment due to wearing surface:
Mws = Wws*L^2/8;
% MLL + I = Refer to Line # 151
fb = ((Mg + Ms)*12/Sb) + (Mb + Mws + 0.8*MLL)*12/Sbc ;
FB = subs(fb, L, 120);
%Compute Allowable Tensile strength at service ( Fb ):
% for dia = 0.5 in,  Ast = 0.153 in2
% for dia = 0.6 in,  Ast = 0.217 in2
% for dia = 0.7 in,  Ast = 0.294 in2
if fcb >= 12000
Fb = 8*sqrt(fcb);
Ast = 0.217;
dia = 0.6;
```

```
ft = 10*sqrt(fci);
fb2 = 0.6*fci;
% where dia = nominal diameter of a 7 wire low relaxation strand in inches
else
Fb = 6*sqrt(fcb);
Ast = 0.217;
dia = 0.6;
ft = 7.5*sqrt(fci);
fb2 = 0.6*fci;
end
disp('The Allowable Tensile strength at service is =(psi)')
disp(Fb)
%Compute Prestress Losses
%Total Losses = fPES + fPLT
%fPES = Prestress Losses due to Elastic Shortening
%fPLT = Prestress Losses due to creep, shrinkage and relaxation
%To compute fPES use Alternative approach from LRFD Eq.(5.9.5.2.3a-1)
%LRFD fifth Edition 2010
Aps = zeros(Nstr,1);
for J =1 : Nstr
Aps(J) = J*Ast;
end
%computing fPES (Prestress Losses due to Elastic Shortening )
fPES = cell(Nstr,1);
for J=1: Nstr
fPES{J,1} = (Aps(J)*Fsi*(Ig+(ec(J)^2)*A)-
ec(J)*Mg*12*A)/(Aps(J)*(Ig+(ec(J)^2)*A)+(A*Ig*Eci/Est));
end
%computing fPLT (Prestress Losses due to creep, shrinkage and relaxation)
%To compute fPLT use Aproximate Estimate of Time-Dependent Losses
%from LRFD Eq. (5.9.5.3.-1)
%Gh=Correction factor for relative humidity of the ambient air
%Gst=Correction factor for concrete strength @ time of transfer
%fPR=Estimate of relaxation loss = 2.4 ksi for low relaxation strands
%RH=Average Annual ambient humidity (%)
RH = 70;
Gh = 1.7-0.01*RH;
Gst = 5/(1+(fci/1000));
```

```
341 fPR = 2.4;
342 fPLT = cell(Nstr,1);
343 for J = 1 : Nstr
344 fPLT{J,1} = (10*Fsi*Aps(J)*Gh*Gst/A) + 12*Gh*Gst + fPR ;
345 end
346 %Total Losses at SErvice Loads
347 %Total Losses = TLOS = fPES + fPLT
348 TLOS = cell(Nstr,1);
349 for J = 1:Nstr
350 TLOS{J,1} = fPES{J,1} + fPLT{J,1};
351 end
352 %subs(TLOS{44,1}, L, 120)
353 %Compute Effective Final Prestress (ksi)
354 %fse = 0.75*f's - Total final losses
355 %fse = 0.75*(270 ksi) - TLOS
356 %Compute Pse = Effective final prestress in Kips
357 %Pse = Number of Strands*Cross sectional Area*fse
358 Pse = cell(Nstr,1);
359 Psi = cell(Nstr,1);
360 for J=1 :Nstr
361 Pse{J,1} = J*Ast*(0.75*fs - TLOS{J,1});
362 Psi{J,1} = J*Ast*(0.75*fs - fPES{J,1});
363 end
364 for J = 1: Nstr
365 Pse2{J,V} = Pse{J,1};
366 Psi2{J,V} = Psi{J,1};
367 end
368 % subs(Pse{44,1}, L, 120)
369 %Set the required precompression (fb - Fb); (Refer to 199 and 212
370 %lines) equal to the bottom fiber stress due to prestress:
371 % fb - Fb = Pse/A   +   Pse*(ec)/Sb
372 % A = Refer to line 48
373 % Pse = Refer to line 285
374 % ec = Refer to line 157
375 % Sb = Refer to line 62
376 %!!!!!! SET EQUATION  FOR SOLVE L : SFL = fb - Fb - Pse/A -
377 Pse*(ec)/Sb =0
378 %SFL = cell(Nstr,1);
```

```
%ROOT = zeros(Nstr, LE);
for J=1:Nstr
SFL{J,1} = fb-(Fb/1000)-(Pse{J,1}/A) - (Pse{J,1}*ec(J)/Sb);
end
% subs(SFL{44,1}, L, 120)
% Get Polinomial coefficient vector and compute polinomial roots
D = cell(Nstr,1);
C = cell(Nstr,1);
RR = cell(Nstr,1);
%ROOT = zeros(Nstr, LE);
%Yst = zeros(Nstr, LE);
RO = zeros(3,1);
for J = 1 :Nstr
D{J,1} = (L+125)*SFL{J,1};
D{J,1} = collect(D{J,1});
C{J,1} = sym2poly(D{J,1});
RR{J,1} = roots(C{J,2});
RO = roots(C{J,1});
for H = 1 : 3
if imag(RO(H,1))==0
RO(H,1) = RO(H,1);
else
RO(H,1) = 0;
end
end
Yst(J,1) = J;
end
cont1 = cont1 + 1;
if cont1 == 1
for Z=1:Nstr
ROOT3(Z,1) = ROOT(Z,1);
end
plot(ROOT3,Yst, 'b')
else
end
if cont1 == 2
for Z=1:Nstr
ROOT3(Z,1) = ROOT(Z,2);
```

```
end
plot(ROOT3,Yst, 'g')
else
end
if cont1 == 3
for Z=1:Nstr
ROOT3(Z,1) = ROOT(Z,3);
end
plot(ROOT3,Yst, 'r')
else
end
if cont1 == 4
for Z=1:Nstr
ROOT3(Z,1) = ROOT(Z,4);
end
plot(ROOT3,Yst, 'k')
else
end
xlabel('SPAN, (ft)'),ylabel('NUMBER OF STRANDS')
if fcb == 7000
title('AASHTO-PCI Bulb-Tee-BT-72, using fc = 7000 psi')
else
title('AASHTO-PCI Bulb-Tee-BT-72, using fc = 12000 psi')
end
grid on, axis([70 170 20 70])
for g = 1 : 100
STR = input('label text for this curve =','s');
RE = input('Is there any error ? (y/n) = ','s');
if RE == 'n'
 break
else
end
end
gtext(STR)
% Flexural Strength: Computing Mu (Ultimate Moment)
% Using Group 1 load factor design loading combination, given in
% Section 9.3.4.3 of the Standard Specifications:
% Mu = 1.3[Mg + Ms + Mb + Mws + 1.67*(MLL+I)]
```

```
Mu{V,1} = 1.25*(Mg + Ms + Mb) + 1.5*Mws + 1.75*(MLL);
MB{V,1} = Mb;
MWS{V,1} = Mws;
ML{V,1} = MLL;
MG{V,1} = Mg;
MS{V,1} = Ms;
STG(V,1)= Stg;
SBC(V,1) = Sbc;
end
hold off

% Flexural Strength Program for Composite T-Beams
% Using Strain Compability
%HT = Overall composite section depth,(in)
HT = h+ts(1,V);
% be =Deck slab width, (in)
%ts = Structural deck slab thickness, (in)
%flange T-Beam thickness, (in): see figs. 1 and 2 on July 4th 2011 Notes
tf = 3.5;
%Width of the Bulb-Tee(Bt-72), (in)
bf = bew;
%bw = input ('Width of girder web, (in)
tw = Ww ;
%fpcs = input ('Design concrete Slab strength, (psi)
fpcs =  fcs ;
%fpcg = input ('Design concrete Girder strength, (psi)
fpcg = fcb;
%Fillets (According to figures 1 and 2 July 4th, 2011) in inches:
f1 = 2;
f2 = 2;
f3 = 2;
% hl = see figs 1 and 2 July 4th, 2011 in inches
hl = 69;
% Strand Location :
Ys = zeros(Nstr,1);
for J = 1:12
Ys(J) = 2;
end
```

```
for J = 13 : 24
Ys(J) = 4;
end
for J= 25: 32
Ys(J) = 6;
end
for J = 33 : 36
Ys(J) = 8;
end
for J = 37 : 2: Nstr
Ys(J) = Ys(J-2) + 2;
end
for J = 38 : 2 :Nstr
Ys(J) = Ys(J-2) + 2;
end
%computing the allowable assumed compressive height, hcr:
hcr = zeros(Nstr,1);
for J=1:Nstr
hcr(J) = HT-Ys(J)-(dia/2);
if hcr(J) > hl
hcr(J) = hl;
else
end
end
%Computing N ; N = Number of Slices to be considered through hcr (the
%allowable assumed copressive heigth):
%assume to have 100 slices
%To control the slices width, it will be considered that the slices
%width can not be greater than 0.33333 = 7/21. This value was taken
%fronm Appendix B (Flexural Strength Calculations for Composite T-Beams
%from Stephen J. Seguirant, Brice, and Khaleghi PCI Journal 2005
N = zeros (Nstr,1);
for J = 1 : Nstr
AN = 100;
for K = 1:5000
if (hcr(J)/AN) > (7/21)
AN = AN + 1;
else
```

```
break
end
end
N(J) = AN;
end
%Computing the number of slices (N1,.. N5)that corresponds to each area A1,
%A2...A5, See Fig. 3 and refer to page 4, on July 4th, 2011 Notes.
N1 = zeros(Nstr,1);
N2 = zeros(Nstr,1);
N3 = zeros(Nstr,1);
N4 = zeros(Nstr,1);
N5 = zeros(Nstr,1);
for J = 1: Nstr
w1 = ts(1,V)*N(J)/hcr(J);
N1(J) = round(w1);
w2 = tf*N(J)/hcr(J);
N2(J) = round(w2);
w3 = f1*N(J)/hcr(J);
N3(J) = round(w3);
w4 = f2*N(J)/hcr(J);
N4(J) = round(w4);
N5(J) = N(J)-N1(J)- N2(J)- N3(J) - N4(J);
%NN = [N(J) N1(J) N2(J) N3(J) N4(J) N5(J);]
end
%Aps = input ('Area of prestressing steel, (in2)
Aps = zeros(Nstr,1);
for J =1 : Nstr
Aps(J) = J*Ast;
end
%dp = input('Depth to centroid of prestressing steel, (in)
dp = zeros(Nstr,1);
for J =1 : Nstr
 dp(J)= HT - Ybs(J);
end
%Ep = input('Modulus of elasticity of prestressing steel, (ksi)
Ep = Est;
%fpe = input('Effective prestress after all losses, (ksi)
% fpe value is computed according to Parametric Study made by
```

```
% Seguirant, Brice and Khaleghi, 2005,page 48, after formula 15.
fpe = zeros(Nstr,1);
for J = 1 : Nstr
fpe(J) = 158-0.2*abs(J-20);
end
%For the Deck and Girder concrete:
Ecs2 = (40000*sqrt(fpcs) + 1000000)/1000;
ns = 0.8 + (fpcs/2500) ;
ng = 0.8 +(fpcg/2500) ;
Ecg = (40000*sqrt(fpcg) + 1000000)/1000;
%Compute Strain in the Slab when fc reaches f'c:
Epcs = (fpcs/Ecs2)*(ns/(ns-1));
Epcg =(fpcg/Ecg)*(ng/(ng-1));
Nmax =max(N);
y = zeros(Nmax,1);
Ecf = zeros(Nmax,1);
fc = zeros(Nmax,1);
Pc = zeros(Nmax,1);
Eps = zeros(Nmax,1);
fsi = zeros(Nmax,1);
SM = zeros(Nmax,1);
Tsi = zeros(Nmax,1);
kON = 0;
J = 0;
OMn = zeros(Nstr,1);
%Compute y(I,1) coordinates for each strip.
for J = 1: Nstr
% Compute girder concrete areas
% A1,A2,......A5= Girder concrete areas.
% For A1:
y(1,J) = ts(1,V)/(2*N1(J));
for I = 2 : N1(J)
y(I,J) = y((I-1),J) + (ts(1,V)/N1(J));
end
%For A2:
y((N1(J) + 1),J) = ts(1,V)+(tf/(2*N2(J)));
for I = (N1(J)+4): N1(J) + N2(J)
y(I,J) = y((I-1),J) + (tf/N2(J));
```

```
end
%For A3:
y((N1(J) + N2(J)+ 1),J) = ts(1,V) + tf + (f1/(2*N3(J)));
for I =(N1(J) + N2(J)+ 2)  : N1(J) + N2(J)+ N3(J)
y(I,J) = y((I-1),J) + (f1/N3(J));
end
%For A4:
y((N1(J) + N2(J)+ N3(J)+ 1),J) = ts(1,V) + tf + f1 + (f2/(2*N4(J)));
for I = (N1(J) + N2(J)+ N3(J)+2) : N1(J) + N2(J)+ N3(J)+ N4(J)
y(I,J) = y((I-1),J) + (f1/N4(J));
end
%For A5:
y(( N1(J) + N2(J)+ N3(J)+ N4(J)+ 1),J) = ts(1,V) + tf + f1 + f2 + ((hcr(J)-
(ts(1,V)+tf+f1+f2))/(2*N5(J)));
for I = ( N1(J) + N2(J)+ N3(J)+ N4(J)+2) : N1(J) + N2(J)+ N3(J)+ N4(J)+
N5(J)
y(I,J) = y((I-1),J) + ((hcr(J)-(ts(1,V)+tf+f1+N3(J)))/N5(J));
end
end
%Computing differential Areas
%DA1, DA2,... DA5 = Differential Areas corresponding to A1.. A5 defined
above.
%Incremental Area = width*slice thickness;
%slice thickness = Deck-girder area thickness/number of slices (N1 or N2 or...
N5)
d1 = max(N1 + N2 + N3);
d2 = max(N1 + N2 + N3 + N4);
DA1 = zeros(Nstr,1);
DA2 = zeros(Nstr,1);
DA3 = zeros(d1,Nstr);
DA4 = zeros(d2,Nstr);
DA5 = zeros(Nstr,1);
A1 = zeros(Nstr,1);
A2 = zeros(Nstr,1);
A3 = zeros(Nstr,1);
A4 = zeros(Nstr,1);
A5 = zeros(Nstr,1);
for J = 1 : Nstr
```

```
DA1(J) = be*ts(1,V)/N1(J);
DA2(J) = bf*tf/N2(J);
for I = N1(J) + N2(J) +1 : N1(J) + N2(J) + N3(J)
x = (((bf-tw)/2)-f3)*(f1-(y(I,J)-tf-ts(1,V)))/f1;
DA3(I,J) = (2*x*f1/N3(J)) + (tw+2*f3)*(f1/N3(J));
end
for I =  N1(J) + N2(J) + N3(J)+1 : N1(J) + N2(J) + N3(J) + N4(J)
x = f3*(f2-(y(I,J)-ts(1,V)-tf-f1))/f2;
DA4(I,J) = (2*x*f2/N4(J)) + (tw*f2/N4(J));
end
DA5(J) = tw*(hcr(J)-(ts(1,V)+tf+f1+f2))/N5(J);
end
for J =1 :Nstr
A1(J) = N1(J)*DA1(J);
A2(J) = N2(J)*DA2(J);
for I = N1(J) + N2(J) +1 : N1(J) + N2(J) + N3(J)
A3(J) = A3(J) + DA3(I,J);
end
for I =  N1(J) + N2(J) + N3(J)+1 : N1(J) + N2(J) + N3(J) + N4(J)
A4(J) = A4(J) + DA4(I,J);
end
A5(J) = N5(J)*DA5(J);
end
cc = 0;
Q = J;
for J=1 : Nstr
for cc = hcr(Q)/N(Q): hcr(Q)/(100*N(Q)):hcr(Q)
%compute Strain in the first concrete slice Ecf(1,1) caused by fc
Ecf(1,J)= (0.003/cc)*(cc-y(1,J));
da  = DA1(J);
nn = ns;
Epc = Epcs;
fpc = fpcs;
if (Ecf(1,J)/(Epc/1000)) < 1.0
k = 1.0;
else
k = 0.67 + (fpc/9000);
end
```

```
%compute compression Force, Pc(I,1)
fc(1,J) = (fpc/1000)*nn*(Ecf(1,J)/(Epc/1000))/(nn-
1+(Ecf(1,J)/(Epc/1000))^(nn*k));
Pc(1,J) = fc(1,J)*da;
%Compute moment related to the top combressive concrete force about top
%compressive T-Beam fiber:
SM(1,J) = fc(1,J)*da*y(1,J);
%Compute tensile strain in prestressing steel:
Eps(1,J) = 0.003*((dp(J)/cc)-1) + (fpe(J)/Ep);
%compute Tensile stress in prestressing steel using power formula:
fsi(1,J) = Eps(1,J)*(887 + (27613/((1 + (112.4*Eps(1,J))^7.36))^(1/7.36)));
if fsi(1,J) > 270
fsi(1,J) = 270;
else
end
%compute Tensile Force:
Tsi(1,J) = fsi(1,J)*Aps(J);
if Tsi(1,J)-Pc(1,J)< 0
% Compute Nominal Flexural strength:
Mn = Pc(1,J)*(dp(J)-y(1,J));
% Compute Factor Resistance O:
dt = HT-2;
O = 0.5 + 0.3*((dt/cc)-1);
if O >1.0
O = 1.0;
else
end
if O < 0.75
O = 0.75;
else
end
% Compute facored flexural resistance:
OMn(J) = O*Mn;
else
end
for I =2 : N(J)
if cc >= y(I,J)
%assume cc = neutral axis depth = t/N
```

```
%cc(I,1) = 34.42;
%compute Strain in the concrete slice Ecfg(I,1) caused by fc
Ecf(I,J)= (0.003/cc)*(cc-y(I,J));
if y(I,J) <= ts(1,V)
fpc = fpcs;
da = DA1(J);
nn = ns;
Epc = Epcs;
else
end
if y(I,J) > ts(1,V) && y(I,J) <= (ts(1,V)+tf)
fpc = fpcg;
da = DA2(J);
nn = ng;
Epc = Epcg;
else
end
if y(I,J) > (ts(1,V)+tf) && y(I,J) <= (ts(1,V) + tf + f1)
fpc = fpcg;
da = DA3(I,J);
nn = ng;
Epc = Epcg;
else
end
if y(I,J) > (ts(1,V)+tf+f1) && y(I,J) <= (ts(1,V) + tf + f1 + f2)
fpc = fpcg;
da = DA4(I,J);
nn = ng;
Epc = Epcg;
else
end
if y(I,J) > (ts(1,V)+tf+f1+f2) && y(I,J) <= (ts(1,V) + tf + f1 + f2 + (hcr(J)-
(ts(1,V)+tf+f1+f2)))
fpc = fpcg;
da = DA5(J);
nn = ng;
Epc = Epcg;
else
```

```
end
if (Ecf(I,J)/(Epc/1000)) < 1.0
k = 1.0;
else
k = 0.67 + (fpc/9000);
end
%Compute concrete strees
fc(I,J) = (fpc/1000)*nn*(Ecf(I,J)/(Epc/1000))/(nn-
1+(Ecf(I,J)/(Epc/1000))^(nn*k));
%Compute resultant compression force in concrete, Pc(I,1)
Pc(I,J) = fc(I,J)*da + Pc((I-1),J);
%Compute sum of moments related to combressive concrete forces about top
%compressive T-Beam fiber:
SM(I,J) = fc(I,J)*da*y(I,J) + SM((I-1),J);
%Compute tensile strain in prestressing steel:
Eps(I,J) = 0.003*((dp(J)/cc)-1) + (fpe(J)/Ep);
%compute Tensile stress in prestressing steel using power formula:
fsi(I,J) = Eps(I,J)*(887 + (27613/((1 + (112.4*Eps(I,J))^7.36))^(1/7.36)));
if fsi(I,J) > 270
fsi(I,J) = 270;
else
end
KON = I;
%compute Tensile Force:
Tsi(I,J) = fsi(I,J)*Aps(J);
else
end
if Tsi(I,J)-Pc(I,J)< 0
break
else
end
end
% cc
%  Tsi(KON,1)
%  Pc(KON,1)
% Tsi(KON,1)-Pc(KON,1)
if Tsi(I,J)-Pc(I,J)< 0
display('Neutral axis Location from the Top T-beam fiber')
```

```
J
cc
KON
Tsi(I,J)
Pc(I,J)
Tsi(I,J)-Pc(I,J)
break
else
end
end
% compute compressive concrete force resultant location from top
% T-Beam fiber:
Yr = SM(I,J)/Pc(I,J);
%Compute Nominal Flexural Moment Resistant :
Mn = Pc(I,J)*(dp(J)-Yr);
Pc(I,J);
Yr
Mn
% Compute Factor Resistance O:
dt = HT-2;
O = 0.5 + 0.3*((dt/cc)-1);
if O >1.0
O = 1.0;
else
end
if O < 0.75
O = 0.75;
else
end
% Compute factored flexural resistance:
OMn(J) = O*Mn/12;
FM = OMn(J);
FM
end
SFL = cell(LE,Nstr);
ROOT2 = zeros(V, LE);
%Yst2 = zeros(V, LE);
Yst2 = zeros(Nstr, 1);
```

```
for V =1 : LE
for J = 1 : Nstr
%SET EQUATION Mu{V,1} = OMn (J)  SOLVING FOR L :
SFL{V,J} = Mu{V,1} - OMn(J);
% subs(SFL{44,1}, L, 120)
%Get Polinomial coefficient vector and compute polinomial roots
D = cell(V,1);
C = cell(V,1);
RR = cell(V,1);
D{V,J} = (L+125)*SFL{V,J};
D{V,J} = collect(D{V,J});
C{V,J} = sym2poly(D{V,J});
RR{V,J} = roots(C{V,J});
RO = roots(C{V,J});
for H = 1 : 3
if imag(RO(H,1))==0
RO(H,1) = RO(H,1);
else
RO(H,1) = 0;
end
end
ROOT2(J,V) = max(RO);
Yst2(J,1) = J;
end
cont2 = cont2 + 1;
if cont2 == 1
for Z=1:Nstr
ROOT3(Z,1) = ROOT2(Z,1);
end
plot(ROOT3,Yst2,'bo:')
else
end
grid on
hold on
if cont2 == 2
for Z=1:Nstr
ROOT3(Z,1) = ROOT2(Z,2);
end
```

```
plot(ROOT3,Yst2, 'go:')
else
end
if cont2 == 3
for Z=1:Nstr
ROOT3(Z,1) = ROOT2(Z,3);
end
plot(ROOT3,Yst2, 'ro:')
else
end
if cont2 == 4
for Z=1:Nstr
ROOT3(Z,1) = ROOT2(Z,4);
end
plot(ROOT3,Yst2,'ko:')
else
end
for g = 1 : 100
STR = input('label text for this curve =','s');
RE = input('Is there any error ? (y/n) = ','s');
if RE == 'n'
break
else
end
end
gtext (STR)
end
AS = input('Do you want to keep Flexural plot(s)? (y/n) = ','s');
if AS == 'y'
hold on
else
hold off
end
SE12 = zeros(Nstr,1);
SE10 = zeros(Nstr,1);
SE08 = zeros(Nstr,1);
SE06 = zeros(Nstr,1);
STR12 = zeros(Nstr,1);
```

```
STR10 = zeros(Nstr,1);
STR08 = zeros(Nstr,1);
STR06 = zeros(Nstr,1);
 for J = 1 : Nstr
SE12(J) = ROOT(J,1);
SE10(J) = ROOT(J,2);
SE08(J) = ROOT(J,3);
SE06(J) = ROOT(J,4);
STR12(J) = ROOT2(J,1);
STR10(J) = ROOT2(J,2);
STR08(J) = ROOT2(J,3);
STR06(J) = ROOT2(J,4);
end

%Finding the Intersection Point between service and Strength
DIF12 = zeros(Nstr,1);
DIF10 = zeros(Nstr,1);
DIF08 = zeros(Nstr,1);
DIF06 = zeros(Nstr,1);
for J = 1 : Nstr
DIF12(J) = abs(SE12(J)-STR12(J));
DIF10(J) = abs(SE10(J)-STR10(J));
DIF08(J) = abs(SE08(J)-STR08(J));
DIF06(J) = abs(SE06(J)-STR06(J));
end
[d12,J12] = min(DIF12);
[d10,J10] = min(DIF10);
[d08,J08] = min(DIF08);
[d06,J06] = min(DIF06);
FIN12 = zeros(Nstr,1);
FIN10 = zeros(Nstr,1);
FIN08 = zeros(Nstr,1);
FIN06 = zeros(Nstr,1);
for J =1 : J12
FIN12(J) = STR12(J);
end
for J = (J12+1) : Nstr
FIN12(J) = SE12(J);
```

```
end
for J =1 : J10
FIN10(J) = STR10(J);
end
for J = (J10+1) : Nstr
FIN10(J) = SE10(J);
end
for J =1 : J08
FIN08(J) = STR08(J);
end
for J = (J08+1) : Nstr
FIN08(J) = SE08(J);
end
for J =1 : J06
FIN06(J) = STR06(J);
end
for J = (J06+1) : Nstr
FIN06(J) = SE06(J);
end
plot(FIN12,Yst,FIN10,Yst,FIN08,Yst,FIN06,Yst)
hold on

%Reproduction of PCI-03 Charts:
X1 = [70;
77.1875
80
88.1818
94.45
98.7878
102.7272
104.5454
107.27
108.8757
111.3939];
Y1 = [22.9;
24.24
26
30
```

```
36
40
46
50
56
60
66];
X2 = [70;
85.75
94.0828
102.7272
107.2727
111.5151
114.4848
118.1818
120.3
121.9393];
Y2 = [21;
26
30
36
40
46
50
56
60
64];
X3 = [78.75;
98.9696
107.5757
115.4545
120
124.5454
127.3939
130.606
132.5454
134.8484];
Y3 = [20;
```

```
26
30
36
40
46
50
56
60
64];
X4 = [91.2121
111.818181
120
127.5757
132.7272
137.5757
140.606
144.1818
146.67
150];
Y4 = [20
26
30
36
40
46
50
56
60
66];
X5 = [78.33333;
99.0303
105.7575
112
116.1818
120.6
130.0];
Y5 = [20;
26
```

```
30
36
40
46.25
66];
X6 = [89.09
108.18
116.36
123.93
128.18
132.42
134.54
138.18
139.39];
Y6 = [20
26
30
36
40
46
50
56
58.78];
X7 =[103.0303
118.7878
126.9696
134.8484
139.3939
144.8484
147.8787
151.818];
Y7 = [20
26
30
36
40
46
50
```

```
54.8484];
X8 = [120
136.0606
143.9393
151.8181
156.0606
161.5151
164.303
168.1818
170];
Y8 = [20
26
30
36
40
46
50
56
58.78];
X9 = [106.25 145.3125];
Y9 = [53.63 57.5757];
X10 = [120.6 142.72 170];
Y10 = [46.25 53.03 58.78];
AS = input('Do you want to plot PCI-03 Charts ? (y/n) = ','s');
if AS == 'y'
hold on
plot(X1,Y1, 'b--',X2,Y2,'g--', X3,Y3,'r--', X4,Y4,'k--', X9,Y9, 'b--')
grid on, axis([70 170 20 70])
end
% Reproduction of Chart BT-4 AASHTO-PCI Bulb-Tee BT-72 based on
% PCI-11
 x12 = [40 45 50 55 60 65 70 75 80 85 90 95 100 105 110 115 120];
y12 = [6 8 10 10 12 14 14 16 18 20 22 24 26 28 30 34 36];
x10 = [50 55 60 65 70 75 80 85 90 95 100 105 110 115 120 125 130];
y10 = [8 10 10 12 14 14 16 18 20 22 24 24 26 30 32 34 38];
x8 = [45 50 55 60 65 70 75 80 85 90 95 100 105 110 115 120 125 130 135
140 145];
y8 = [6 8 8 10 10 12 14 14 16 18 18 20 22 24 26 28 30 32 36 40 42];
```

```
x6 = [40 45 50 55 60 65 70 75 80 85 90 95 100 105 110 115 120 125 130 135
140 145 150 ];
y6 = [4 6 6 8 8 10 10 12 12 14 14 16 18 20 20 22 24 26 28 32 34 38 40];
AS = input('Do you want to plot PCI-11 Charts ? (y/n) = ','s');
if AS == 'y'
hold on
plot(x12,y12, x10,y10, x8,y8, x6,y6);
end
% Concrete Stresses at Transfer or Release
% Data :
%Allowable stress limits:
%For normal strength concrete:
%Allowable Concrete Tensile Stress at release = 7.5*Sqrt(f'ci)
%Allowable Concrete compressive Stress at release = 0.6*(f'ci)
 %For high strength concrete:
%Allowable Concrete Tensile Stress at release = 10*Sqrt(f'ci)
%Allowable Concrete compressive Stress at release = 0.6*(f'ci)
 % for dia = 0.5 in,  Ast = 0.153 in2
% for dia = 0.6 in,  Ast = 0.217 in2
% for dia = 0.7 in,  Ast = 0.294 in2
%Compute Allowable Tensile strength at service ( Fb ):
if fcb >= 12000
Ast = 0.217;
dia = 0.6;
ft = 10*sqrt(fci)/1000;
fb2 = 0.6*fci/1000;
ft1 = ft + 0.00000000001;
fb22 = fb2 + 0.00000000001;
% where dia = nominal diameter of a 7 wire low relaxation strand in inches
else
Ast = 0.217;
dia = 0.6;
ft = 7.5*sqrt(fci)/1000;
% ft = 0.200;
fb2 = 0.6*fci/1000;
ft1 = ft + 0.00000000001;
fb22 = fb2 + 0.00000000001;
end
```

```
% Compute Top and Bottom Stresses at Harped Points and Midspan:
% Harped Point:
%HP = .40*L + 0.5;
%Due to the camber on the beam at release, the beam sel-weight is acting
%on the overall beam length. It is assumed that the beam extends 6 in
%beyond the bearing centerline. Therefore the overall length will be =
% L + 1 ft. Where L is the design span.
%Compute Psi
%Psi = Effective pretension force after allowing for the initial losses
%(computed before at 336 and 341 steps)
% Compute concrete strese at the top fiber of the beam, ft:
% ft = Psi/A - Psi*e/St + Mg/St
% Compute concrete stresses at the bottom fiber of the beam,
% fb2 = Psi/A + Psi*e/St - Mg/St
% Bending Moment at the HARP POINT (0.4L) due to beam self-weight is
% calculated using the followin equation :
% Mx = 0.5*w*x*(L-x)
% where w = 0.799 Kip/ft
% x = HP = 0.40L + 0.5 [=] ft
%Total length = TL = L + 1  [ft]
%Mgt3 = 0.5*(0.799)*HP*(TL-HP);
%Bending Moment at MIDSPAN (x = MS = TL/2) due to beam self-weight is
% calculated using the followin equation :
%Mgt4 = 0.5*(0.799)*MS*(TL-MS);
for J = 1 : Nstr
Psi3(J,1) = subs(Psi{J,1}, L, FIN12(J));
HP = 0.40*(FIN12(J))+0.5;
TL = FIN12(J) + 1;
MS = TL/2;
Mgt3(J,1) = 0.5*(0.799)*HP*(TL-HP);
Mgt4(J,1) = 0.5*(0.799)*MS*(TL-MS);
end
for J = 1 : Nstr
Psi3(J,2) = subs(Psi{J,2}, L, FIN10(J));
HP = 0.40*(FIN10(J))+0.5;
TL = FIN10(J) + 1;
MS = TL/2;
Mgt3(J,2) = 0.5*(0.799)*HP*(TL-HP);
```

```
Mgt4(J,2) = 0.5*(0.799)*MS*(TL-MS);
end
for J = 1 : Nstr
Psi3(J,3) = subs(Psi{J,3}, L, FIN08(J));
HP = 0.40*(FIN08(J))+0.5;
TL = FIN08(J) + 1;
MS = TL/2;
Mgt3(J,3) = 0.5*(0.799)*HP*(TL-HP);
Mgt4(J,3) = 0.5*(0.799)*MS*(TL-MS);
end
for J = 1 : Nstr
Psi3(J,4) = subs(Psi{J,4}, L, FIN06(J));
HP = 0.40*(FIN06(J))+0.5;
TL = FIN06(J) + 1;
MS = TL/2;
Mgt3(J,4) = 0.5*(0.799)*HP*(TL-HP);
Mgt4(J,4) = 0.5*(0.799)*MS*(TL-MS);
end
for V =1 : LE
for J = 1 : Nstr
if V == 1
FINN(J,V) = FIN12(J);
end
if V == 2
FINN(J,V) = FIN10(J);
end
if V == 3
FINN(J,V) = FIN08(J);
end
if V == 4
FINN(J,V) = FIN06(J);
end
end
end
% Check stresses at Release at Harp Points
for V =1 : LE
for J = 1 : Nstr
ftr =  (Psi3(J,V)/A)-(Psi3(J,V)*ec(J,1)/St)+((Mgt3(J,V)*12)/St);
```

```
fbr =  (Psi3(J,V)/A)+(Psi3(J,V)*ec(J,1)/Sb)-((Mgt3(J,V)*12)/Sb);
if V == 1
ftrH12(J) = ftr;
fbrH12(J) = fbr;
end
if V == 2
ftrH10(J) = ftr;
fbrH10(J) = fbr;
end
if V == 3
ftrH08(J) = ftr;
fbrH08(J) = fbr;
end
if V == 4
ftrH06(J) = ftr;
fbrH06(J) = fbr;
end
if ftr >= 0
if ftr > fb2
LRTCH(J,V) = FINN(J,V);
end
end
if ftr < -ft
LRTTH(J,V) = FINN(J,V);
end
if fbr >= 0
if fbr > fb2
LRBCH(J,V) = FINN(J,V);
end
end
if fbr < -ft
LRBTH(J,V) = FINN(J,V);
end
end
end
% Check stresses at Release at Midspan
for V =1 : LE
for J = 1 : Nstr
```

```
ftr =  (Psi3(J,V)/A)-(Psi3(J,V)*ec(J,1)/St)+((Mgt4(J,V)*12)/St);
fbr =  (Psi3(J,V)/A)+(Psi3(J,V)*ec(J,1)/Sb)-((Mgt4(J,V)*12)/Sb);
if V == 1
ftrM12(J) = ftr;
fbrM12(J) = fbr;
end
if V == 2
ftrM10(J) = ftr;
fbrM10(J) = fbr;
end
if V == 3
ftrM08(J) = ftr;
fbrM08(J) = fbr;
end
if V == 4
ftrM06(J) = ftr;
fbrM06(J) = fbr;
end
if ftr >= 0
if ftr > fb2
LRTCM(J,V) = FINN(J,V);
end
end
if ftr < -ft
LRTTM(J,V) = FINN(J,V);
end
if fbr >= 0
if fbr > fb2
LRBCM(J,V) = FINN(J,V);
end
end
if fbr < -ft
LRBTM(J,V) = FINN(J,V);
end
end
end
for V = 1 : LE
for J = 1 : Nstr
```

```
if LRTCH(J,V) > 0 && V == 1
Hx1 = LRTCH(J,V);
Hy1 = J;
HFT1 = 'Top Compression at Harp points';
break
end
if LRTCH(J,V) > 0 && V == 2
Hx2 = LRTCH(J,V);
Hy2 = J;
HFT2 = 'Top Compression at Harp points';
break
end
if LRTCH(J,V) > 0 && V == 3
Hx3 = LRTCH(J,V);
Hy3 = J;
HFT3 = 'Top Compression at Harp points';
break
end
if LRTCH(J,V) > 0 && V == 4
Hx4 = LRTCH(J,V);
Hy4 = J;
HFT4 = 'Top Compression at Harp points' ;
break
end
if LRTTH(J,V) > 0 && V == 1
Hx1 = LRTTH(J,V);
Hy1 = J;
HFT1 = 'Top Tension at Harp points';
break
end
if LRTTH(J,V) > 0 && V == 2
Hx2 = LRTTH(J,V);
Hy2 = J;
HFT2 = 'Top Tension at Harp points';
break
end
if LRTTH(J,V) > 0 && V == 3
Hx3 = LRTTH(J,V);
```

```
Hy3 = J;
HFT3 = 'Top Tension at Harp points';
break
end
if LRTTH(J,V) > 0 && V == 4
Hx4 = LRTTH(J,V);
Hy4 = J;
HFT4 = 'Top Tension at Harp points';
break
end
if LRBCH(J,V) > 0 && V == 1
Hx1 = LRBCH(J,V);
Hy1 = J;
HFT1 = 'Bottom Compression at Harp points';
break
end
if LRBCH(J,V) > 0 && V == 2
Hx2 = LRBCH(J,V);
Hy2 = J;
HFT2 = 'Bottom Compression at Harp points';
break
end
if LRBCH(J,V) > 0 && V == 3
Hx3 = LRBCH(J,V);
Hy3 = J;
HFT3 = 'Bottom Compression at Harp points';
break
end
if LRBCH(J,V) > 0 && V == 4
Hx4 = LRBCH(J,V);
Hy4 = J ;
HFT4 = 'Bottom Compression at Harp points' ;
break
end
if LRBTH(J,V) > 0 && V == 1
Hx1 = LRBTH(J,V);
Hy1 = J;
HFT1 = 'Bottom Tension at Harp points';
```

```
break
end
if LRBTH(J,V) > 0 && V == 2
Hx2 = LRBTH(J,V);
Hy2 = J;
HFT2 = 'Bottom Tension at Harp points';
break
end
if LRBTH(J,V) > 0 && V == 3
Hx3 = LRBTH(J,V);
Hy3 = J;
HFT3 = 'Bottom Tension at Harp points ';
break
end
if LRBTH(J,V) > 0 && V == 4
Hx4 = LRBTH(J,V);
Hy4 = J;
HFT4 = 'Bottom Tension at Harp points';
break
end
end
end
for V = 1 : LE
for J = 1 : Nstr
if LRTCM(J,V) > 0 && V == 1
Mx1 = LRTCM(J,V);
My1 = J;
MFT1 = 'Top Compression at midspan';
break
end
if LRTCM(J,V) > 0 && V == 2
Mx2 = LRTCM(J,V);
My2 = J;
MFT2 = 'Top Compression at midspan';
break
end
if LRTCM(J,V) > 0 && V == 3
Mx3 = LRTCM(J,V);
```

```
My3 = J;
MFT3 = 'Top Compression at midspan';
break
end
if LRTCM(J,V) > 0 && V == 4
Mx4 = LRTCM(J,V);
My4 = J;
MFT4 = 'Top Compression at midspan' ;
break
end
if LRTTM(J,V) > 0 && V == 1
Mx1 = LRTTM(J,V);
My1 = J;
MFT1 = 'Top Tension at midspan';
break
end
if LRTTM(J,V) > 0 && V == 2
Mx2 = LRTTM(J,V);
My2 = J;
MFT2 = 'Top Tension at midspan';
break
end
if LRTTM(J,V) > 0 && V == 3
Mx3 = LRTTM(J,V);
My3 = J;
MFT3 = 'Top Tension at midspan ';
break
end
if LRTTM(J,V) > 0 && V == 4
Mx4 = LRTTM(J,V);
My4 = J;
MFT4 = 'Top Tension at midspan';
break
end
if LRBCM(J,V) > 0 && V == 1
Mx1 = LRBCM(J,V);
My1 = J;
MFT1 = 'Bottom Compression at midspan';
```

```
break
end
if LRBCM(J,V) > 0 && V == 2
Mx2 = LRBCM(J,V);
My2 = J;
MFT2 = 'Bottom Compression at midspan';
break
end
if LRBCM(J,V) > 0 && V == 3
Mx3 = LRBCM(J,V);
My3 = J;
MFT3 = 'Bottom Compression at midspan';
break
end
if LRBCM(J,V) > 0 && V == 4
Mx4 = LRBCM(J,V);
My4 = J ;
MFT4 = 'Bottom Compression at midspan' ;
break
end
if LRBTM(J,V) > 0 && V == 1
Mx1 = LRBTM(J,V);
My1 = J;
MFT1 = 'Bottom Tension at midspan ';
break
end
if LRBTM(J,V) > 0 && V == 2
Mx2 = LRBTM(J,V);
My2 = J;
MFT2 = 'Bottom Tension at midspan';
break
end
if LRBTM(J,V) > 0 && V == 3
Mx3 = LRBTM(J,V);
My3 = J;
MFT3 = 'Bottom Tension at midspan';
break
end
```

```
if LRBTM(J,V) > 0 && V == 4
Mx4 = LRBTM(J,V);
My4 = J;
MFT4 = 'Bottom Tension at midspan';
break
end
end
end
if Hx1 < Mx1;
x1 = Hx1;
y1 = Hy1;
%FT1 = HFT1;
else
x1 = Mx1;
y1 = My1;
%FT1 = MFT1;
end
if Hx2 < Mx2;
x2 = Hx2;
y2 = Hy2;
%FT2 = HFT2;
else
x2 = Mx2;
y2 = My2;
%FT2 = MFT2;
end
if Hx3 < Mx3;
x3 = Hx3;
y3 = Hy3;
%FT3 = HFT3;
else
x3 = Mx3;
y3 = My3;
%FT3 = MFT3;
end
if Hx4 < Mx4;
x4 = Hx4;
y4 = Hy4;
```

```
%FT4 = HFT4;
else
x4 = Mx4;
y4 = My4;
%FT4 = MFT4;
end
X =[x1,x2,x3,x4];
Y =[y1,y2,y3,y4];
if Hx1 == 0;
X = [x2, x3, x4];
Y = [y2, y3, y4];
end
if Hx2 == 0;
X = [x1, x3, x4];
Y = [y1, y3, y4];
end
if Hx3 == 0;
X = [x1, x2, x4];
Y = [y1, y2, y4];
end
if Hx4 == 0;
X = [x1, x2, x3];
Y = [y1, y2, y3];
end
if Mx1 == 0;
X = [x2, x3, x4];
Y = [y2, y3, y4];
end
if Mx2 == 0;
X = [x1, x3, x4];
Y = [y1, y3, y4];
end
if Mx3 == 0;
X = [x1, x2, x4];
Y = [y1, y2, y4];
end
if Mx4 == 0;
X = [x1, x2, x3];
```

```
Y = [y1, y2, y3];
end
AS = input('Do you want to plot Release Stresses ? (y/n) = ','s');
if AS == 'y'
hold on
% TOP AND BOTTOM RELEASE STRESSES AT HARP POINTS
plot(FIN12,ftrH12,'b--',FIN10,ftrH10,'g--', FIN08,ftrH08,'r--',FIN06,ftrH06,'k-
-', FIN12,fbrH12,'b',FIN10,fbrH10,'g', FIN08,fbrH08,'r', FIN06,fbrH06,'k' )
%grid on, axis([70 170 20 70])
RRR = input('Please save the file and press return','s');
hold off

% TOP AND BOTTOM RELEASE STRESSES AT MIDSPAN
plot(FIN12,ftrM12,'b--',FIN10,ftrM10,'g--', FIN08,ftrM08,'r--
',FIN06,ftrM06,'k--', FIN12,fbrM12,'b',FIN10,fbrM10,'g', FIN08,fbrM08,'r',
FIN06,fbrM06,'k' )
end
plot (X,Y)
```

Curriculum Vitae (Resume)
September 2016

Name: Jorge Márquez Balderrama.
Place of birth: Chihuahua, México
Gender: Male.
Marital Status Married.

Work and Academic History:

1981-1985 **Bachelor degree in Civil Engineering from the University of Chihuahua,** Chihuahua, México.

1986-1989 **Civil Engineer. W**orked in Portillo y Young S.C consulting company. Design of steel and concrete buildings. Worked also in Estructuras y Edificaciones de Acero S.A de C.V., Steel Construction Company. Construction Manager and Lead designer of a five store steel building (El Amacén S.A de C.V) and other concrete and steel structures.

1990-1991 **Master of Applied Science degree** with specialization in Structures from the **University of Toronto, Canada.** My **M.A.Sc thesis (An Experimental Study of Bond in Earthquake Conditions)** was devoted to develop design, fabrication, and test procedures for an overall test program planned for two main purposes: (1) to find measures that prevent bond deterioration and failure through low cycle fatigue and (2) to establish an experimental basis for formulation of development length provisions applicable to earthquake conditions. The **experimental work** was carried out in **the Structural Laboratories of the Department of Civil Engineering at the University of Toronto**. My advisor was Dr. John F. Bonacci. Test procedures, and results from my experimental research work were published in the **Journal of Structural Engineering of the American Society of Civil Engineers (Vol. 120**
No. 3 Mar. 1994) under the title of "Tests of Yielding Anchorages under Monotonic Loadings. During my graduate studies I took five courses: Energy methods in Structural Engineering, Structural Dynamics, Design of Steel Structures, Prestressed Concrete, and Finite Element Method in Mechanical Engineering.

1989-2004 **Instructor for math and physics courses** in the Engineering Department **at Tecnológico de Monterrey campus Chihuahua,** Chihuahua, México.

1991-2010	**Worked on my own and formed an engineering company named Diseño Estructural y Construcciones S.A de C.V. Design, construction, supervision and consulting services for steel and concrete buildings** for the Mexican government and private clients in Chihuahua; Chihuahua México **(see attached performed work)**. Lead Designer of twenty meters cantilever steel frames to build the sports park baseball Manuel L. Almanza located in the University of Chihuahua. Design and construction of steel and concrete buildings for Colgate, Altec, and VTC West (Virginia Transformer Corporation) companies.
2002-2010	**Instructor for analysis and design of concrete and steel structure graduate and undergraduate courses** including, concrete, structural analysis, advanced calculus, applied mathematics, numerical methods, advanced steel structures design, structural dynamics, advanced concrete behavior and advanced structural analysis in the Civil Engineering Department at the **University of Chihuahua, Chihuahua**, Mexico. **Instructor for math, production management, statics, and linear programming courses** in the **Accounting and Administration Department at the University of Chihuahua**; Chihuahua, Mexico.
2010-2011	**Student in four graduate courses in PhD program** (continuum mechanics, mathematical modeling, applied mathematics, and design of experiments) offered in conjunction between New Mexico State University and the University of Chihuahua; Chihuahua, México.
2011-2015	**Doctoral studies in Civil Engineering at New Mexico State University**. During the course of my graduate studies, I maintained a **4.0/4.0 grade point average**. I took **11 courses including**, Advanced Mechanics of Steel Structures, Advanced Mechanics of Concrete, Advanced Concrete Design, Structural Systems, Advanced Mechanics of Materials, Masonry Design, and Design of Experiments, Continuum Mechanics, Mathematical Modeling, and Applied Mathematics. **The aim of my Ph.D. research was to develop preliminary design charts and design guidelines for simple and two-span continuous prestressed concrete girder bridges using ultra-high performance concrete (UHPC), high performance concrete (HPC), and normal strength concrete (NSC).** Findings from this research were **accepted for publication and presentation** in several conferences including, the 2012 Prestressed Concrete Institute (PCI) and National Bridge **Conference in Nashville Tennessee**, the 93rd Transport Research Board (TRB) annual meeting in **Washington D.C in 2014**, and the 7th International Conference on Bridge Maintenance, Safety and Management (IABMAS 2014) held **in Shanghai, China** on July 2014.

2011 **Administrative assistant for the NMSU Bridge Inspection Program** funded by the New Mexico Department of Transportation.

2012 **Community service at Centennial High School in Las Cruces New Mexico**. The activities I developed were to prepare lectures and structural engineering experiments to encourage students to choose a Civil Engineering career. This community service was under Dr. Peter T. Martin´s (**Professor and Head of Civil Engineering Department at New Mexico State University)** supervision.

2012-2015 **Load rating engineer to evaluate prestressed concrete and steel highway bridges**. This work was funded by the **New México Department of Transportation.**

2013 **Lead designer of a steel frame for testing ultra-high performance concrete (UHPC) prestressed girder specimens** in the NMSU Structures Laboratory.

2013-2014 **Instructor for an undergraduate class (CE 444 – Elements of Steel Design)** offered in the Fall 2013 and 2014 semesters in the Civil Engineering Department at New Mexico State University.

2015 **Bridge Inspection training course** in the Civil Engineering Department at New Mexico State University.

2016 **Research stay** at New Mexico State University in the Structural Laboratories of Civil Engineering Department. Research work was related to Ultra-High Performance Concrete

Publications:

1994 **Bonacci, J.F. and Márquez, J., 1994**, "Tests of Yielding Anchorages under Monotonic Loadings", *Journal of Structural Engineering*, **American Society of Civil Engineers (ASCE), Vol. 120, No. 3, pp. 987-997.**

2012 **Márquez, J., Jáuregui D.V., Weldon B.D., and Newtson C., 2012**, "Development of Preliminary Design Charts for Prestressed UHPC Bridge Girders", CD-ROM, **PCI (Precast/Prestressed Concrete Institute) and National Bridge Conference in Nashville, Tennessee.**

2014 **Márquez, J., Jáuregui D.V., Weldon B.D., and Newtson C., 2014**, "A Preliminary Design Aid for Prestressed NSC, HPC, and UHPC Bridge Girders", **The 93rd Transportation Research Board (TRB) Annual Meeting in Washington D.C.** http://amonline.trb.org/14-0718-1.859599?qr=1 http://amonline3.prod.omnipress.atex.cniweb.net/trb-55856-2014a-1.823612/t-1110-1.858709/488-1.859588?qr=1

2014 **Márquez, J., Jáuregui D.V., Weldon B.D., and Newtson C., 2014**, "A Preliminary Design Aid for Prestressed Concrete Bridge Girders using LRFD", **Bridge Maintenance, Safetey, Management an Life Extension Book**, Airong Chen, Dan M. Frangopol & Xin Ruan, Crc Press/Balkema, **ISBN: 978-1-138-00103-9 (hardback + DVD), ISBN: 978-1-315-76069-8 (eBook PDF),** Pages: 542, 2410-2415, **The 7th International Conference on Bridge Maintenance, Safety and Management (IABMAS 2014) in Shanghai, China. https://www.crcpress.com/Bridge-Maintenance-Safety-Management-and-Life-Extension/Chen-Frangopol-Ruan/p/book/9781138001039**

2015 **Márquez, J., Jáuregui D.V., Weldon B.D., and Newtson C., 2015**, "A Simpified Procedure to Obtain LRFD Preliminary Design Charts for Simple Span Prestressed Concrete Bridge Girders, **American Society of Civil Engineers (ASCE) Practice Periodical on Structural Design and Construction, ISSN (online) 1943-5576, ISSN (print): 1084-0680 Volume 21, Issue 1 (February 2016) http://ascelibrary.org/doi/10.1061/%28ASCE%29SC.1943-5576.0000274**

2016 **Márquez, J., Jáuregui D.V., Weldon B.D., and Newtson C., 2016**, "LRFD Preliminary Design Charts for Simple and Two-Span Continuous Prestressed Concrete Bridges", **Maintenance, Monitoring, Safety, Risk, and Resilience of Bridges and Bridge Networks Book**, Túlio N. Bittencourt, Dan M. Frangopol & André T.Beck, Crc Press/Balkema, **ISBN: 978-1-138-02851-7 (hardback + DVD), ISBN: 978-1-4987-7703-2 (eBook PDF),** Pages: 480, 1908-1913, **The 8th International Conference on Bridge Maintenance, Safety and Management (IABMAS 2016) in *Foz Do Iguazu, Brazil.***

https://www.crcpress.com/Maintenance-Monitoring-Safety-Risk-and-Resilience-of-Bridges-and-Bridge/Bittencourt-Frangopol-Beck/p/book/9781138028517

Oral Presentations:

2012 "Development of Preliminary Design Charts for Prestressed UHPC Bridge Girders", presented at **The 2012 Prestressed Concrete Institute (PCI) and National Bridge Conference Nashville Tennessee, U.S.A.**

2013 "Development of Preliminary Design Charts for Prestressed UHPC Bridge Girders", presented at the **Graduate Research and Arts Symposium in March 2013, and 58th Transportation Engineering Conference in April 2013 at New Mexico State University, U.S.A.**

2014 "A Preliminary Design Aid for Prestressed NSC, HPC, and UHPC Bridge Girders", presented at **The 93rd Transportation Research Board (TRB) Annual Meeting in Washington D.C, U.S.A in January 2014.**

2014 "A Preliminary Design Aid for Prestressed Concrete Bridge Girders using LRFD", presented at **The 7th International Conference on Bridge Maintenance, Safety and Management (IABMAS 2014) in *Shanghai, China in July 2014*.**

2016 "LRFD Preliminary Design Charts for Simple and Two-Span Continuous Prestressed Concrete Bridges", presented at **The 8th International Conference on Bridge Maintenance, Safety and Management (IABMAS 2016) in *Foz Do Iguazu, Brazil in July 2016.***

Awards:

1986 **First-in-class** in the **Civil Engineering Department** at the University of Chihuahua.

1986 **First-in-class** in the University of Chihuahua certified by the **College of Civil Engineers of Chihuahua.**

2012 **Graduate School Merit Award** at **New Mexico State University**.

2012 **Graduate School Preparing Future Faculty Award** at **New Mexico State University.**

2015 **Poster Research Award** in T**he 60th Transportation Engineering Conference 2015** in Las Cruces New México.

2015 **Ph.D. Honors Graduate** in School of **Graduate Studies at New Mexico State University.**

Continuing Education:

1987 Intensive **English course**, **University of Texas at Austin**, U.S.A

1988 Intensive **English course**, **University of Toronto, Canada**.

1989 **Total quality control**, Tecnológico de Monterrey campus Chihuahua, México.

1995 **STAAD III** training course, Research Engineers, Las Vegas, U.S.A.

2002 **Building Regulations** and Technical Standards Municipality of Chihuahua, College of Civil Engineers of Chihuahua A.C., Mexico

2005 **New Technical Standards complementary Concrete DF**, Mexican Society of Structural Engineering, College **of Civil Engineers** of Chihuahua A.C., Mexico.

2006 **Seismic Design Criteria (**Manual updated Civil works CFE, Mexican Society of Structural Engineering, University of Chihuahua, Mexico

2007 **Soil-Structure Interaction**, Mexican Society of Structural Engineering, University of Chihuahua, Dr. Jose M. Rosette from University of Texas at Austin, TX.

2007 **Seminar Clays**, College of Civil Engineers of Chihuahua A.C., Mexico.

2008 **Building Regulations** and Technical Standards Municipality of Chihuahua, College of Civil Engineers of Chihuahua A.C., Mexico

2012 **Emerging Bridge Technologies**, Evaluating Design Assumptions, Unique Transportation Solutions, Box and Post-Tensioned Bridges, Bridge Technologies-Seismic and Foundation Pile Design, 2012 PCI National Bridge Conference Nashville, Tennessee, U.S.A

2015 **Bridge Inspection Training Course**, Federal Highway Administration (FHWA), New Mexico State University, U.S.A.

2016 **Autodesk Civil3D Basics,** University of Chihuahua.

Didactic Courses:

2003 **Diploma in Teaching Focused on Learning,** University of Chihuahua.

2004 **Problem-based learning**, Tecnológico de Monterrey campus Chihuahua, México.

2005 **Approach to model Based Educational Competences**, University of Chihuahua.

2014 **Preparing Future Faculty** Graduate Assistant Program, New Mexico State University, Graduate School.

2016 **Diploma in Tutoring,** University of Chihuahua.

Professional and Honor Societies:

1993-1995 **Cámara Nacional de la Industria del Comercio**, Chihuahua; Chihuahua, México.

1995-2010 **College o f Civil Engineers of Chihuahua A . C** , Chihuahua; México.

2004-2006 **Mexican Society of Structural Engineering**, Chihuahua; Chihuahua, México.

2012-2015 **The Honor Society of Phi Kappa Phi**.

2014-2015 **Alpha Chi National College Honor Society**.

Dr. Jorge Marquez Balderrama., Ph.D.
E-mail: jomaba@nmsu.edu
Office: (614) 442-9500
Address: Facultad de Ingeniería - Universidad Autónoma de Chihuahua
Circuito No. 1, Campus Universitario 2
C.P. 31125, Chihuahua, Chih. México